Field Measurement and Numerical Analysis of Long-term Deformation of Rock Slope at Higashi-shikagoe Limestone Quarry, Japan

Dissertation for the Degree of Doctor of Engineering

Clement Amagu Amagu

Division of Sustainable Resources Engineering

Graduate School of Engineering

Hokkaido University, Japan

September 2023

Field Measurement and Numerical Analysis of Long-term Deformation of Rock Slope at Higashi-shikagoe Limestone Quarry, Japan
(東鹿越鉱山における岩盤斜面の長期変位計測と数値解析)

By

Clement Amagu AMAGU

A dissertation submitted in partial fulfillment of the requirements for the Degree of Doctor of Engineering

Laboratory of Rock Mechanics

Division of Sustainable Resources Engineering

Graduate School of Engineering

Hokkaido University

Japan

September 2023

Declaration

I, Clement Amagu Amagu, declare that this dissertation titled "Field Measurement and Numerical Analysis of Long-term Deformation of Rock Slope at Higashi-shikagoe Limestone Quarry, Japan" is an original report of my study and was carried out entirely under the supervision of Professor Jun-ichi Kodama. It was written by me and references have been duly provided on all supporting literature and resources. I also declare that this dissertation has not been submitted previously, either in whole or part, for application of any degree.

Amagu

Candidate's signature

18/08/2023

Date

Certified by

Professor Jun-ichi Kodama
(Supervisor)

18/08/2023

Date

Acknowledgements

My most esteemed gratitude goes to the Almighty God for His abundant grace and mercies in my life especially during this PhD work. I am grateful for everything!

I wish to express my heartfelt gratitude to my Supervisor: Professor Jun-ichi Kodama for guiding and providing valuable suggestion throughout the period of my studies. I highly obliged his kindly help, parental advices, patient and all kind of supports till completion of this research. Thank you for your time and your advice sir, I deeply appreciate your efforts so far!

I am very thankful to Professor Fujii Yoshiaki, Professor Tatsuya Ishikawa and Professor Satoru Kawasaki for their co-supervision, significant academic support and encouragements.

I am highly indebted to all instructors in the Laboratory of Rock Mechanics, Hokkaido University, for their assistance in various lectures and material support towards the success of this work, especially our lab advisors, Assoc. Professor Daisuke Fukuda; and our lab assistant, Mr. T. Sugawara for his continuous assistance during the experimental works. I also offer my sincere thanks to all the instructor of the Division of Sustainable Resources Engineering, Hokkaido University for their fruitful suggestions and kind help to provide information and material related to this work. Their contributions in my academic life are highly appreciated.

I want to thank Japan's Ministry of Education, Culture, Sports, Science and Technology (MEXT) for the scholarship provided to support my studies and stay in Japan. My huge thanks also go to Nittetsu Mining Co. Ltd, Japan for permitting me to do this research at their mining site and also allowed me to use their data throughout this work. My deep and cordial gratitude goes to the staff of the JPSRE office for the financial supports.

My special thanks goes to Dr. Pardon Sinkala, Dr. Sophea Boeut, Dr. Li Zhaoxin, Mr. Minami Kazuki, Mr. Cheng Zhang, Mr. Nevaid Dzimunya and other of my fellow lab mates for their care, encouragement and assistance during my stay in Rock mechanics laboratory. I am also thankful to HUISA, E3, HUASA family and the host of others, who helped me to sustain and improve my social life during my stay in Sapporo.

I am grateful to my beloved Mother, Mrs. JN. Amagu for her love for education which spurred her to afford me basic education, and my siblings for their encouragements. To my close friends and supports, Rev. Fr. FU. Akam, Rev Sis. MD. Aham, Rev Sis. B. Iwu, Dr. S. Ikporo, Dr. RO Nwakirikor, Hon. V. Nwibo, Barnabas, Blessing, Sussan, Ujunwa, Michael, Francis, Ugochukwu, Godwin and many more. I deeply appreciate their love and support in my studies.

Abstract

A massive rock slope of about 250 m height, intersected by 70-m-thick clay-bearing rock at its foot wall, has been formed at the Higashi-shikagoe limestone quarry, and has experienced slope failures four times. Consequently, behavior of the rock slope has been monitored by measuring surface displacement along the rock slope with an automated polar system (APS) since 2002. In this study, the mechanism of long-term deformation of the rock slope observed at the quarry was investigated using field measurement and numerical analysis.

The relative displacement at 18 mirror points for more than seven years was analyzed to clear deformation characteristics of the rock slope. It was found that the distance between the beam generator and each mirrors revealed a continuous rate of gradual decrease. It was also found that forward movement of the rock slope toward the southern side of the quarry is the dominant component of the displacement vectors.

Thus, the main cause of the observed continuous deformation was evaluated using two-dimensional (2-D) finite element method. Firstly, the effects of limestone excavation at foot wall of the rock slope, the deterioration of the 70-m-thick clay-bearing rock distributed at foot of the rock slope, and shear failure of rock mass due to water infiltration on the slope displacement were investigated. It was found that the calculated results of rock slope displacement induced by deterioration of the existing layer of clay-bearing rock qualitatively agreed with measured results at the north-side and center of the quarry. However, the magnitude of the calculated displacements is significantly smaller than that of measured displacements. This implied that the rock slope at the quarry is likely not deformed mainly by deterioration of the clay-bearing rock. The results also reveal that the rock slope displacement at south- side of the quarry is mainly caused by excavation at the floor wall if the horizontal stress is sufficiently large. To clarify effect of the existing layer of clay-bearing rock on the slope displacement, elasto-plastic analysis was carried out. Again, it was found that displacement induced by excavation is quite significant if clay-bearing rock behaves as an elasto-plastic material and the horizontal stress is large enough.

Three-dimensional (3-D) elastic analysis was proposed to evaluate the effect of regional stress arising from mining on the rock slope deformation. At first, three 3-D meshes of different model sizes were generated to clear the effect of boundary conditions. The results show that model with a size of four times larger than that of the mining area is large enough for simulation.

Subsequently, regional stress state and Young's modulus were estimated by back analysis of mining-induced deformation. The findings are as follows; (a) the estimated stress state of the quarry is almost uniaxial compression with the maximum principal stress range of -2.10 to -2.62 MPa, (b) the magnitude and direction of regional stress is independent of Young's modulus of the existing layer of clay-bearing rock, (c) Young's modulus, 3.5 - 4.6 GPa estimated by back analysis is close to that of Young's modulus, 4.01 GPa estimated by GSI, and (d) the direction, N21°W of the estimated maximum principal stress is close to that of measured stress, N18°W. Thus, the stress state in the quarry could also be influenced by regional stress due to tectonic activity.

Finally, to interpret mining-induced deformation from 2014 to 2017, a 3-D elasto-plastic analysis under regional stress was carried out using a model rotating technique newly proposed. The results show that the calculated results of the elasto-plastic analysis are closer to the measurement results than those of the elastic analysis. This means that the clay-bearing rock at the foot of the rock slope has shown plastic behaviors. However, countermeasure by rock bolts and shotcrete, which commenced in 2018, is expected to have inhibited the plastic deformation of the rock slope because the decreasing rate of change in distance became smaller since 2018.

Contents

List of Figures

List of Tables

1 Introduction

1.1 Background

The prediction and analysis of the stability of rock slopes are becoming more and more important research in rock engineering projects worldwide, including open-pit mines especially of large-scale slopes (Read and Stacey, 2009). In open-pit mining, as mining activities increase yearly, the depth of the mine increases as well as the height of its slope. Consequently, massive open rock slopes are often formed at the mining site, and such huge final slopes are sometime left after mining. Thus, the risk of landslides and instability of rock slope become inescapable. It is worth noting that the instability of the rock slopes in an open-pit mine endangers the lives of workers, damage property, affect mining operations and often cost excess dollars to restore the mine (Bye and Bell 2000; Kodama et al., 2009), consequently lead to economic losses. It is therefore, practical essential to study the stability of rock slopes to assess its stability, predict failure, and design possible countermeasures. These can ensure safe, smooth and effective open-pit mining, and moreover minimize risks of landslides and slope failure. Traditionally, continuous monitoring of rock slope deformation has been the main method for assessing slope stability, mostly during the operation stage in open pit mines (Kodama et al., 2009).

At Higashi-shikagoe limestone quarry, a massive rock slope of about 250 m height has been formed due to continuous mining activities (Amagu et al., 2021a, 2021b). The rock slope is intersected by 70-m-thick clay-bearing rock at its foot wall. Not only that the rock slope at the quarry has experienced slope failures four times since 1996, but continuous deformation of the rock slope was also observed. In addition, the mechanism and the causes of the observed continuous rock slope displacement at the quarry are not well understood for more than two decades. Thus, monitoring of rock slope deformation through field measurement of surface displacement and numerical simulation are deemed necessary in assessing slope stability at Higashi-shikagoe limestone quarry.

1.2 Literature review

Many researchers have focused on prediction and analysis of the stability of rock slopes (Hoek and Bray, 1981; Goodman, 1989; Kaneko et al., 1997; Willie and Mah, 2004; Kodama et al., 2009). However, assessment of rock slope stability still poses a major challenge to rock engineering projects worldwide, including open-pit mines, especially of large-scale slopes (Read

and Stacey, 2009) as it requires wide knowledge of the geological structure, lithology, and geotechnical properties of the rock mass. Thus, case study of deformation and failures of rock slope, causes and analysis of rock slope deformation are reviewed in this section. Estimation of regional stress by back analysis and rock slope deformation due to excavation are also reviewed.

1.2.1 Case study of deformation and failure of rock slope

Instability of rock slopes have been a concern issue that commonly occurred in open-pit mines around the world. Cases of landslides and slope failures have commonly been reported in many countries such as Japan, China, Chile, South Africa, Indonesia, and so on (Yamaguchi and Shimotani, 1986; Fujita, 1997; Kolapo et al., 2022). For instance, sudden collapsed of 300,000-400,000 m^3 of rock slope has been reported in the Kagemori limestone quarry, Japan which was followed by the continuous development of cracks on the slope surface (Yamaguchi and Shimotani, 1986). Fujiita (1997) reported, for example, nearly 2700 landslides and slope failure disasters induced by rainfall effects in Japan (Fujiita, 1997). Some cases of slope failures in the studied quarry have also been described by Amagu et al (2021a) and Bandazi (2017).

Hu et al. (2019) reported the slope failure that occurred at Yanqianshan iron mine in China. They confirmed that the eastern part of the slope collapsed as a result of mining activities and creeping of rock mass; these initiated the potential sliding of strata in the mine. Voight et al. (1979) also reported notable incident of slope failure in Chuquicamata mine, northern Chile, which was triggered by an earthquake. They stated that the slope movement progressed at a more or less steady rate until it fell in 1968. The Bingham Canyon landslide which occurred on 10 April 2013 in the canyon open-pit copper mines, United States of America has been reported (Serna et al., 2016). Pankow et al (2014) examined seismograph, which showed that the landslide was triggered by several small earthquakes.

An example of a slope failure that occurred during the transition of extraction from open-pit to the underground block caving method in Palabora mine, South Africa was reported by Brummer et al. (2006). They confirmed that the occurred slope failure was evident by the daylight caving of the zone as a result of intersections of four main faults crossing the pit and three dominant joint sets present at the mine. These studies implied that rock slope instabilities are becoming a major hazard in open-pit mines and often causing economic losses, property damages and maintenance costs, as well as injuries or fatalities. Thus, an understanding of the

continuous rock slope deformation mechanism at the Higashi-shikagoe limestone quarry is therefore a crucial issue to assess stability of the rock slope.

1.2.2 Causes of deformation and failure of rock slope

Identifying the causes of rock slope failures in mine is extremely important to ensure certain degree of the rock slope stability and design potential countermeasures to minimize risks related to operation safety. There have been significant researches on slope stability that investigated the causes of slope failure and its triggering factors (Read and Stacey, 2009; Gao et al., 2017; Kolapo et al., 2022). Failure in rock slopes occurs due to many reasons. Traditionally, there are several considerable factors governing stability of rock slope including geometry of the slope, characteristics of potential failure plane, geological structure and/or mechanical behavior of rock mass (Study committee on slope stability and environmental preservation in Chichibu area, 1996; Yamaguchi et al., 1981; Nakamura et al., 2003), hydrogeological properties, rainfall and groundwater conditions (Fujiita, 1997; Sugiyama et al., 1995; Ishikawa et al., 2015; Sharifzadeh and Javadi, 2017; Ayalew et al., 2004, Cai and Ugai, 2004), seismicity and earthquake events (Ohtsuka and Matsuo, 1995; Orense, 2012; Dahal et al., 2006; Bommer and Rodrı'guez, 2002; Keefer, 2000), excavation (He et al., 2008; Kodama et al., 2013, Kaneko et al., 1996, Obara et al., 2000) and so on.

Sha (2016) categorized factors affecting stability of rock slope as internal factors and external factors including mineral composition of the rock, rock types, geotechnical and structural strengths etc. Environmental factors such as earthquakes, rainfall, and weathering that can reduce the strength of the rock mass are also categorized as internal factors, while the external factors are mainly caused by human activity (Nicholas and Sims, 2000). Failure of slope walls depends on cracking of rock mass, weathering, increase in pore pressure, presence of decomposed clay rock filling materials, leaching, increase in water permeability, strain softening, and change in groundwater, which causes an increment in shear stress (Sha, 2016). Hustrulid et al. (2000) argued that instability of rock slopes is largely caused by mining activities such as rock drilling, blasting, and the use of heavy machines. Similarly, Read and Stacey (2009) indicated that the presence of groundwater, slope design, complex geology, discontinuities on rock mass, and mining operations are factors that affect the stability of rock slopes in mines. Eberhardt (2003) reviewed redistribution of in situ stresses, complexity in geology, anisotropy

and inhomogeneity of the rock materials, pressure pores and seismic loading as the most common factors that influence the stability of rock slopes.

Many studies have shown that rainfall, especially heavy storms in summer and long-term infiltration of melting snow, induced landslides and slope failures (Fujita, 1997; Cai and Ugai, 2004; Okata et al., 1994; Sugiyama et al., 1995; Shuin et al., 2012). Such rainfall-induced slope failures are closely facilitated by variations in the groundwater table and the increases in pore water pressure (Yeh et al. 2015); consequently, decreases the shear strength of rock mass, and possibly leads to landslides and slope failures (Sharifzadeh et al. 2002). Cai and Ugai (2004) pointed out that rainfall infiltration resulted in the rise of groundwater level, and the increase in the pore-water pressure, consequently, decreases the shear strength of rocks, and possibly leads to landslides and slope failures.

During recent seismic events, several cases of slope failures induced by ground motion have been also reported (e.g., Ohtsuka and Matsuo, 1995; Lu et al., 2014, 2015). Particularly, Orense (2012) reported cases of slope failure induced by large-magnitude ground shaking and soil liquefaction of weathered tuffaceous sandstones, mostly at the boundaries between fill and cut slope sections during the 2011 Tohoku earthquake in Japan. Lu et al. (2014) clarified that slope failure induced by an earthquake occur when a cumulative plastic displacement induced by a dynamic response exceeds a critical displacement value estimated by a static parameter.

The above studies affirmed that assessment of slope stability in open-pit mines required vast knowledge of the geological structure, lithology, geotechnical and hydrogeological characteristics of the rock mass, tectonic processes and mining activities (Read and Stacey, 2009). Hence, the rock slope deformation at the Higashi-shikagoe limestone quarry is likely induced by mining activities, geological conditions, rainfall and/or earthquake activity. However, the effect of earthquakes is not considered particularly serious because rock slope surface displacement changes were not observed before and/or after the large 2018 Hokkaido Eastern Iburi earthquake. In contrast, rainfall and snowmelt are considered to be more strongly affect rock slope stability at the Higashi-shikagoe limestone quarry because the maximum rainfall per day is at least 150 mm and the cumulative snowfall is >1000 mm. Previously, Bandazi (2017) investigated the effects of temperature, rainfall and snowfall, excavation and backfilling on the observed rock slope displacement at Higashi-shikagoe quarry by field measurement and elastic analysis. He concluded that observed displacement at the quarry is not induced by excavation,

but strongly by water infiltration through discontinuities. In this study, assessment of slope stability is therefore, based on the consideration of the geological conditions, properties of rock mass, excavation-induced stress changes and mining progression in the quarry to well-understand behavior of the rock mass.

1.2.3 Analysis of rock slope deformation

In open-pit mines, field measurements and continuous monitoring of rock slope deformation has been considered as vital method to assess the slop stability (Rose and Hungr 2007), predict its future failure, and possibly design countermeasure works. In that light, various methods of assessing slope stability including laboratory tests of rock cores, rock mass classification (Hoek and Bray, 1981, Hassan and Hani 2017; Pantelidis 2009; Liu and Chen 2007), numerical analysis (Jing and Hudson, 2002; Jing, 2003; Eberhardt et al., 2004; Kodama et al. 2009, Barla, 2016), and limit equilibrium analysis (Bishop 1955; Yamaguchi and Shimotani 1986; Ataei and Bodaghabadi 2008; Stead et al. 2006) have been in practical use. In Japan, the automated polar system, APS (Study committee on slope stability and environmental preservation in Chichibu area 1996), tiltmeters (Sugawara 2000), Global positioning system, GPS (Shimizu et al. 1997; Sugawara 2000; Matsuda et al. 2003), and extensometers (Noguchi and Okada 1999; Nakamura et al. 2003) have been used for rock slopes displacement measurements. Obara et al. (2000) and Kodama et al. (2009) suggested the use of integral joint of field measurement and elastic analysis for assessment of rock slope stability, mainly because inelastic deformation can be inferred from a comparison between the measured results and calculated elastic deformation once the elastic deformation of rock slope is estimated. Based on these studies, the long-term deformation behavior of rock slopes in Higashi-shikagoe limestone open-pit quarry was investigated by field displacement measurement and numerical analysis (Amagu et al., 2021), considering the influence of geological conditions, heterogeneity of rock mass, excavation-induced stress changes and mining progression to assess its stability, predict its future failure, and design countermeasure works.

1.2.4 Estimation of rock slope deformation due to excavation

Displacement induced by excavation has been deduced as one of the considerable factors for assessing the deformation mechanism. Many scholars have carried out a series of research on the stability of rock slopes subject to continuous excavation (Kaneko et al., 1997; Obara et al., 2000;

Kodama et al., 2009; He et al., 2008)). He et al (2008) conducted a 3-D model to assess the impact of excavation and backfill process on the stability of rock slope at Antaibao open pit coal mine. Yamaguchi and Shimotani (1986) studied the mechanism of slope failure in Kagemori quarry, concluded that the rock slope slide along the geological boundary between the limestone and the schalstein footwall. Even though excavation at the quarry had ceased 6 months before the slope collapsed, continuous cracks were observed on the slopes. Nakamura et al. (2003) presented measurement of rock slope deformation due to excavation in a pit-type limestone mine using multi-stage extensometers and proposed that elastic deformation of rock slope formed in the pit-type quarry can be affected by geological structure and/or mechanical properties of rock types. Kaneko et al. (1997) studied the effects of the initial stress on the deformation mode of a rock slope using a 2-D elastic analysis and confirmed that the rock slope shows contraction when the ratio of horizontal stress to vertical stress is small, but it shows extended deformation when the ratio is larger. Kodama et al. (2009) used 3D mesh technique to evaluated long-term deformation of a rock slope at Ikura limestone quarry, which are significantly affected by excavation progresses. Najib et al. (2015) investigated the deformation modes of rock slopes due to excavation in mountain-type mines using a two-dimensional finite element method. They found out that the direction of the surface displacement of the rock slope can change from forward to backward as the excavation progresses.

In the previous studies, they predicted elastic deformation of homogeneous rock slope. Thus, mining-induced elastic deformation of homogeneous rock slope has been clear. However, mining-induced elastic deformation of heterogeneous rock slope intersected by weak rock formation such as layer of clay-bearing rock (as the case of Higashi-shikagoe quarry) has not been investigated, although elastic behavior of such heterogeneous rock slope is essential in assessing rock slope stability. In addition, it has been confirmed that understanding the behavior of slope excavated within the presence of swelling clay plays key role in assessing stability of rock slope over time (Nilsen, 2011). It is expected that clay-bearing rocks exhibit plastic deformation and/or squeezing when it is overstress due to excavation (Zhang et al., 2018). However, study on mining-induced plastic deformation of heterogeneous rock slope with weak rock formation (e.g. clay-bearing rock) is still limited, even though weak rock formation is often intercalated host rock mass in many mines.

Based on the previous studies, excavation is thus expected to have deformed the rock slope at the Higashi-shikagoe quarry because limestone on the floor of the quarry has been excavated by the bench cut method. Previously, Bandazi (2017) investigated effect of excavation on rock slope deformation at the Higashi-shikagoe quarry by 3-D elastic analysis. He concluded that observed displacement at the quarry is not induced by excavation. Mainly because the displacements induced by the effect of horizontal rock stress was not considered. It is well known that as mining progresses, change in stress state of rock mass induced by gravity and horizontal regional stress plays an important role in estimating the rock slope stability (Kodama et al.2013). Thus, estimation of mining-induced elastic deformation of the rock slope by the effect of gravity and the effect of horizontal regional stress using field measurement and numerical analysis are vital in assessing stability of rock slope at the quarry. Furthermore, deformation resulting from the plastic behavior of clay-bearing rock at the quarry is also considerable to interpret mining-induced deformation within the mining area.

1.2.5 Estimation of regional stress by back analysis

In mining and civil engineering projects, information on the stress field in rock mass around excavation is of fundamental importance for ensuring the stability of the structures. In open-pit mines, changes in the stress state of rock mass arising from mining activities have been extensively investigated by some researchers (Kaiser et al., 1990; Kaneko et al., 1997; Obara et al., 2000; Nishiyam et al., 2010; Nara et al., 2011; Kodama et al., 2013). Excavation activities at open pit mines often cause stress redistribution, which can significantly affect the strength, failure mode and deformational behavior of rock mass (Nara et al., 2011; Kodama et al., 2013). During the excavation in open pit mine, stress redistribution around the excavated area can lead to stress concentration and deformation arising from the changes in the surface geometry of the mines. This often results in the failure of excavation reaming wall. Additionally, stress in a rock mass may induce time-dependent deformation and fracture development (Nara and Kaneko, 2006; Nara et al., 2006). These changes in the stress state of rock mass in open pit mine are mainly due to mining induced by the release of gravity and horizontal stresses. Also, stress state of rock is affected by earthquakes, tectonic and/ or geological structures such as faults (Li et al., 2009; Matsuki et al., 2009).

Severally methods such as hydro-fracturing technique, the Acoustic Emissions (AE), and Deformation Rate Analysis etc (Yamamoto et al., 1997; Sano 2005) have been used in

engineering projects to estimate rock stress. Conversely, the rock stress in a rock mass around the mine can be estimated by back analysis. Thus, Kaneko et al. (1996), Kodama et al. (2013) and Obara et al. (2000) have estimated stress field in a rock mass by back analysis using field measurement and numerical model of the rock mass considering surface geometry and tectonic stress. Kaneko et al. (1997) and Obara et al. (2000) calculated rock slope deformation resulting from floor excavation in an open pit mine using a 2D boundary element method. Kodama et al. (2013) successfully estimated regional stress and young's modulus of rock at the torigatayama limestone mine by back analysis of mining-induced deformation using a 3-D finite element. They found out that the excavation-induced stress changes of rock slope is dependent on the level and direction of rock stress, especially on the ratio of horizontal stress to vertical stress, as the excavation causes stress relief and relaxation in a rock mass (Obara et al., 2000; Kodama et al., 2009).

In the previous studies, excavation-induced stress changes of homogeneous rock slope were estimated by back analysis. However, excavation-induced stress changes of heterogeneous rock slope intersected by clay-bearing rock have not been estimated. Effect of model size on excavation-induced stress changes has not also been investigated. Therefore, estimation of excavation-induced stress changes of rock slope considering model size and heterogeneity of rock mass intersected by clay-bearing rock by 3-D back analysis is crucial to clarify the effect of regional stress on stability of rock slope. Hence, it is important to evaluate a stress state and the elastic moduli in heterogeneity of rock mass around mining area of Higashi-shikagoe limestone quarry to ensure the long-term stability of the rock slope.

1.3 Objectives

The main objectives of this research are to clarify mechanisms of the long-term deformation of rock slope observed at Higashi-shikagoe limestone quarry, identify the causes of the slope deformation. As described in section 1.2, understanding deformation of rock slope influenced by geological conditions, heterogeneity of rock mass, excavation-induced stress changes and mining progression plays important role in assessing long-term stability of the slope. However, as also described in section 1.2, deformation of heterogeneous rock slope with weak rock formation (e.g. clay-bearing rock) considering excavation-induced stress changes and plastic deformation of clay-bearing rock has not been investigated in detail. In this dissertation, the mechanism and causes of continuous deformation of heterogeneous rock slope observed at the quarry were

investigated using the field measurement and elastic analysis. First, characteristics of long-term deformation of rock slope at the quarry are cleared by analyzing the change in distance between the beam generator and each of the 18 mirrors on the rock slope, and 3-D relative surface displacements arising from mining activities at the quarry for more than seven years. Based on the deformation characteristics, geological conditions and mining progression, probable causes of the long-term continuous slope deformation were deduced. Secondly, the main cause of the long-term continuous slope deformation at the quarry was identified by 2-D elastic analysis and plastic behavior of the existing layer of clay-bearing rock on the slope deformation was also considered. Thirdly, effect of model sizes on the slope deformation was cleared by 3-D elastic analysis. Then, the regional stress state of the quarry and the elastic moduli in heterogeneity of rock mass were estimated by 3-D back analysis. Furthermore, deformation resulting from the plastic behavior of clay-bearing rock at the quarry is cleared by 3-D elasto-plastic analysis.

1.4 Content of the research

In chapter 1, the general overview on the assessment of rock slope stability is given. The objectives of the research are explained.

In chapter 2, the characteristics of rock slope deformation observed at Higashi-shikagoe quarry are given. The geologic condition and strength of the rock as well as the characteristics of the measured result and the possible causes of the slope displacement at the quarry are explained.

In chapter 3, the numerical investigation of the deterioration effect of the existing clay rock at the footwall of the rock slope on the deformation using 2D analysis in terms of reduction in the Young's modulus of the clay based on the experimentally results are explained. The estimation of rock slope displacement due to shear failure using Shear strength reduction (SSR) methods and effects of excavation on rock slope displacement using 2D analysis were presented.

In chapter 4, the estimation of regional stress state of the quarry and Young's modulus of the rock mass by 3-D back analysis are presented. The numerical investigation of the clay-bearing rock effect at the footwall of the cut rock slope on the deformation using 3D analysis is also explained.

In chapter 5, estimation of mining-induced deformation by 3-D numerical analysis, considering the elastic and elasto-plastic behavior of the clay-bearing rock are presented. Finally, the conclusions obtained from the present investigation and recommendations for future work are given in Chapter 6.

2 Overview and characteristics of rock slope deformation at Higashi Shikagoe Quarry

2.1 Introduction

A massive rock slope of about 250 m height, intersected by 70-m-thick clay-bearing rock at its foot wall, has been formed at the Higashi-shikagoe limestone quarry. The quarry has experienced slope failures four times since 1996. Therefore, an understanding of the geological conditions and mechanisms of the rock slope deformation are important in order to assess its stability, to predict its future failure, and to design countermeasure works. Hence, this chapter discusses the geological conditions and the characteristics of surface displacement of the rock slope measured for more than seven years by automated polar system (APS). The behavior of the rock slope monitored by measuring surface displacement along the rock slope was analyzed to understand mechanism of the continuous rock slope displacement observed at the quarry. Also, the probable causes of the continuous rock slope deformation observed at the quarry were deduced based on deformation characteristics, geologic conditions and mining progression of the quarry.

2.2 Higashi-shikagoe limestone quarry

The Higashi-shikagoe limestone quarry is a small-scale mine situated on Minami Furano, Central Hokkaido Prefecture, Japan. The site is about 400 m to artificial Lake Kanayama as shown in Fig.2.1a. The quarry has been under operation for about 80 years since February 1943, and operated by Nittestsu mining Co., Ltd, with annual production of more than 300,000 tons. More than 95% of limestone quarried is mainly used in sugar production because of its grade. Other products are used for feed/fertilizer, roads, and industrial use. Due to severe winter conditions within the region of the quarry, the operations are undertaken mainly from April to November. The topographical map of the quarry at the middle of July 2022 showing layout of the rock slope is depicted in Fig. 2.1b. The quarry has been developed by bench cut method with bench height of 10 m at the final slope angle of 55° as sketched in Fig.2.1b. During this period, mining has been undertaken at 340 m and 400 m levels whereas backfilling has been done on the northern side of the quarry (Fig. 2. 2). Massive rock slope of 250 m high has been formed as the level of excavation increases in height and width as seen in Fig. 2.1b.

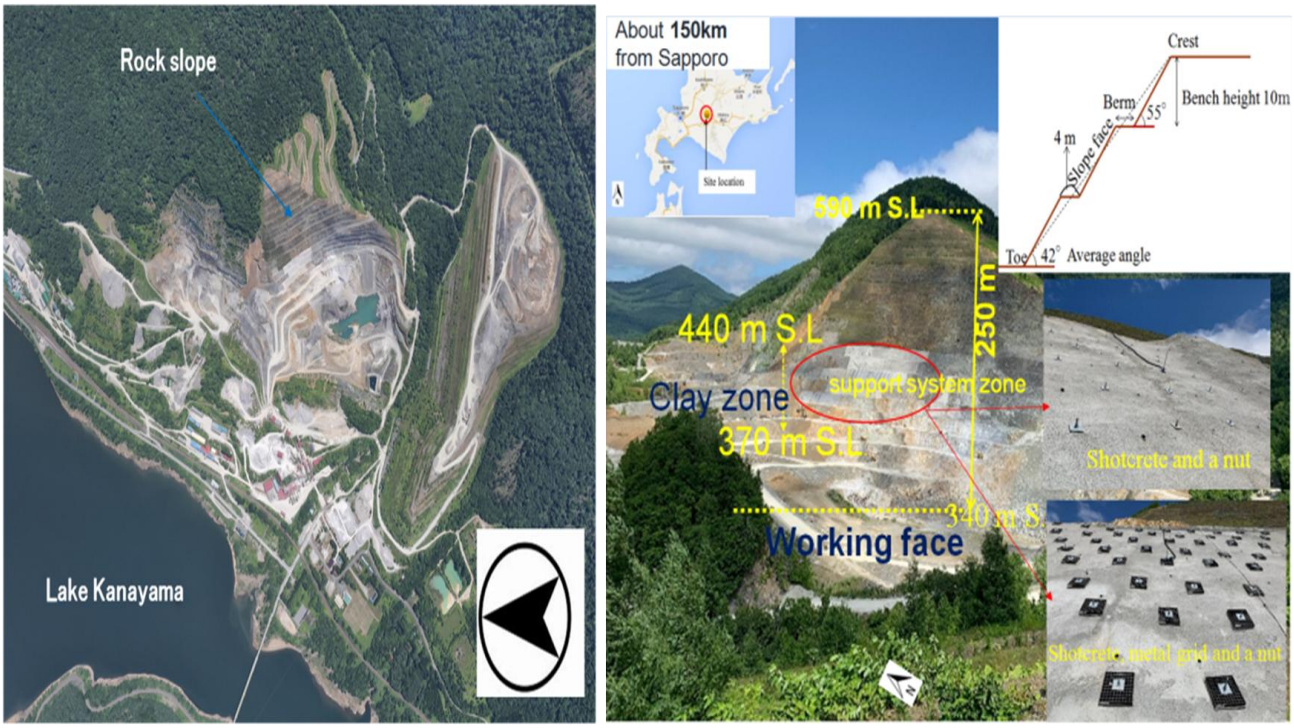

(a) (b)

Fig.2.1: Plane view of the mining area (a) and the rock slope layout (b) at Higashi Shikagoe quarry.

Fig. 2.3 illustrated the series of past events at the quarry from 1996 till 2021. In the past years, slope failures have occurred four (4) times at the quarry. In December 1996, first massive slope failure occurred at 515 m level. In July, 2004, the slope failure extended to 480 m level (Fig. 2. 4). In April, 2009, failure occurred at the north end of the face of 2004's failure (Fig. 2.4) and re-occurred in May, 2017. After the first slope failure, measurement of the rock slope displacement using automated polar system (APS) started in July 2002 for monitoring the rock slope behavior by installing two mirrors at 480 m and 500 m level (ET480-1 and ET500-1). It was found that the magnitude of displacement at the collapsed time in July 2004 was observed to be on the order of 1,000mm. To ensure stability of the rock slope, reduction in the slope angle, and cutting at upper part of the slope were adopted from April, 2007 till July, 2009 as seen in Fig. 2.5. Then, the rate of the displacements along the rock slope from July 2002 till July 2004, gradually increased with time when compared with the displacement from April 2014-March 2017 when the maximum deformation of the slope surface was less than 30mm. Recently, countermeasures such planting and installation of support systems (Shotcrete and rock bolt shown in Fig. 2.1b) have been undertaken since 2018.

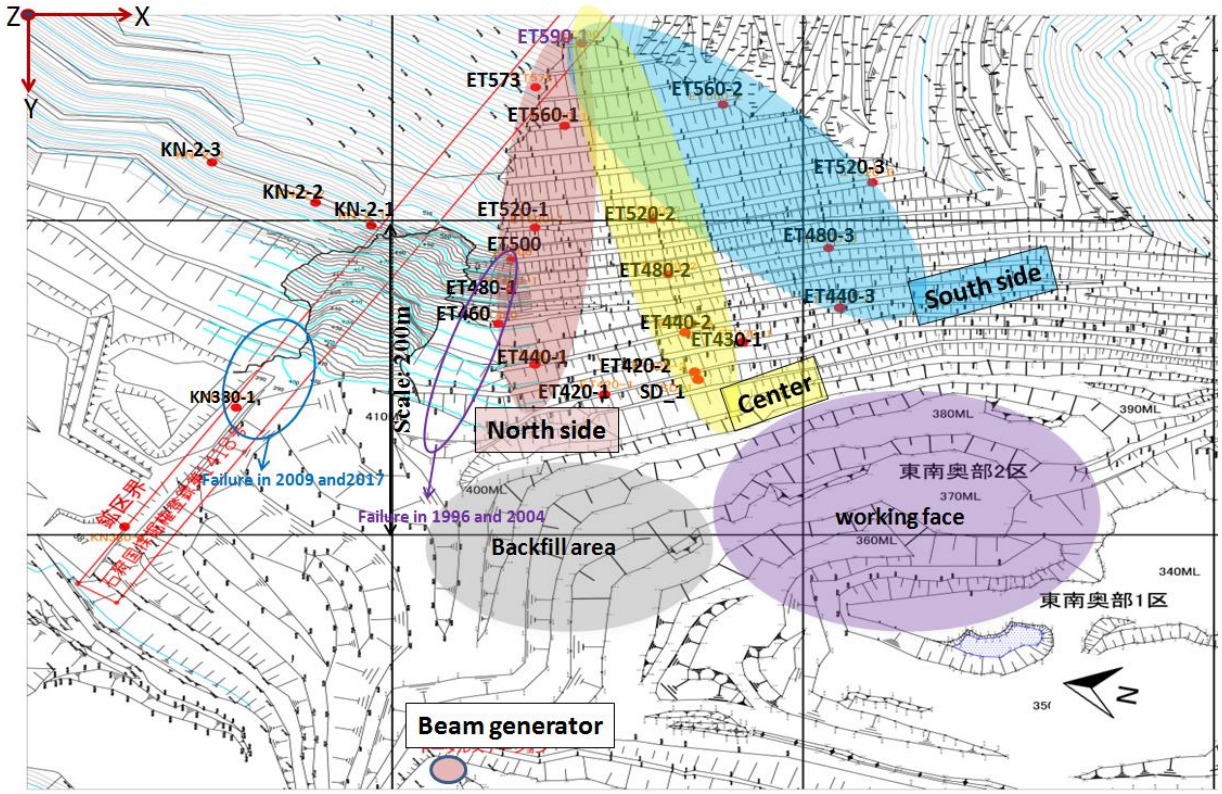

Fig.2.2: Plane view of the mining area. The ET represents the mirror point locations of automated polar system (APS) set on the rock slope. Each mirror point is represented with a number that indicates its level of elevation.

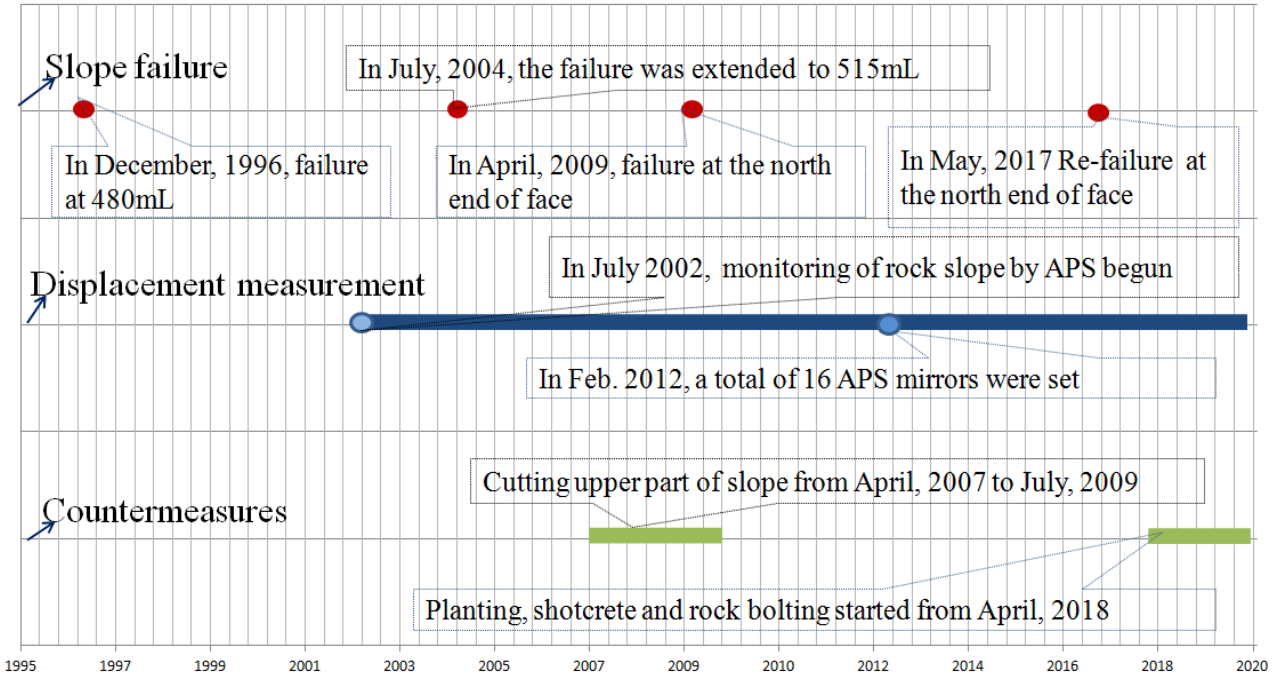

Fig.2.3: An illustration of events that have occurred at the quarry.

Fig.2.4: Plane view of rock slide that occurred at the quarry in 2004, 2009 and 2017.

(a) (b)

Fig. 2.5: Layout of the rock slope before (a) and after (b) cutting upper part of the slope in July, 2004 and November, 2009.

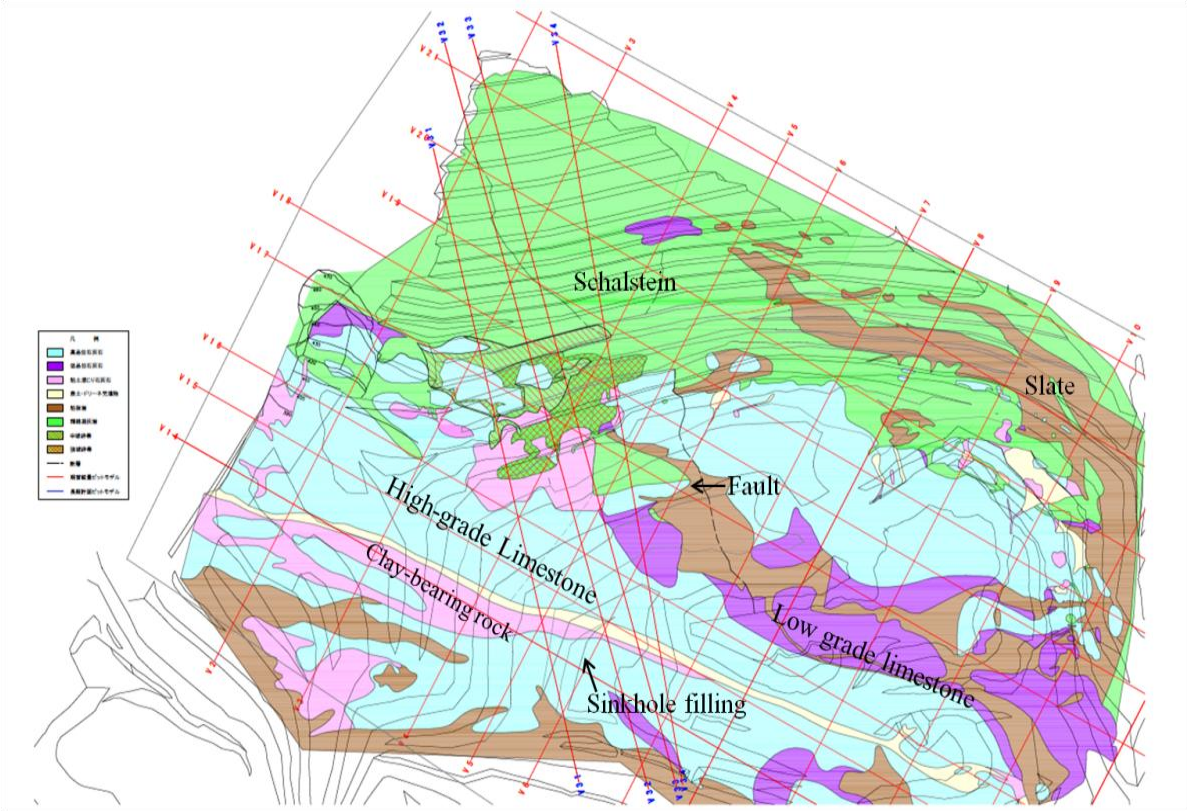

Fig.2.6: Geological map at the quarry.

Table 2.1: The mechanical properties of limestone and schalstein specimens.

Material	Young's modulus (GPa)	Poisson's ratio, v	UCS (MPa)	Friction angle, ϕ (°)	Cohesion,*C* (MPa)
Limestone	60.4	0.10	135.0	41.9	30.1
Schalstin	70.0	0.07	204.8	51.1	36.2

2.3 Geological conditions and mechanical properties of rock and rock mass

Geologically, the rock mass at the quarry composed of complex bedrock consisting of mainly limestone, schalstein (andesitic schalstein and dacitic schalstein) and slate rocks as main rock types as shown in Fig. 2.6, which belongs to the pre-cretaceous Hidaka Group. Fig.2.7 shows examples of the geological cross sections. The limestone deposit lies irregularly and lenticular with strike N30°E and length of 680 m and 100-200 m thickness. The rock masses are fractured with right lateral faults as a major discontinuity. The orientation of the dominant geologic structure strike and dip at N70° E-80° S and N70° E-75° N respectively. Interestingly, the schalstein and slate rocks have undergone intensive weathering, thereafter formed clay seams

of about 70 m thick at foot wall of the rock slope (elevations of 440-370 m) as illustrated in Fig. 2.1b. Fig.2.8 shows typically geologic conditions and weathered zones as observed at the quarry. These can lead to decrease in strength and deformability characteristics of the rock mass (Erguler and Ulusay, 2009), which in-turn can influence the behavior of the rock slopes.

In order to understand the geotechnical classification of the limestone, the mechanical properties of rock materials were examined through uniaxial compression tests conducted on 9 and 5 representative samples of limestone and schalstin rocks, respectively. However, it was difficult to prepare specimens of fresh slate and weathered slate because rock blocks were highly fractured. Based on the experimental results as presented in Table 2.1 and Fig. 2.8, the rock mass is characterized as blocky intersected by presence of clay-bearing rock with fair surface condition, moderately weathered with geological strength index (GSI) design value of 45 (Marinos, 2010). The elastic moduli of the rock mass was estimated by empirical method as presented in Table 2.2 based on Eq. (2.1) given by Majdi et al. (2012).

$$ERM = \sqrt{(\frac{Ei}{100})}10^{(\frac{GSI-20}{35})} \quad (2.1)$$

Where ERM is elastic modulus of rock mass, Ei is the laboratory value of Young's modulus of intact rock.

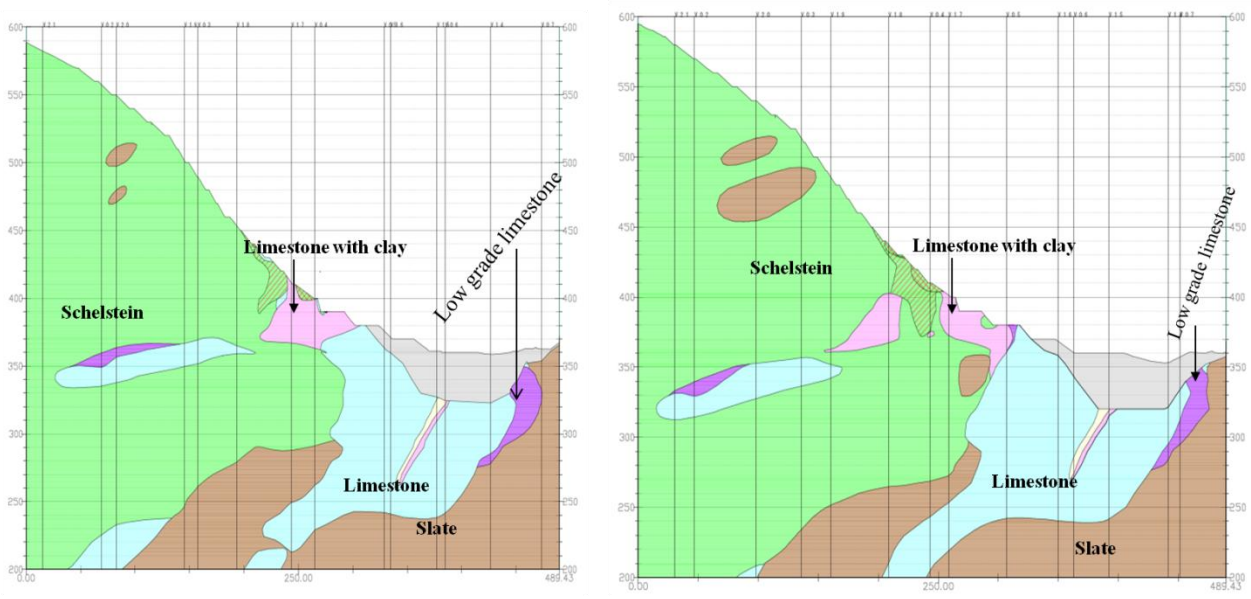

(a) Cross sectional view, V32 (b) Cross sectional view, V33

Fig.2.7: Examples of cross sectional view of the geological map as seen in Fig. 2.6.

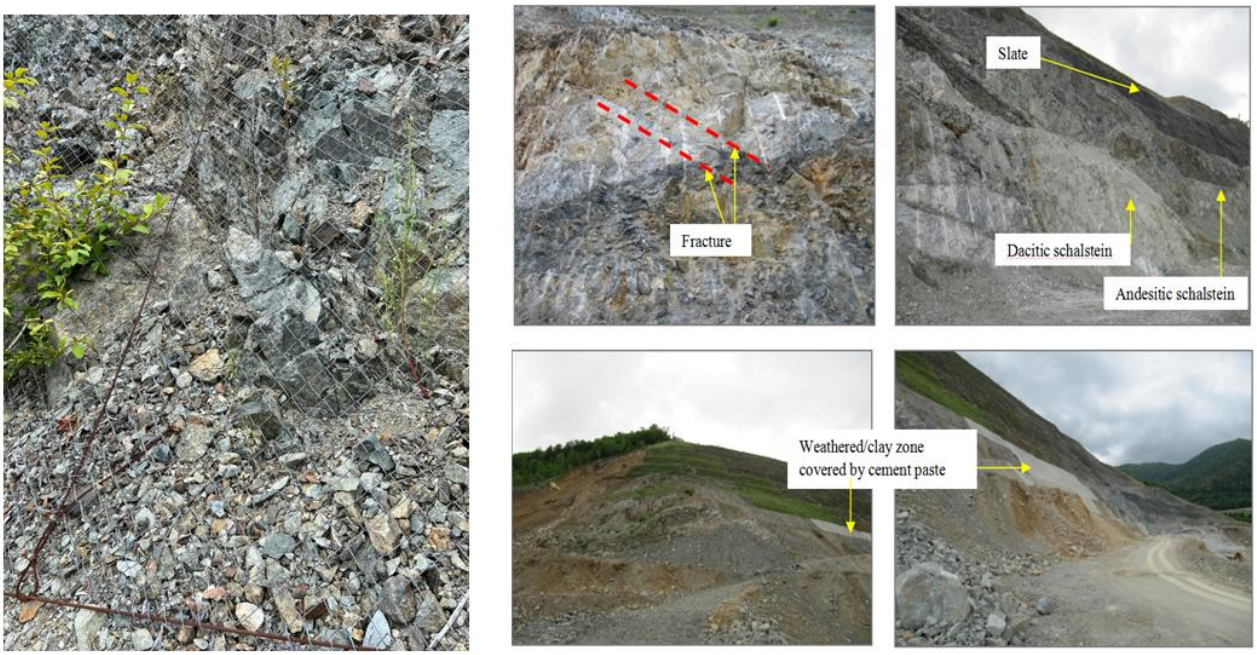

Fig.2.8: Geologic conditions and weathered zones as observed at the quarry.

Table 2.2: The mechanical properties of rock mass.

Ei (GPa)	GSI	ERM (GPa)
60.4	45.0	4.01

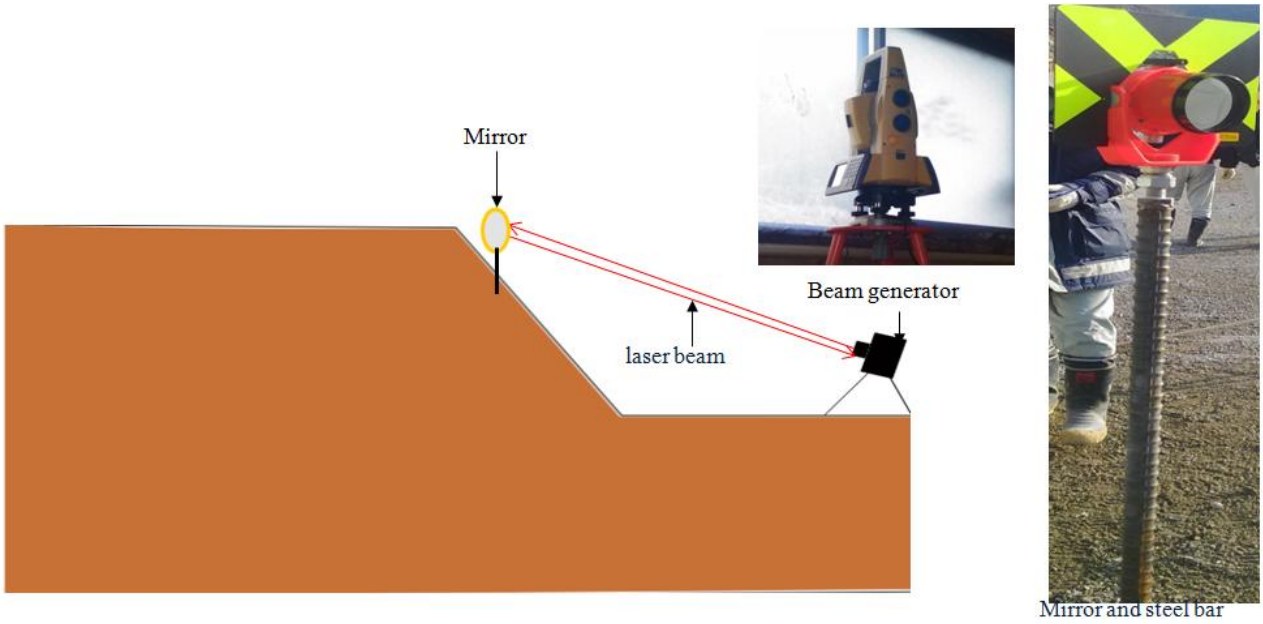

Fig.2.9: Schematic illustration of APS operation.

2.4 Displacement measurements by an automated polar system (APS)

2.4.1 Deployment of APS stations in the rock slope

After the collapsed of the rock slope in 1996, an automated polar system (APS) was set up to monitor the rock slope deformation in July 2002. The system consists of a laser beam generator, located 470 meters away from the slope at an altitude of 380 meters on the western side of the quarry. Data from three nearby stations of the nationwide GPS array of Japan were undertaken to determine stability of the base point. Firstly, APS measured travelling times of laser beam from a beam generator to mirrors located at various points along the slope as illustrated in Fig.2.9. Thereafter, changes in distance between each of the mirror points and the beam generator were calculated from the change in travelling time and velocity of laser beam. In July, 2002, two mirror points were set at the elevation of 480 and 500 m above sea level (ML). In February 2012, 16 surface displacement monitoring points (mirrors) were set along the rock slope to monitor the deformation of the entire quarry. Additionally, 7 APS mirrors were set at foot of the rock slope within 440-420 m level in May 2016 amounting to a total of 23 surface displacement monitoring points were set along the rock slope in April 2016 (Fig. 2.2), but in this study, the change in distance from 18 monitoring points (the APS mirror points), which covered the whole quarry were used in order to understand the overall deformation behavior of the present rock slope at the quarry.

2.4.2 Change in distance

The change in distance from 18 mirrors from April 1, 2014 to August 30, 2021, which covered the whole quarry are analyzed to understand the overall characteristics of the slope displacement. It can be seen in Fig. 2.10 that the distance at all the mirrors decreases gradually with time. The total values of the change in distance ranges from 20 to 140 mm approximately. The trends of decreases in the distance at all mirrors are similar, although the decreasing rate differs at each mirror. This implies that rock slope deformation depends on the position of the quarry. To understand long-term deformation characteristic of the rock slope at the quarry since 2002, change in distance from July 2002-July 2004 and April 2014-March 2019 at the elevation of 480 and 500 m level were compared as shown in Fig. 2.11. The result indicated that the rate of displacement along the rock slope at elevation 480 m and 500 m, between July 2002 to July 2004 increases rapidly with the maximum value of about 1500 mm. The rate of the displacement was

greatest in July 2004 during the slope failure, implying there was high risk of shear failure in 2004 as seen in Fig.2.4. In contrast, the rate of change in distance from April 2014-March 2019 decreases gradually, almost at a constant rate with the maximum of about 30 mm. The sudden decrease in the rate of change in distance was attributed to the effect of countermeasures such cutting upper part of the slope, planting, and installation of support systems (Shotcrete and rock bolt) as shown in Fig.2.5. Till now, it can be concluded the slope shows stable behavior, although it still deform continuously.

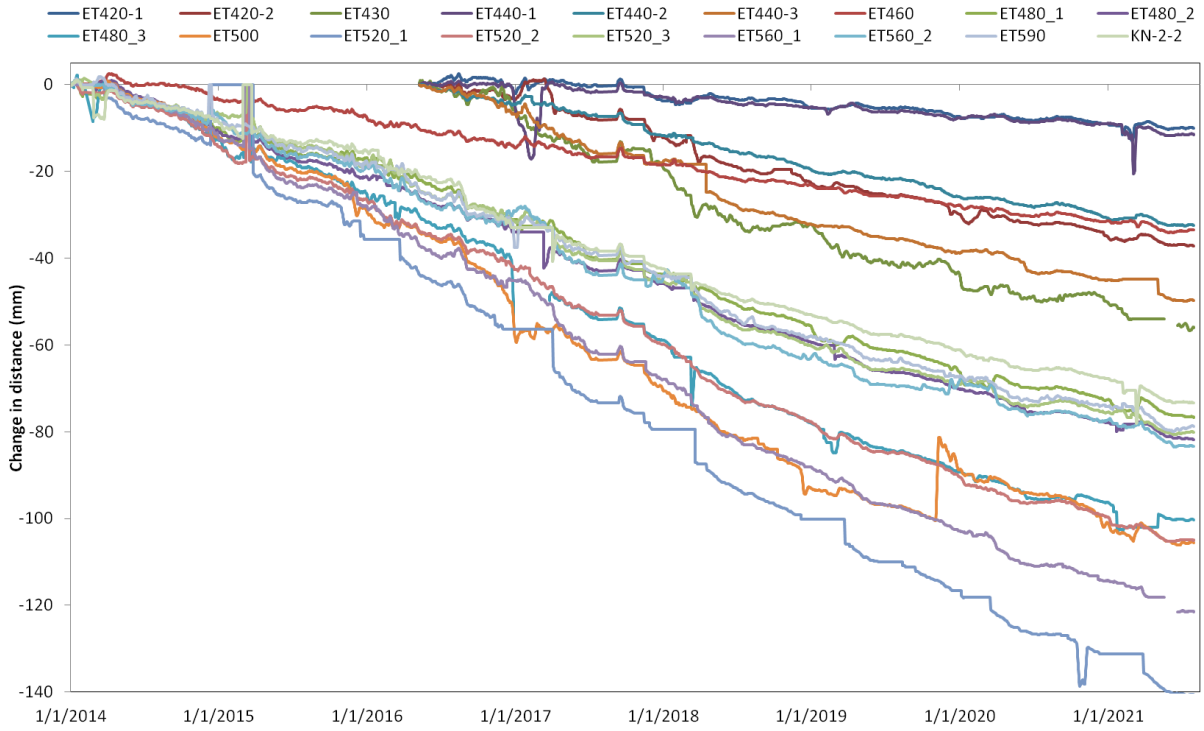

Fig.2.10: Change in distance with time for the periods of 2014 ~2021.

To get a better insight into deformation characteristic of the rock slope at the whole quarry, the monitoring mirrors were grouped to three, namely: North-side (ET42-1, ET440-1, ET460-1, ET480-1, ET500-1, ET520-1, ET560-1 and ET590-1), center (ET420-2, ET430-1, ET440-2, ET480-2, ET520-2 and ET590-1) and south-side (ET440-3, ET480-3, ET520-3, ET560-2 and ET590-1) based on the position of the quarry as shown in Fig.2.2. The change in distance was correlated with their elevations as shown in Fig. 2.12. Fig. 2.12 shows that maximum change in distance at north and center of the quarry occurred at middle (elevation 520 m) of the rock slope, which also decreases with time. In contrast, change in distance at the south-side of the quarry shows the maximum at the foot of the slope as seen in Fig. 2.12c. These results show that the

factors influencing the slope deformation at the north-hand side and the centre of the quarry are similar whereas causes of the slope deformation at the south-hand side of the quarry are different. Furthermore, Fig. 2.12 was used to validate the simulation results because it is essential to evaluate the measured results by numerical analysis (Corkum and Martin 2004).

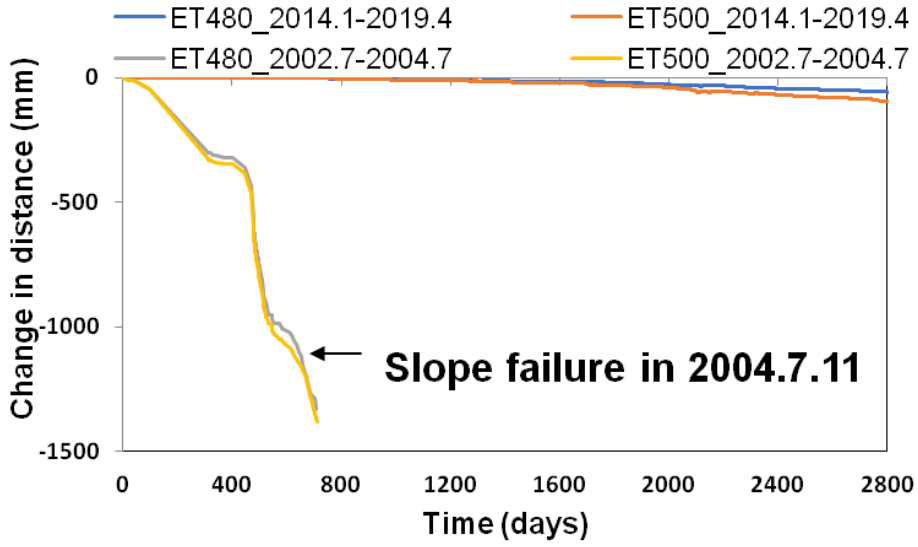

Fig. 2.11: The change in distance from 2002.4 to 2004.7 and 2014.1 to 2019.4.

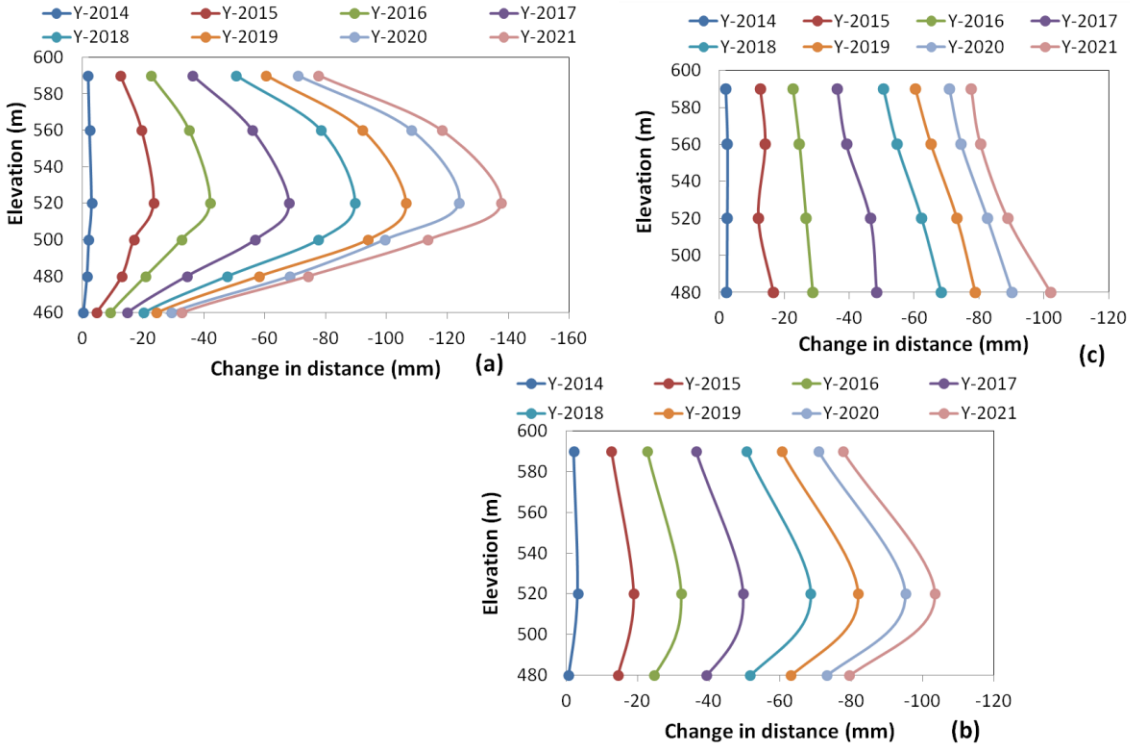

Fig.2.12: Relationship between change in distance from 2014 to 2021 and elevations. (a) North-side, (b) center and (c) south-side of the quarry.

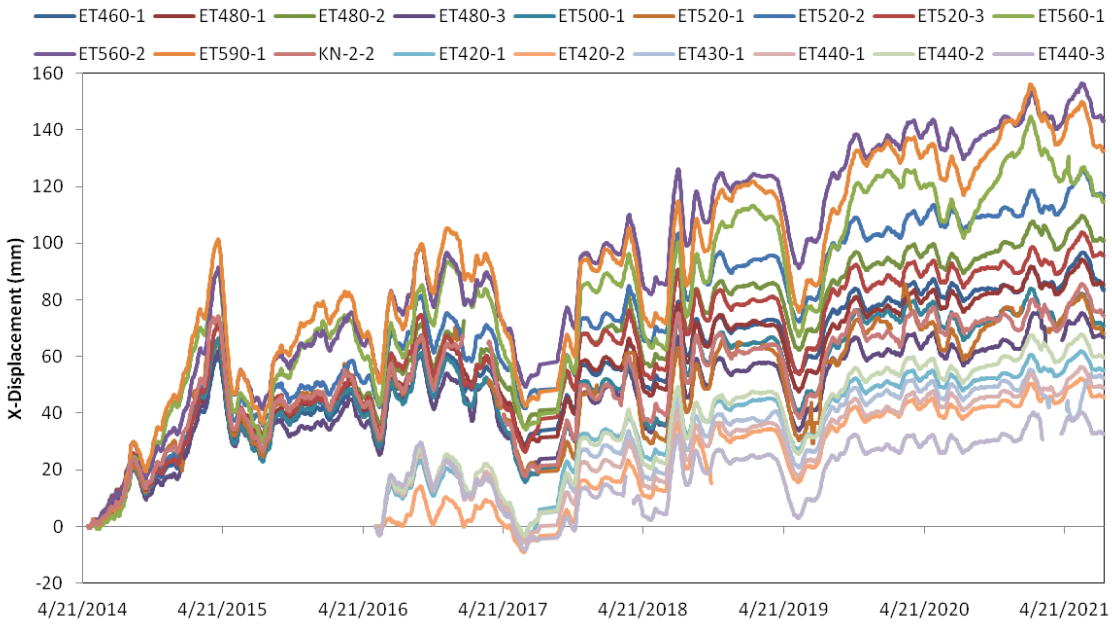

Fig.2.13: X-displacement measured by APS for more than 7 years.

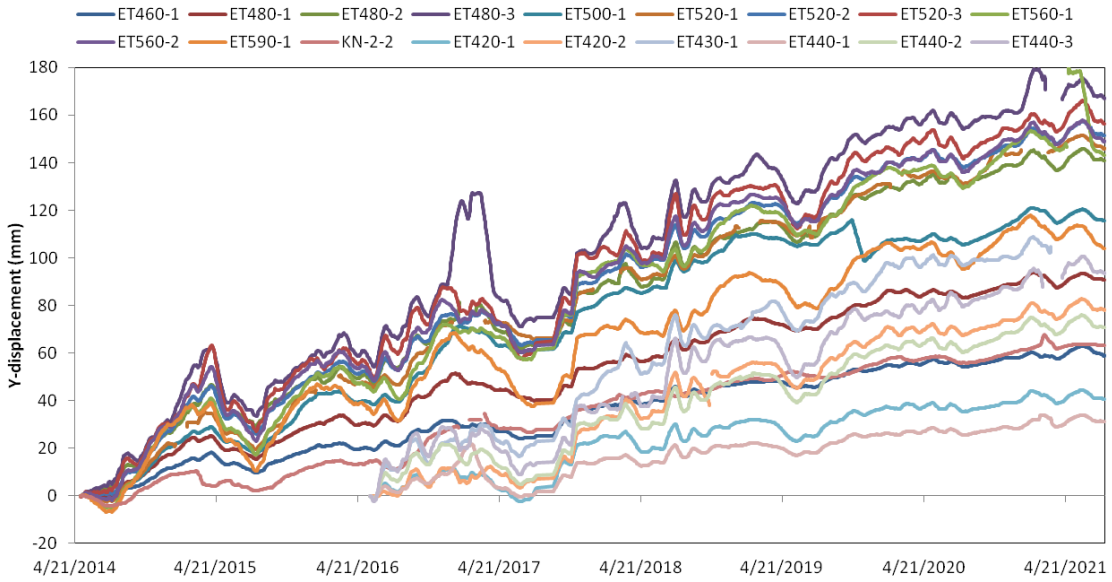

Fig. 2.14: Y-displacement measured by APS for more than 7 years.

2.4.3 3-dimensional component

The 3-D displacement data were analyzed to understand the overall characteristics of slope deformation in x-, y- and z-direction. The 3-D measured displacements are resolved into horizontal and vertical components. The horizontal displacement is denoted by x and y directions. Displacement in X-direction indicates sideways movement of the rock slope or

displacement to the left and right of the beam generator (north-south direction). The positive values of x-displacement indicate rightward movement where negative values indicate leftward movement. In Y-direction, the measured displacement indicates forward and backward (east-west) movement of the rock slope. And positive values represent forward movement whereas the negative values show backward movement. In z-direction, the vertical displacement denotes upward (positive values) and downward (negative) movement of the rock slope.

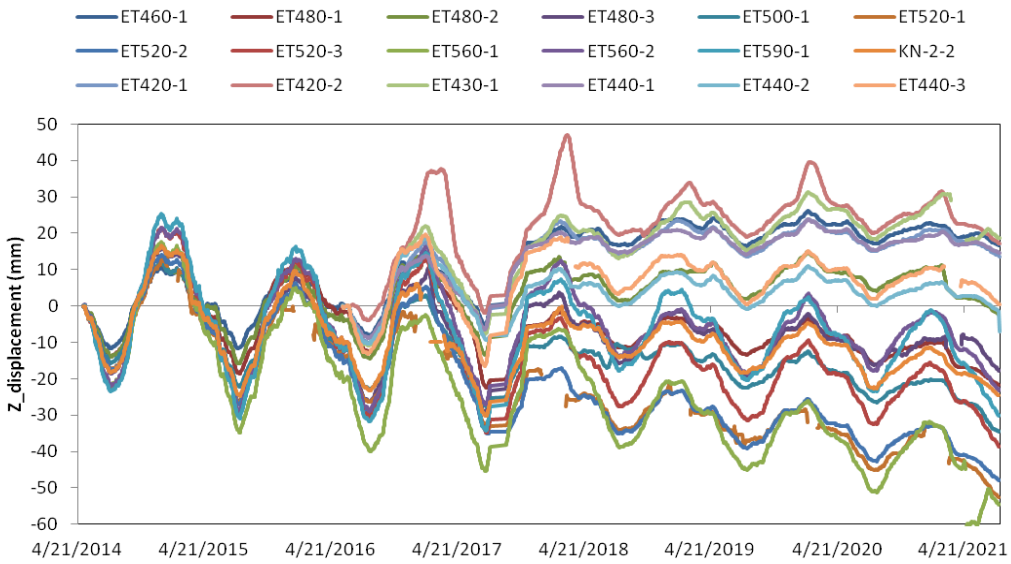

Fig.2.15: Z-displacement measured by APS for more than 7 years.

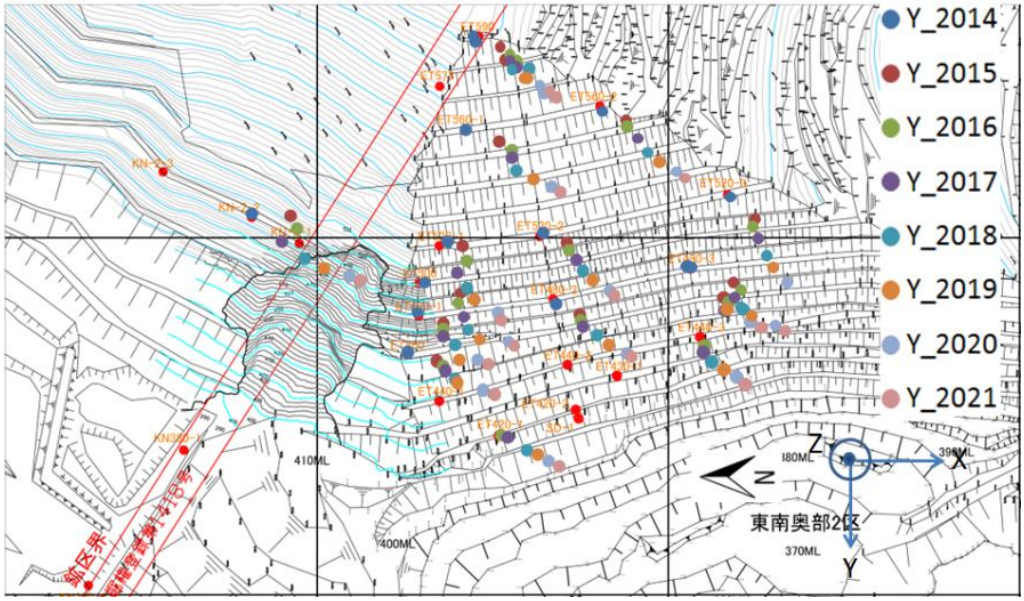

Fig.2.16: Vector of measured displacement. Each bullet represents yearly average of measured displacement starting from 2014 - 2021.

3-D surface displacement measurement from 18 APS stations (see Fig. 2.2), from April, 2014 to July 30, 2021 were analyzed. 30 days moving average method was used to eliminate the annual variation. The displacement at beam generator point was used as a reference point. Figs.2.13-15 shows the 3-D surface displacement measurement in x-, y-, and z-direction. As seen in Fig.2.13-14, the displacement at all elevations shows similar trend of rightward and forward in x and y-direction, respectively. In Fig.2.15, it is observed that displacement in the z direction shows a cyclic pattern of upward and downward movement depending on season. The slope moves downward during the summer period and upward as temperature decreases during winter. Fig. 2.16 depicts horizontal displacement vectors. A yearly average of measured displacement starting from 2014 to 2021 was used. It can be seen that the slope moved forward horizontally toward the southern side of the quarry. Fig.2.17 shows the relationship between the horizontal and vertical measured displacement. A yearly average of measured displacement in y- and z-direction starting from 2014 to 2021 was used. The sliding angle of the rock slope at differ elevations were determined. It can be seen in Fig.2.17 that the rock slope slides at an average angle of 16.5^0 toward the southern side of the quarry. The low sliding angle indicates that the rock slope has low risk of shear failure.

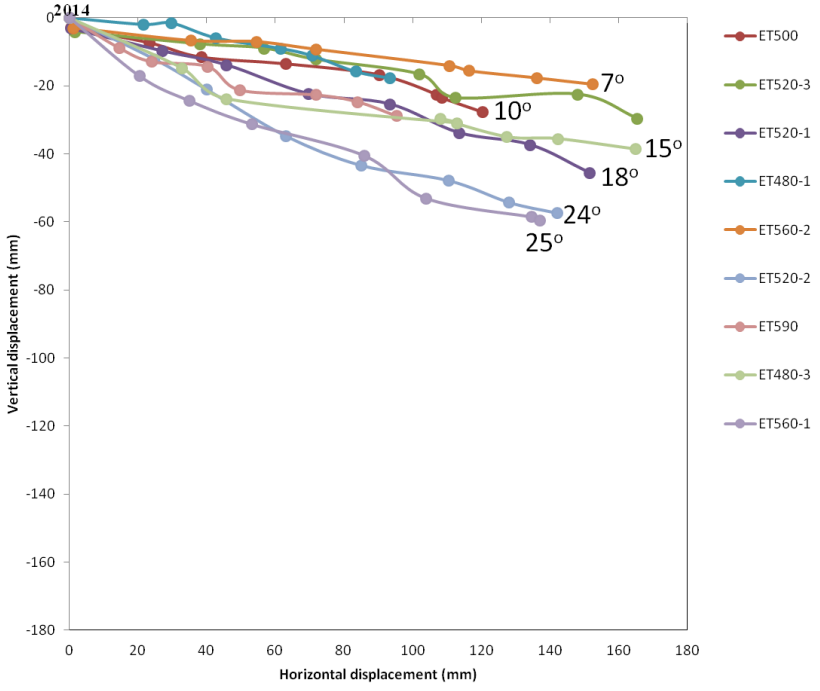

Fig. 2.17: Relationship between the horizontal and vertical displacement with sliding angle. Each bullet represents yearly average of measured displacement starting from 2014 - 2021.

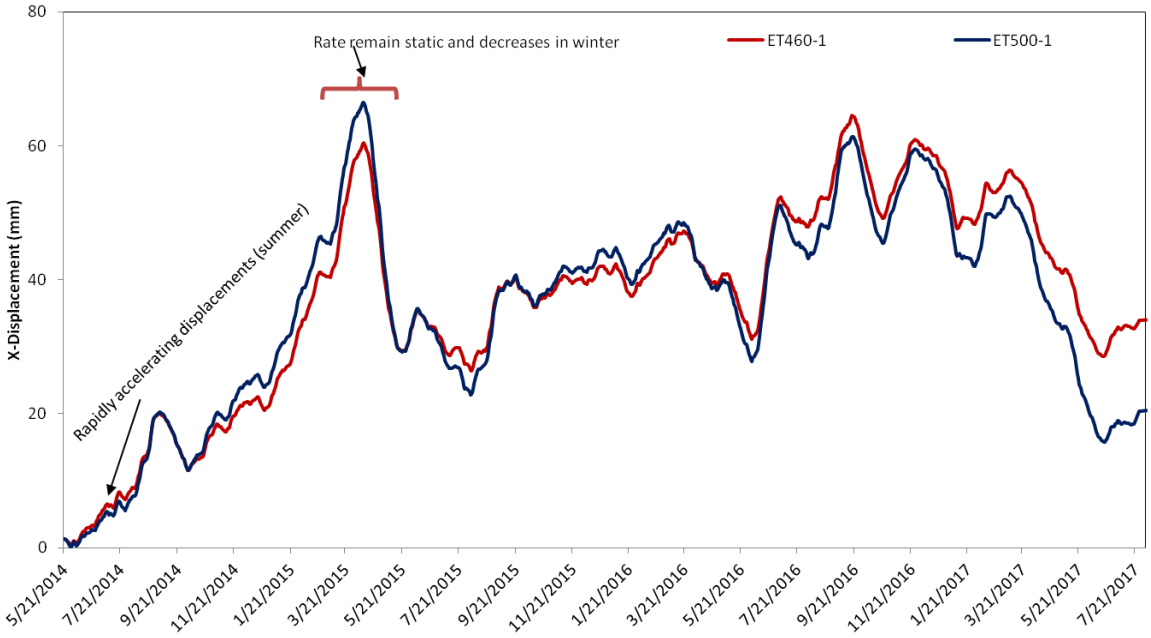

Fig.2.18: Seasonal displacement in x-direction.

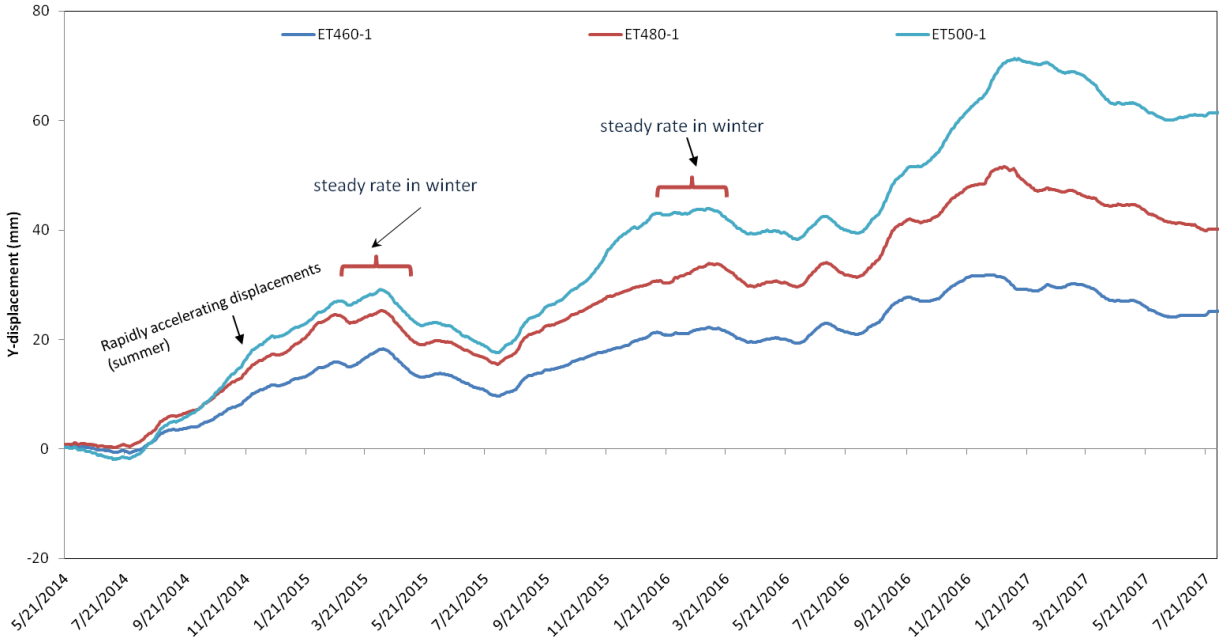

Fig.2.19: Seasonal displacement in y-direction.

2.4.4 Seasonal changes in displacement and mining progression

As described in section 2.2, mining activities at the quarry are mainly undertaken from April to November. Thus, it is expected that the patterns of displacements may be influenced by seasonal variation. Figs.2.18-20 shows seasonal displacements in x-, y-, and z-directions. In

Figs.2.18 and 2.19, it can be seen that rates of the displacements accelerate in summer and remain almost constant in winter. In contrast, it can be seen in Fig.2.20 that rate of the displacements decreases in summer and increases in winter. Also, it can be seen that the displacement in z-direction differs depending on the elevation of the quarry. It was observed that the entire slope moves slightly downward and upward during the warm period and cold period till 2017, respectively. After 2018, the entire slope at elevation 460 m and below move upward with similar displacement rates as mining progresses whereas the slope at the elevations 480 m and above move downward continuously with constant rates.

These observed characteristics of slope displacement imply that excavation activities and excavation sequence have significant effects on the slope displacement in x- and y-direction. This was evident by the monthly production of the limestone as shown in Fig.2.21. Fig. 2.21 revealed highest production during the summer season. Thus, this continuous excavation of limestone on the floor of the quarry is expected to induce deformation of the rock slope.

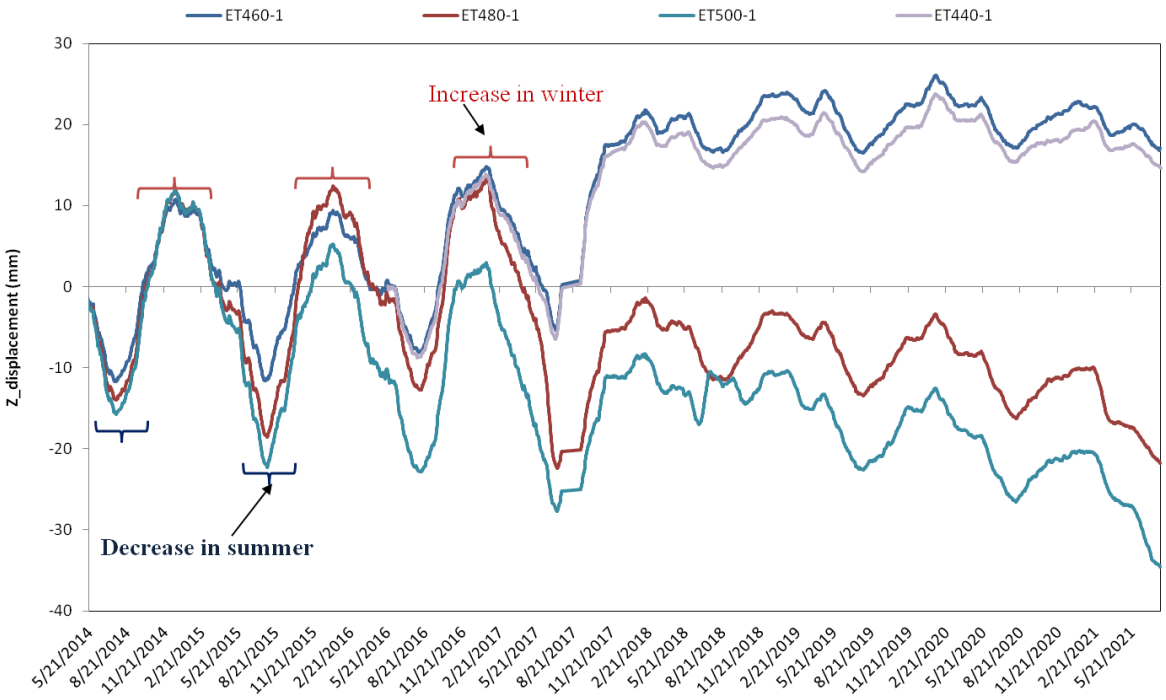

Fig.2.20: Seasonal displacement in z-direction.

2.4.5 Relationship between displacement and rainfall

In Japan, high amounts of precipitation occur in the form of rainfall during summer and severe snowfalls in winter with more than 500 cm of snow accumulated annually. Nakai et al.

(2006) established that precipitation has strong influence on rock slope deformations with time. As mentioned in section 1.2.2, rainfall and snowmelt are considered to be more strongly affect rock slope stability at the Higashi-shikagoe limestone quarry because the maximum rainfall per day is at least 150 mm and the cumulative snowfall is >1000 mm. Thus, it is important to consider the effects of water infiltration on the behavior of the rock slope. It is also understood that accumulation of snowfall creates a loading effect on the rock slope, consequently induces displacement.

To clear this effect, the influence of rainfall infiltration on the slope deformation was evaluated through comparative time series analyses. Thereafter, the cumulative rainfall was used to evaluate rock slope displacements induced by rainfall. This is because a sharp rise in cumulative rainfall can give a good indication of pressure increase in a rock mass which can be correlated with accelerated displacements. Fig.2.22 shows a comparison of cumulative rainfall and displacement. The comparison confirms that the distance tends to decrease with increasing rainfall accumulation rate. This relationship indirectly verifies that rainfall is likely facilitated rock slope deformation at the quarry. The groundwater level might increased by the water infiltration. This possibly increases the pore-water pressure, which in-turn led to decrease in the shear strength of rock mass. Thus, reduces the strength and deformability characteristics of the rock slope. Thus, enhance deterioration of the existing layer of clay-bearing-rock by water contact.

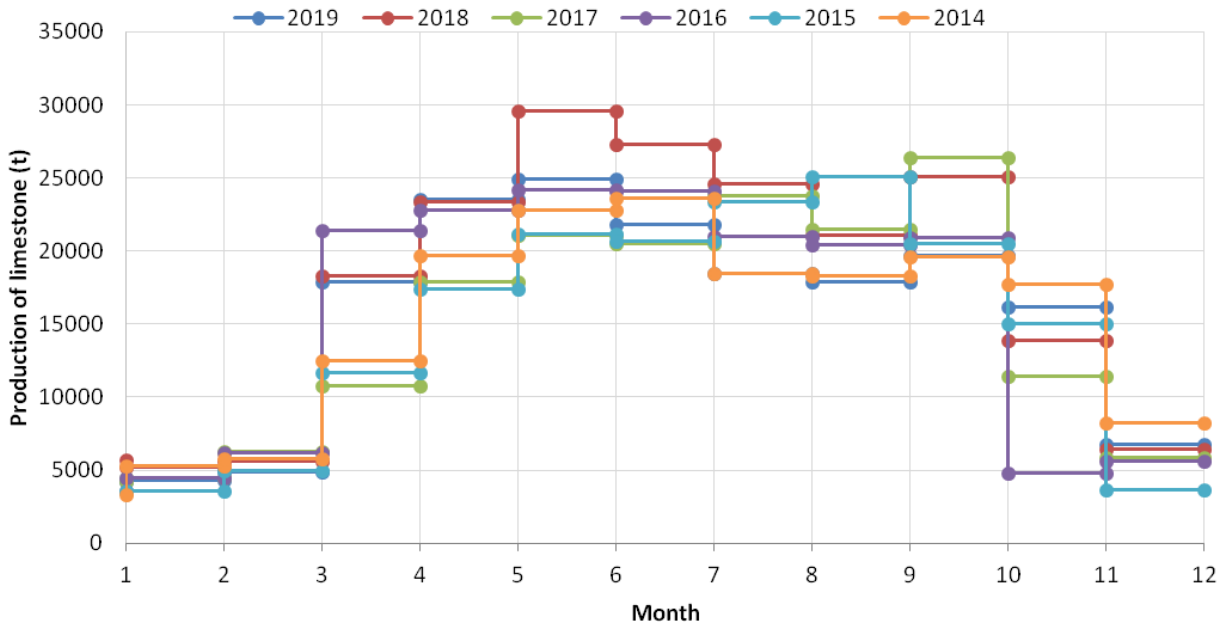

Fig.2.21: Monthly production of limestone at the quarry.

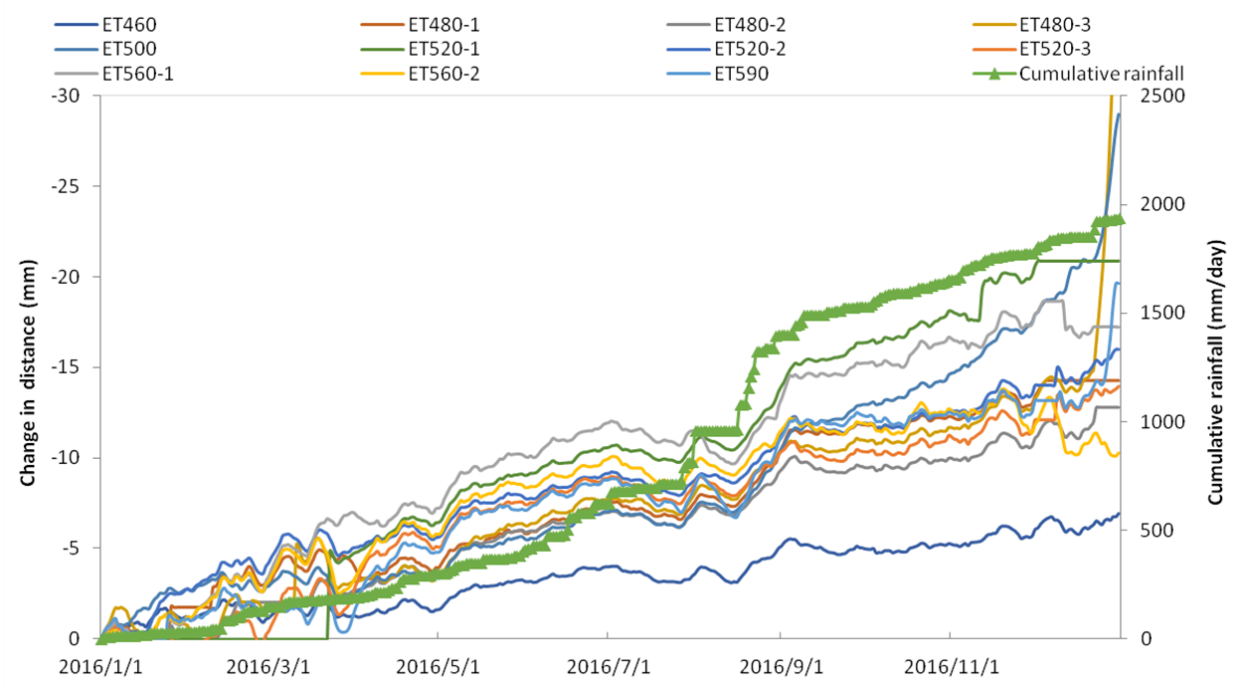

Fig.2.22: Relationship between cumulative rainfall and measured change in distance

2.5 Probable causes of the observed rock slope displacement

Based on deformation characteristics, geologic conditions and mining progression of the quarry, the probable causes of the continuous rock slope deformation observed at the quarry were deduced as follows: (1) the effects of excavation at the floor wall of the rock slope, (2) effect of deterioration of the existing layer of clay-bearing rock, 70-m thick at footwall of the rock slope, and (3) effect of decrease in shear strength of rock mass induce by water infiltration.

Displacement induced by excavation has been one of the considerable factors for assessing the deformation mechanism. The deformation of rock slope often occurs because the rock mass within an excavation zone is subjected to considerable redistributions of the initial stress state (He et al., 2008). In Japan, the deformation of rock mass due to excavation in pit-type mines has been extensively investigated (Kaneko et al., 1997; Obara et al., 2000; Kodama et al., 2009, 2013). As mentioned in section 2.1, the limestone at Higashi-shikagoe quarry has been excavated by the bench cut method on the floor of the quarry. Excavation is thus expected to have deformed the rock slope because both gravity and horizontal stress applied to the floor were released during excavation.

Another factor that likely affects slope deformation at the quarry is probably deterioration of the 70-m-thick layer of clay-bearing rock distributed at the foot wall of the rock slope. In Japan,

limestone deposit is often found on the bedrock such as sandstone, slate and schelstein. For instance, limestone deposit inclined on slate formations at Shiriya limestone quarry have been extracted (Nakamura et al., 2003). However, Higashi-shikagoe limestone quarry has similar geological formation (composed of limestone, schalstein and slate) with that of Shiriya limestone quarry. Interestingly, parts of the schalstein and slate rocks have weathered, forming clay-bearing rock of about 70 m thick (elevations of 440-370 m) at foot wall of the rock slope as illustrated in Fig.2.1b, which could exhibit reduction in the strength and deformability of the rock slope due to its weak strength and high sensitivity to the variation in water content when expose to the natural climatic conditions such as heating and cooling, wetting and dying, and freezing and thawing cycles (Va´n Eeckhout 1976; Erguler and Ulusay 2009, Nicholson, 2010). Particularly, Erguler and Shakoor (2009) showed that the exposure of clay-bearing rocks to natural climatic conditions (e.g., freeze-thaw cycles) effectively causes rock slaking and disintegration. These may consequently reduces the strength and deformability of the rock mass, and in-turn, possibly leads to the rock slope deformation. Erguler and Ulsuay (2009) reported the variation in mechanical properties of clay-bearing rocks at different water content. They revealed reductions in uniaxial compressive strength, modulus of elasticity and tensile strength of clay-bearing rocks with increase in the water content. Generally, mechanical properties of clay-bearing rock tend to deteriorate by the presence of water as a result of reaction between water and clay minerals, mostly kaolinite and montmorillonite. Thus, knowledge of the mechanical properties of clay is of great significant for clarifying the cause of the observed displacement at the quarry as clay-bearing rocks play a vital role in the stability of slopes in tunnels and mines (e.g. Ivasuc and Olinic, 2015; Park and Kutter, 2015; Bian et al., 2016; Jessu et al., 2017). Therefore, assessing the deterioration effect of the existing layer of clay-bearing rock on the rock slope stability is important to clarify mechanism of the slope displacement at Higashi-shikagoe limestone quarry.

Reduction in shear strength of rock mass induce by water infiltration from rainfall and long-term snow melting (Okata et al., 1994; Sugiyama et al., 1995; Shuin et al., 2012) is also expected to affect the rock slope deformation at the Higashi-shikagoe limestone quarry. In Japan, for example, nearly 2700 landslides and slope failure disasters have been induced owing to rainfall effects (Fujiita, 1997). In cold regions like Hokkaido, reduction in strength of rock mass may likely been attributed to the effects of snowmelt water infiltration (Ishikawa et al., 2015,

Matsuoka, 2008), which causes a large amount of surface water flowing through tension cracks to recharge potential surface weaknesses, thus triggering landslides and slope failure. Significantly, accumulation of snowfall creates a loading effect on the rock slope, which in-turn subdues the slope displacement or expansion (Ishikawa et al. 2015). These indicate that freeze-thaw action, snowfall and snowmelt might affect the slope deformation of Higashi-shikagoe limestone quarry.

3 Investigation of the causes of slope displacement by 2-D numerical analysis

3.1 Introduction

In this chapter, the possible causes of the observed continuous deformation as described in section 2.5 were evaluated using two-dimensional (2-D) finite element method. Firstly, the effects of limestone excavation at the floor of the quarry, the deterioration of the 70-m-thick clay-bearing rock distributed at foot of the rock slope, and shear failure of rock mass on the slope displacement were investigated. Thereafter, tendency and magnitude of the calculated results were discussed, and then compared with the measured displacement results. Afterward, the main factor affecting the rock slope deformation observed at the quarry was ascertained.

3.2 Effects of clay-bearing rock deterioration on rock slope displacement

As discussed in section 2.5, the layer of clay-bearing rock at the foot wall may influence the strength reduction and deformability of the rock slope (Erguler and Ulusay, 2009). To clear these, effect of increasing water content on deformability of clay-bearing rock was first investigated experimentally in terms of the effect on the Young's modulus. Afterward, deterioration effect of the existing layer of clay-bearing rock on slope deformation at the quarry was investigated using 2-D elastic analysis based on reduction in the Young's modulus of clay-bearing rock by water contact. Thereafter, the calculated results were compared with the measured displacement to ascertain its possible affect on the rock slope deformation observed at the quarry.

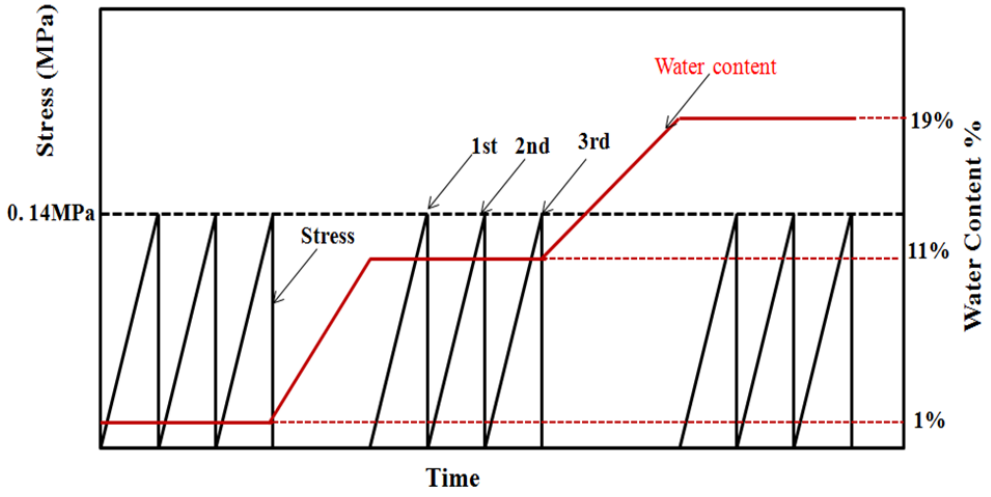

Fig. 3.1: Stress-water content-time curves showing loading cycles.

3.2.1 Mechanical properties of clay-bearing rock specimen

Cylindrical specimens of the clay-bearing rock were difficult to prepare by drilling due to its inherently weak nature. Therefore, cubic specimens with approximate dimensions of 50 × 50 × 50 mm were cut from a block of the clay-bearing rock. All the specimens were dried at 80^0C in an oven for more than 24 hours until a constant mass was reached. Thereafter, the specimens were cooled at room temperature for a minimum of one week before the testing. Afterwards, the uniaxial compressive stress was applied to specimens at a constant loading rate of 0.4 kN/s using load frame manufactured by Instron Company. The experiments were carried out at three different stages of water content of the specimens as illustrated in Fig. 3.1. At first stage, each specimen was subjected to cyclic loading of three cycles. The peak stress of the cyclic loading was set at 0.145 MPa whereas the water content of the specimens was approximated to 1%. Secondly, the specimens were covered with wet towel for 24 hours to increase its water content. Subsequently, three cycles of loading were applied to the specimens under water content of approximately 11%. Finally, the specimens were covered with wet towel for another 24 hours. Then, three cycles of loading were applied again under water contents of approximately 19%. Water content of each tested specimens was calculated as define in Eq. (3.1):

$$W_m = \frac{M_w - M_d}{M_d} \times 100 \tag{3.1}$$

Where W_m ; the water content expressed on a mass, M_w ; the weights of the specimen before drying and M_d ; the weights of the specimen after drying.

Fig. 3.2 shows the typical compressive stress–axial strain curve. The stress-strain curve show concave shape at the lower stress level although it is getting linear. The values of Young's modulus were obtained from the best fit to linear part of the stress-stain curve in each cycle. The relationship between Young's modulus and water content of clay was shown in Fig. 3.3. It show that Young's modulus of the specimens decreases rapidly with an increase in the water content. It indicate that the Young's modulus of the clay-bearing rock specimens decreases from 21, 55, and 50 MPa at water content of 0.62 % approximately to 3, 17 and 21 MPa at water content of about 19.05 % during the first, second and third cyclic loading, respectively. This implies that the clay-bearing rock has high sensitivity to the variation in water content. Thus, the mechanical

properties of clay-bearing rock in the quarry considerably decrease with increase in water content (Va´n Eeckhout 1976; Erguler and Ulusay 2009).

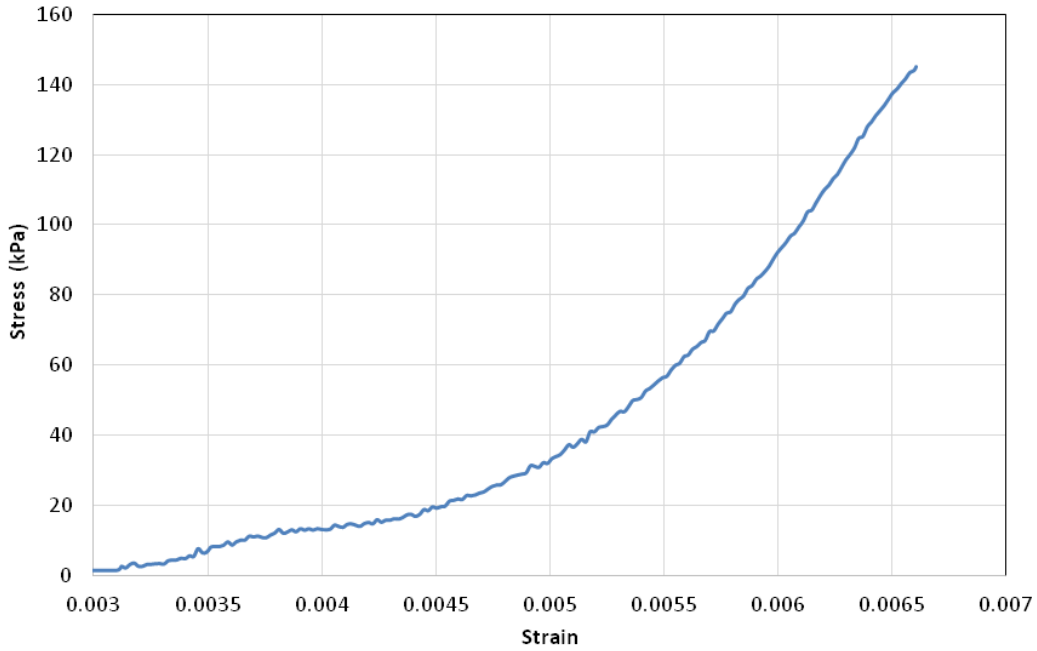

Fig. 3.2: Stress–strain curves of the clay-bearing rock specimens.

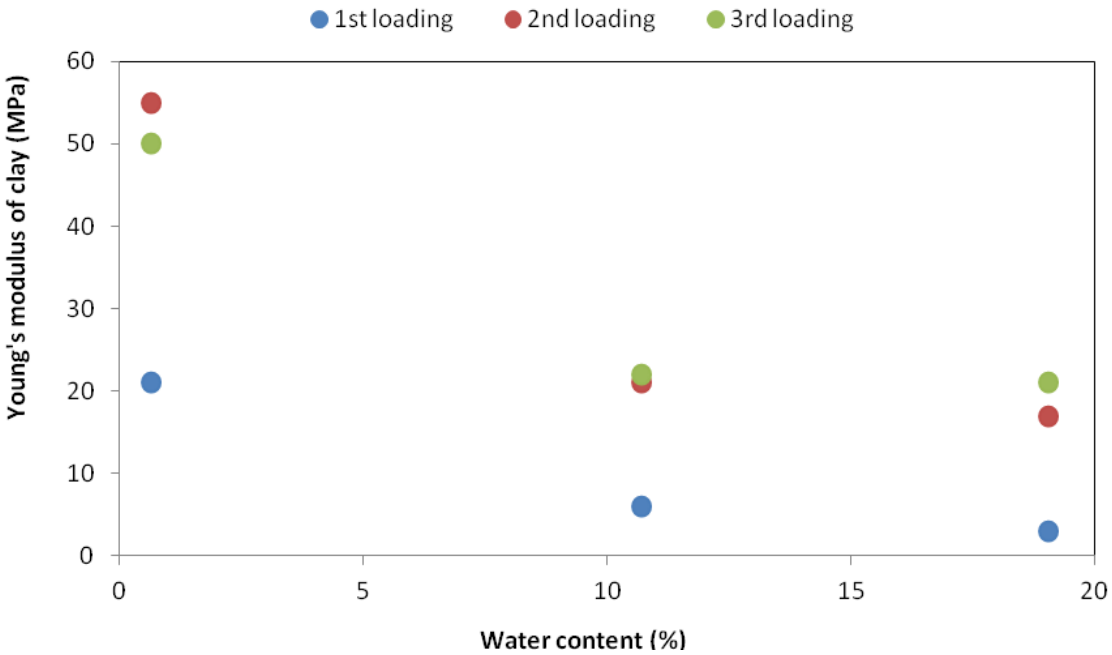

Fig. 3.3: Young's modulus of the clay specimens at different water contents.

3.2.2 Analytical method

Numerical models of layered rock slope were generated using a commercial finite element program (MIDAS GTS/NX 2014 (V2.1)). The geological profile of the rock slope along the

cross-sectional area of the quarry designated as V32 and V33 (Fig.2.7) were used to build the numerical models shown in Fig. 3.4. The finite element meshes shown in Fig. 3.4 were generated using six-node triangular elements based on the elevation readings from the cross-sectional area of the quarry (see Fig. 2.7). The entire analytical model has dimensions of 830 m in vertical direction (from north to south) and 1489 m in horizontal direction (from east to west).

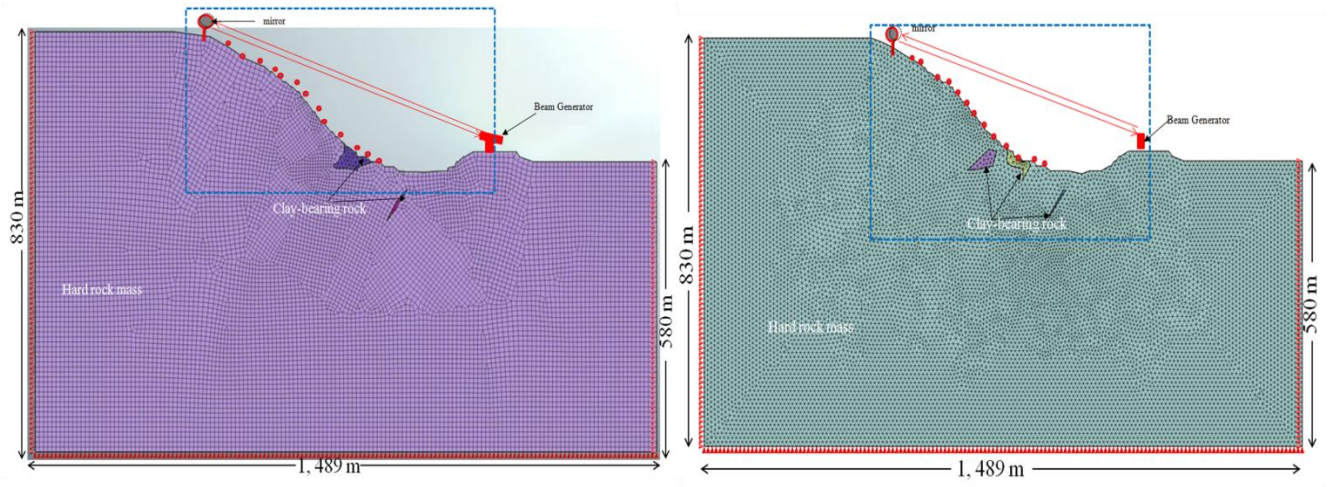

(a) V32 (b) V33

Fig.3.4: The entire analytical 2-D models of the quarry. The blue rectangle represents the area of displayed simulated result of induced displacement.

In this model, the ground types are classified into two groups, hard rock mass (limestone, schalstein and slate) and clay-bearing rock (limestone with clay), based on their notably different Young's modulus (Sakurai, 1982). Both the hard rock and clay-bearing rock are assumed to be isotropic and elastic materials. The Young's modulus of the rock specimens can be relatively evaluated by various laboratory tests (Sakurai, 1982). However, an estimation of rock mass mechanical properties from test results of rock specimens can be difficult, because the rock specimens are strongly affected by inhomogeneity (Willie and Mah, 2004). The qualities of the hard and clay-bearing rock are therefore assumed to average and poor, respectively. The Young's modulus of the hard rock was set to 4.01 GPa estimated by GSI (see Table 2.2) with the aim of examining the key role played by the presence of clay-bearing rock in assessing rock slope stability. The unit weight and Poisson's ratio of the hard rock were assumed to be 26.2 kN/m^3 and 0.2, respectively, which fall within the reasonable range of values for a good quality rock mass (Hoek and Brown, 1997; Bell, 2000). These properties are presented in Table 3.1. The

unit weight and Poisson's ratio of the clay-bearing rock were set to 18.0 kN/m^3 and 0.3, respectively, which fall within the properties of soft clay estimated by Chai and Miura (1999). All analyses were carried out under plane strain conditions. Normal displacements to the surface at the right and left sides and bottom face of the model (Fig. 3.4) were fixed to zero.

To clarify the effect of reduction in Young's modulus of the existing clay-bearing rock on the cut rock slope deformation, two basic cases were modeled. Based on the experimental results described in 3.2.1, the Young's modulus of clay-bearing rock was set to be 50 MPa and 20MPa at initial stages; then assume it deteriorated to 20 MPa and 3 MPa by water contact. The two analyses were defined as Case A and Case B. Afterwards, the relative displacements induced by reduction in Young's modulus of clay-bearing rock were calculated for each of the models by subtracting the displacement at the initial model from that of the deteriorated model. For comparison with the measurement results, the change in distance was analyzed between several points on the slope surface at different elevations and beam generator points as seen in Fig.3.4. The displacement vector on the slope surface and beam generator point was also analyzed to understand the causes of the distance change.

Table 3.1: Mechanical properties of the rock materials.

Properties	Hard rock mass	Clay-bearing rock
Unit weight, γ (kN/m^3)	26.2[a]	18.0[b]
Young's modulus, E (GPa)	4.01[c]	0.05 and 0.02[d]
Poisson's ratio, v	0.2[a]	0.3[b]

[a]The unit weight adopted from Bell (2000)
[b]Adopted from Chai and Miura (1999).
[c]Estimated by GSI
[d]Calculated from laboratory test results

3.2.3 Analytical results and discussion

Fig. 3.5 shows examples of the displacement vectors at the surface of the rock slope in case A (50 MPa → 20 MPa) and case B (20 MPa → 3 MPa). As seen in Fig. 3.5, the displacement vectors show an overall trend of downslope displacement of the rock mass from the top to the toe of the rock slope surface in both cases. The maximum displacements of 0.088 and 0.83 m in case A (50 MPa~20 MPa) and case B (20 MPa~3 MPa), respectively were observed mostly within the zone of clay-bearing rock near the foot of the slope.

Fig. 3.6 depicts the change in distance at an elevation of 430-590 m calculated from the displacement vectors. It is observed that trend of the calculated results are similar in both geologic cross-sectional lines, V32 and V33. The distance decreased at all elevations between 430 to 590 m. The change in distance is considered to decrease because a large displacement within the clay-bearing rock zone due to deterioration induces down slope displacement above the zone. It can be seen that both cases show similar tendencies along all the elevations (430 to 590 m) although the magnitudes differs. This shows that the magnitude of displacement depends on the Young's modulus of the clay-bearing rock, implies that rock slope deformation tends to continues as the rock keeps deteriorating. It should be noted that the maximum decreasing rate was observed in the middle (~520 m) of the rock slope in both cases.

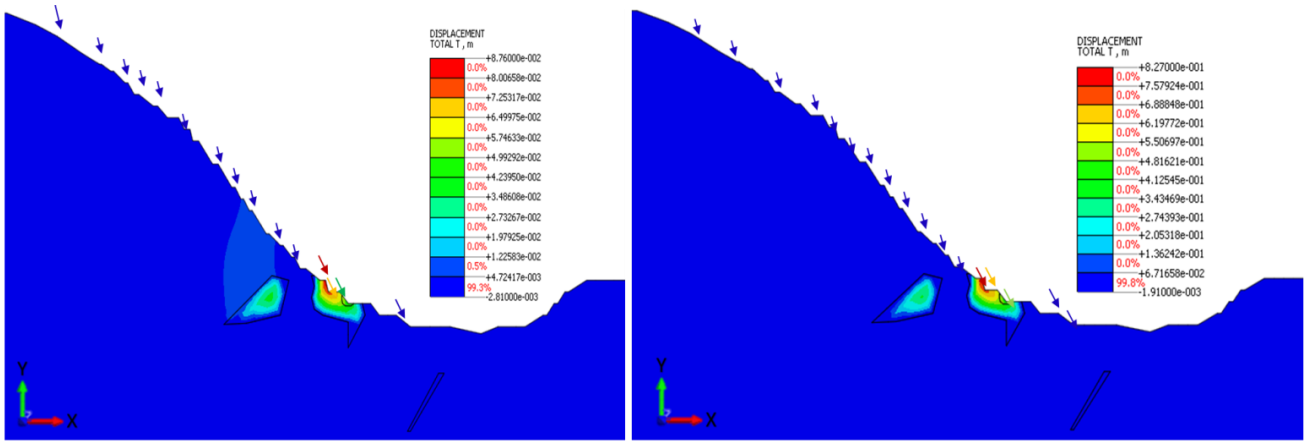

(a) Case A (50 MPa → 20 MPa) (b) Case B (20 MPa → 3 MPa)

Fig.3.5: Example of total displacement vector at the surface of rock slope induced by reduction in Young's modulus of clay-bearing rock zone, in the blue dotted rectangle in Fig.3.4b. The arrows indicate the direction of the displacement whereas length of arrow is proportional to magnitude of the displacement.

Table 3.2: Young's modulus of hard rock mass and clay-bearing rock.

Cases	clay-bearing rock (GPa)		Hard rock mass (GPa)
	Initial	After deterioration	
A (50 MPa ~ 20 MPa)	0.05	0.02	4.01
B (20 MPa ~ 3 MPa)	0.02	0.003	4.01

From the comparison between Fig 3.6 and Fig.2.12, it can be seen that the measured results at the north and center of the quarry qualitatively have a similar tendency of displacement with

the calculated result (Fig. 3.6). As seen in Fig. 2.6, the clay-bearing rock is mainly distributed on the north- side and centre of the quarry, which consequently exhibit significant strength reductions and deformability as a result of its deterioration by water contact (Erguler and Ulusay, 2009). For simplicity, clay-bearing rock deterioration owing to water was modeled by reducing its Young's modulus. However, clay-bearing rocks also show other deterioration types, including plastic deformation, cracking and breaking (Zhang et al., 2018). This relationship indirectly verifies that the clay-bearing rock deterioration is induced by water. Nicholson and Hencher (1997) explained that deterioration of clay-bearing rocks includes the progressive physical and chemical alteration of rock, which is facilitated by stress release, freeze-thaw and wet-dry cycles (Matsuoka, 2008; Erguler and Shakoor, 2009) when exposed to natural climate conditions. In particular, slaking, which is caused by repeated exposure to dry and wet conditions, is also an important mechanism of clay-bearing rock deterioration (Erguler and Shakoor, 2009; Gautam and Shakoor, 2013). The clay-bearing rock in the quarry is therefore also possibly susceptible to deterioration via slaking. However, the magnitude of displacement in Fig.3.6 is significantly smaller than that of Fig.2.10a and b. This implied that the rock slope at the Higashi-shikagoe limestone quarry is likely not deformed mainly as a result of deterioration of the clay-bearing rock the foot wall of the rock slope, mostly at the north-side and center of the quarry even thought the clay-bearing rock is widely distributed. Thus, the slope displacement is induced by other factors.

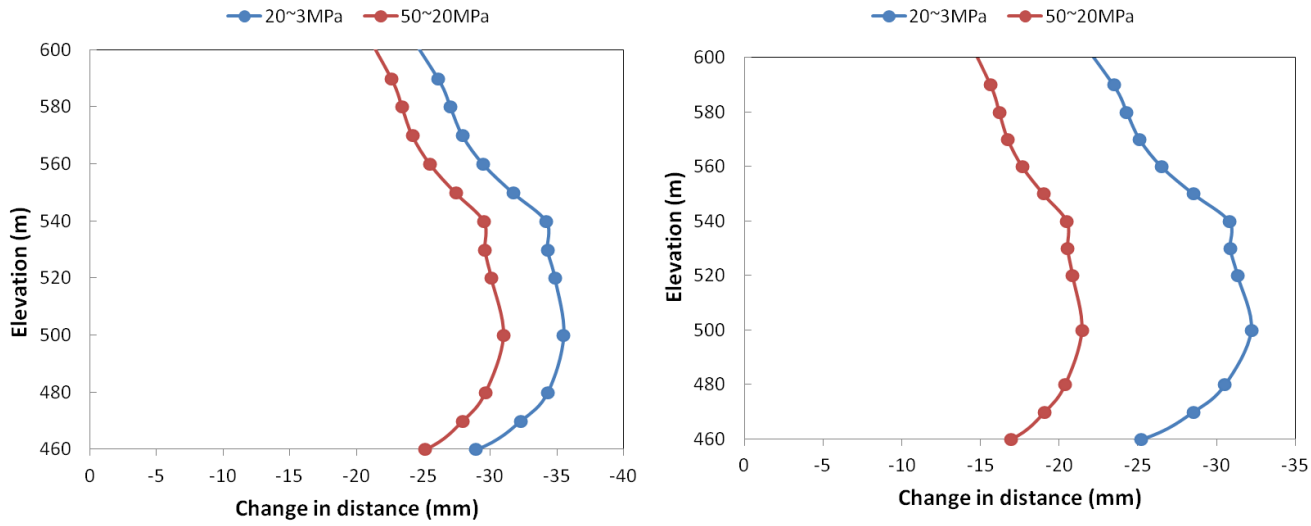

(a) V32 (b) V33

Fig.3.6: Change in distance calculated from displacement as shown in Fig.3.4.

3.3 Effects of excavation on rock slope displacement

As discussed in section 2.5, the limestone at Higashi-shikagoe quarry have been excavated by the bench cut method on the floor of the quarry. Excavation is thus expected to have deformed the rock slope because both gravity and horizontal stress applied to the floor were released during excavation. To address these effects, the elastic and elasto-plastic deformations of the rock slope induced by excavation were investigated by 2-D analysis. The displacements induced by the effect of gravity and the effect of horizontal regional stresses were analyzed to clear the characteristics of the cut rock slope deformation arising from excavation at the floor of the rock slope progressively from 2014 to 2019. Then, the deformation mechanism of the cut rock slope was discussed based on the comparison between the measured and calculated results.

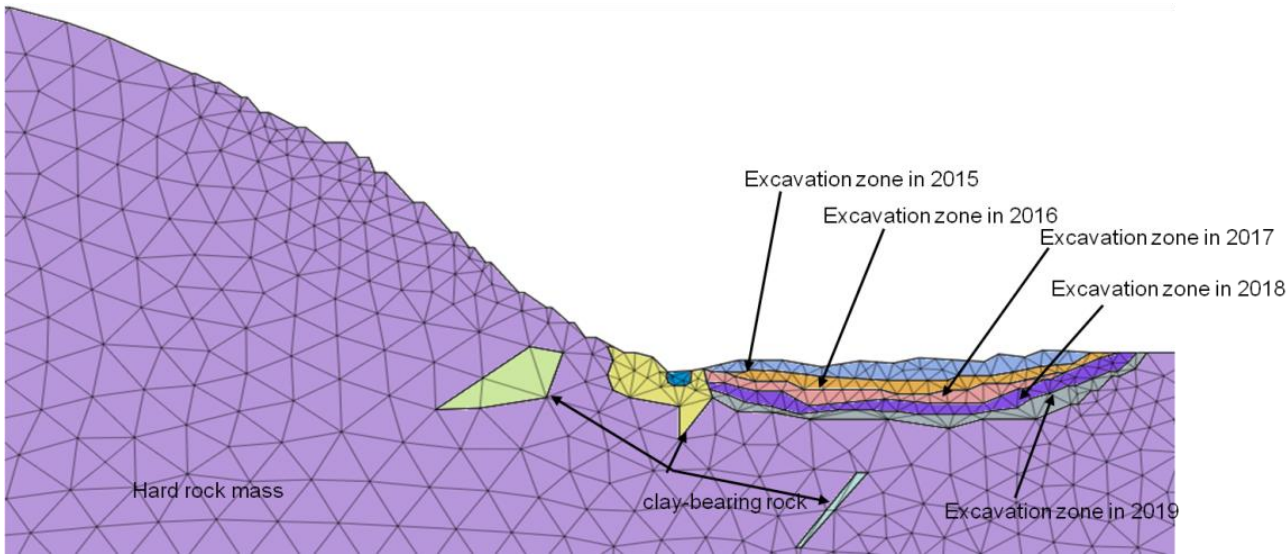

Fig. 3.7: FEM meshes in terms of excavation yearly, in blue dotted rectangle in Fig.3.6b.

3.3.1 Analytical method

Numerical models for two stress conditions are build using a commercial finite element program (MIDAS GTS/NX 2014 (V2.1)) based on elevation reading of the geological profile of the rock slope along the cross-sectional area of the quarry designated as V32 and V33 (Fig. 2.7). Five cases are modeled in each cross-section of the quarry for the progressive excavation levels from 2015 to 2019 for each of the two stress conditions. Excavation at the 400-m level was completed at the end of 2015, and resumed at the 360-m level in 2019. The basic configuration of the analytical models is the same as that discussed in section 3.2.2 using the mechanical properties presented in Table 3.1. However, the geometry of the blue dotted square in Fig. 3.4

changed as the excavation progressed. Fig. 3.7 shows an example of the analytical models of the quarry in 2015-2019 of V33. For the analysis of displacement induced by release of gravity, the simulation conditions including the boundary conditions are the same as with the conditions described in section 3.2.2. For analyzing displacement induced by the release of horizontal stress, a unit horizontal rock stress (σ_{xx}) of 1 MPa was applied to the right-hand side of the model. Mechanical properties for elastic analysis are shown in Table 3.1 whereas those shown in Table 3.3 were used for elasto-plastic analysis. In both analyses, the displacement increment due to excavation from 2014 was simulated using the excavation analysis function equipped in MIDAS GTS/NX 2014 (V2.1).

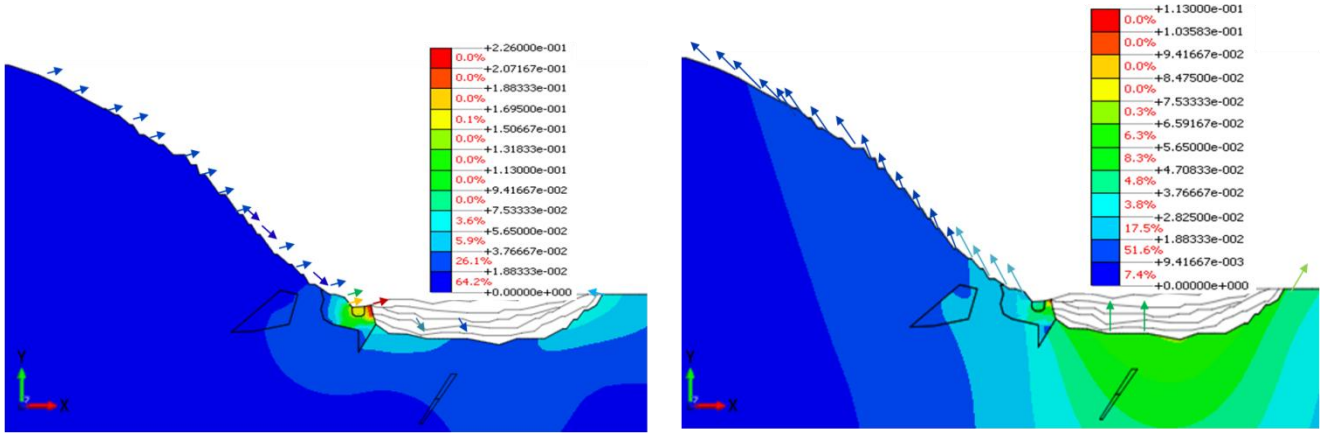

(a) Release of horizontal stress (b) Release of gravity

Fig. 3.8: Examples of total displacement vector at the surface of rock slope induced by excavation in 2019 at the blue dotted rectangle in Fig.3.4b**.** The arrows indicate the directions of the displacement whereas length of arrow is proportional to magnitude of the displacement.

3.3.2 Results of elastic analysis

Examples of contours of surface displacement induced by excavation were shown in Fig. 3.8. It can be seen in Fig. 3.8 (a), forward surface displacement of the cut rock slope was observed due to the release of horizontal stresses as a result of excavation of the rock mass. As expected, the displacement magnitude increased yearly when approaching the slope foot with the greatest displacement concentrated near the zone of clay-bearing rock. Significantly, the displacement of the rock slope and the stress at the toe of the slope is redistributed gradually as a result of the excavation of the rock mass. In contrast, the displacement vectors along the rock slope shown in Fig. 3.8b indicate upward and leftward movement of the rock mass, whereas the

vectors at the beam generator point show upward and rightward displacement due to the release of gravity when the rock floor of the pit was excavated.

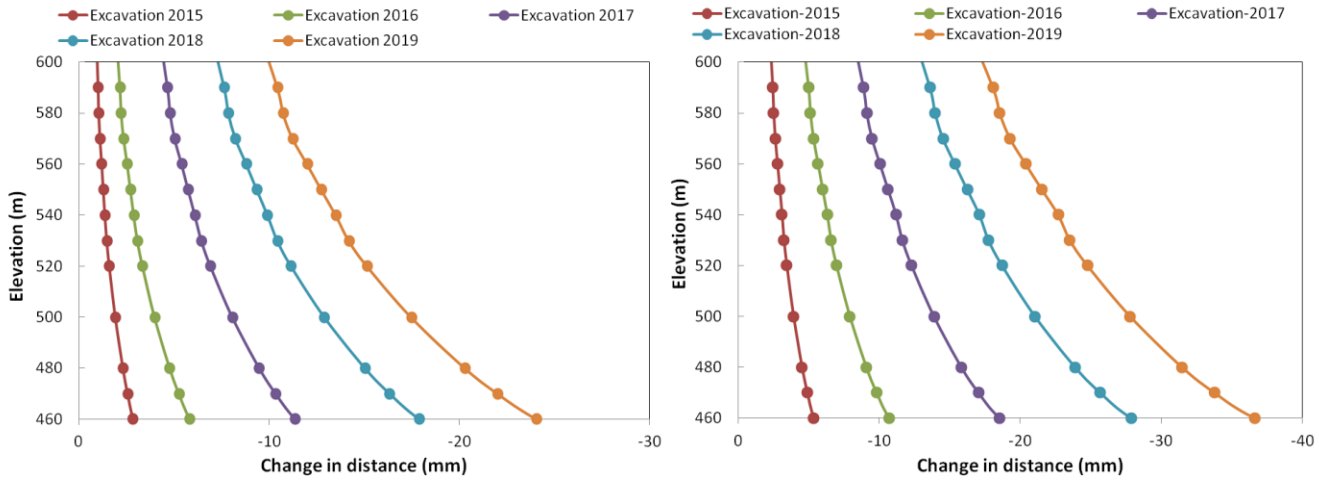

(a) V32 (b) V33

Fig. 3.9: Change in distance of the simulated results of displacement induced by release of horizontal stress, (a) V32 and (b) V33**.**

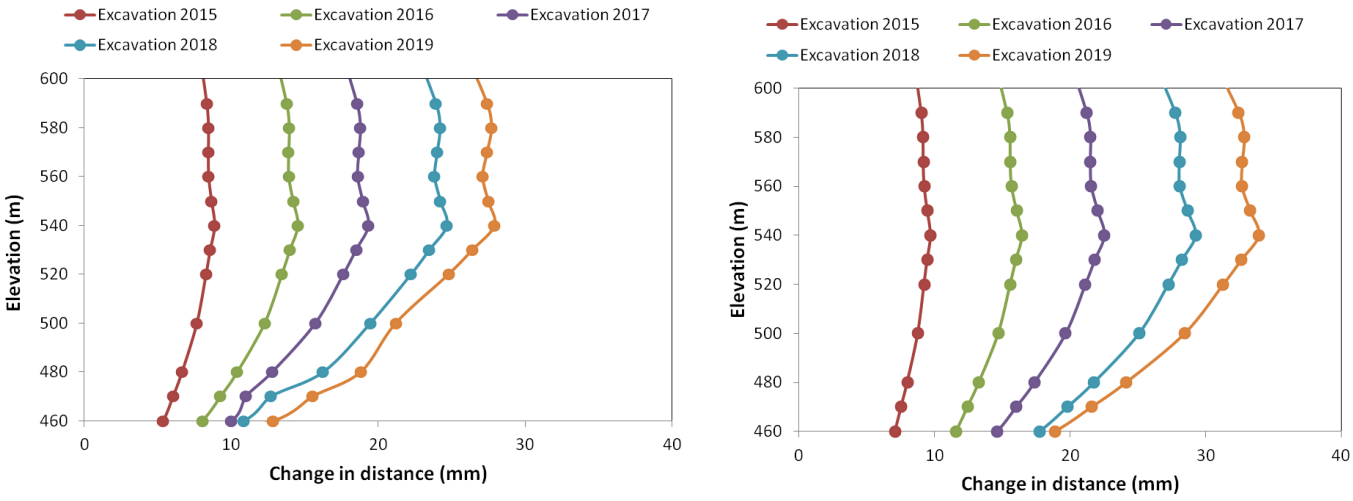

(a) V32 (b) V33

Fig.3.10: Change in distance of the simulated results of displacement induced by release of gravity, (a) V32 and (b) V33.

Fig. 3.9-10 shows the changes in distance calculated from the distribution of the surface displacement vectors along the slope and beam generator point plotted relative to elevation of the quarry between 460 and 590 m. It is clearly seen in Fig. 3.9 that the distance decreased with similar tendencies at both cross-sectional lines due to the release of horizontal stress as the rock

floor was excavated likely because of the forward displacement of the rock mass. The highest decreasing distance rate is also notably observed near the foot of the rock slope. Fig. 3.10 shows that the distance at elevation 590–460 m increased with progressive yearly excavation due to the leftward and rightward displacement of the rock mass along the slope and at the beam generator point. The maximum distance increase is observed near the foot of the rock slope, where the largest displacement magnitude is concentrated. From Fig.3.9-10, it can be said that the change in distance due to excavation of the pit floor depends on the rock stress conditions. The distance increases under gravity force conditions and decreases under horizontal stress conditions.

From the comparison between measured result (Fig.2.12c) and calculated results, it is observed that the change in distance under horizontal stress conditions has similar tendency of displacement with the measured results at the south-side of the quarry although their magnitude differs. Thus, excavation is expected to be one of the dominant causes of the slope displacement on the south-side of the quarry if the regional horizontal stress at the quarry is sufficiently high. For example, Obara et al. (2000) suggested that rock slope exhibits elastic extension by excavation, resulting in forward displacement of the rock slope at a horizontal stress to vertical stress ratio of 1.0. However, this ratio tends to increase with inverse depth and is therefore likely to be greater than 1.0 in open pit mines (Brown and Hoek, 1978).

Table 3.3: Mechanical properties of the rock materials.

Parameters	**Hard rock mass**	**Clay-bearing rock**
Material type	Isotropic	
Material model	Mohr–Coulomb	
Unit weight, γ (kN/m^3)	26.20[a]	18.00 [b]
Young's modulus, E (GPa)	4.01[c]	0.05[d]
Poisson's ratio, v	0.20[a]	0.30[b]
Cohesion, c (MPa)	30[e]	0.02[f]
Friction angle, ϕ (^{o})	40 and 50[e]	35[f]

[a]The unit weight adopted from Bell (2000)
[b]Adopted from Chai and Miura (1999).
[c]Estimated by GSI
[d]Calculated from laboratory test results
[e]Calculated from laboratory test results by Bandazi (2017)
[f]Adopted from Chai et al (2013)

3.3.3 Results of elsato-plastic analysis

To estimate a sufficient horizontal stress, elasto-plastic analysis was carried out, based on simulation condition of displacement by the effect of horizontal stress using model of cross sectional lines, V32 and V33. It is expected that the rock slope can be deformed by plastic behavior of clay resulting from stress state change due to excavation. Therefore, the clay-bearing rock was assumed to behave as an elasto-plastic material. The displacement increment due to excavation at footwall of the rock slope progressing from 2015 to 2019 as shown in Fig.3.7, were simulated using the mechanical properties presented in Table 3.3. From Fig.3.11, it can be seen that the distance decreases under horizontal stress condition. From the comparison between Fig. 3.9 and Fig.3.11, it is seen that the magnitude of displacement from elasto-plastic analysis is notably greater than that of elastic analysis. As can be seen from comparison of calculated result with measured results (see Fig.2.12c), the magnitude of displacement from elasto-plastic analysis is closer to that of measured results. Thus, this indicates that consideration of plastic deformation of clay-bearing rock is important assessing displacement due to excavation.

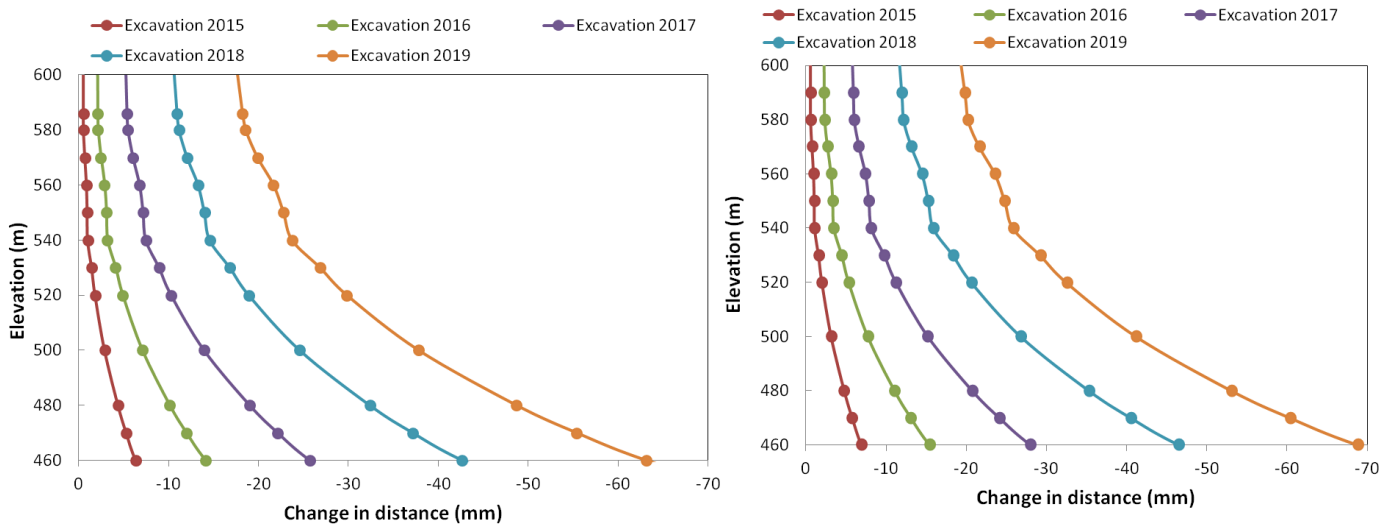

(a) V32 (b) V33

Fig.3.11: Calculated change in distance from surface displacement induced by excavation due to release of horizontal stress (a) and gravity (b) under elasto-plastic analysis.

3.4 Slope displacement induced by shear failure using shear strength reduction method

To understand rock slope displacement due to shear failure, shear strength reduction method (SSRM) was adopted. The shear strength reduction method (SSRM), where both the hard rock

mass and clay are assumed to behave as perfect elasto-plastic materials, was adopted to understand rock slope displacement caused by reduced shear strength after rainfall infiltration. The SSRM is one of the most popular techniques for performing FEM slope analysis (Dawson et al., 1999; Griffiths and Lane, 1999) mainly because it simulates progressive shear failure of the slope under complex geometric conditions (Matsu and San, 1992; Shen et al., 2012). The SSRM also determines a stress reduction factor or factor of safety value that brings a slope to the verge of its failure limit (Zienkiewicz et al., 1975; Farshidfar and Nayeri, 2015) according to:

$$C_F = \frac{C}{F} \tag{3.2}$$

$$\phi_F = tan^{-1}\left(\frac{\tan \phi}{F}\right) \tag{3.3}$$

where C and ϕ are the actual cohesion and frictional angle, respectively, C_F and ϕ_F are the reduced strength characteristics (cohesion and frictional angle) and F is a reduction factor that controls the reduction rate of C and ϕ. As noted by Dawson et al. (1999) and Griffiths and Lane (1999), C and ϕ gradually decrease until the final slope failure is detected.

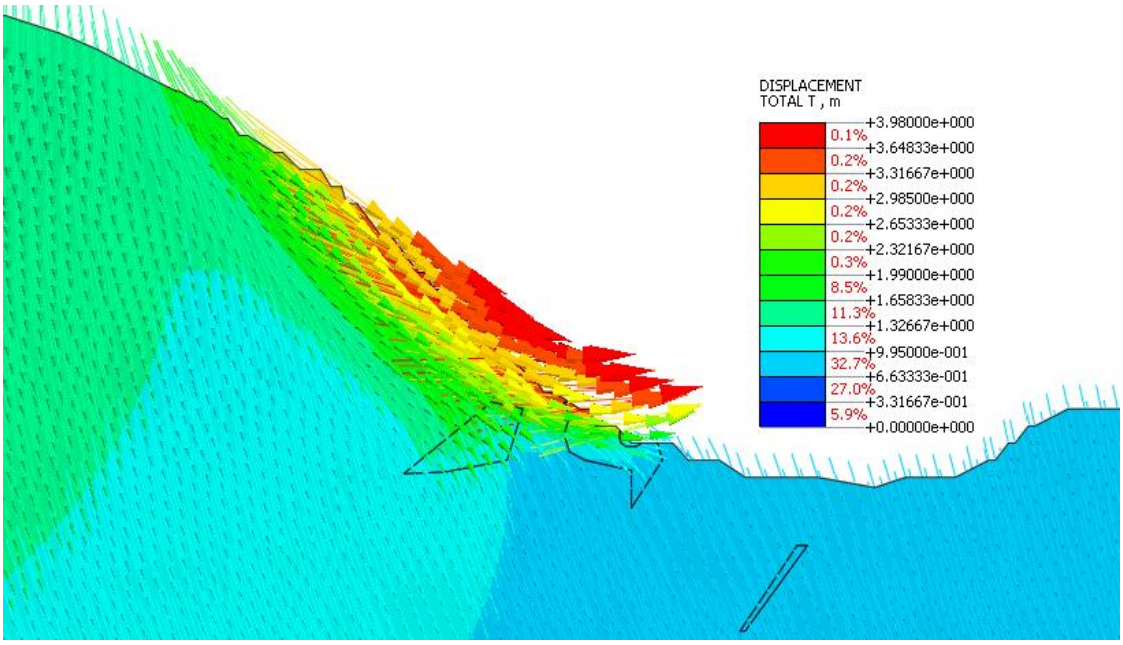

Fig.3.12: Displacement vector along the rock slope at ϕ = 40(°), with shear strain distribution in the blue dotted rectangle in Fig.3.6b.

3.4.1 Analytical method

The basic configuration of the models including the shape, size and boundary conditions was the same as described in section 3.2.2. However, in addition to the elastic modulus and unit weight, the cohesion and frictional angle were also included in the simulation. The values C and ϕ of the hard rock mass were estimated from standard uniaxial compression tests (Bandazi, 2017). In these laboratory tests, the friction angles of limestone and schalstein were approximated as 40° and 50°, respectively. The friction angle of hard rock was set to 40° and 50° for two analytical cases. The shear strength parameters of the weak rock were adopted from Chai et al. (2013), as presented in Table 3.3. In this simulation, increment of reduction factor ΔF and the maximum number of iteration are set to 0.01 and 50, respectively. The displacement increment induced by plastic deformation owing to sequential failure of elements was analyzed.

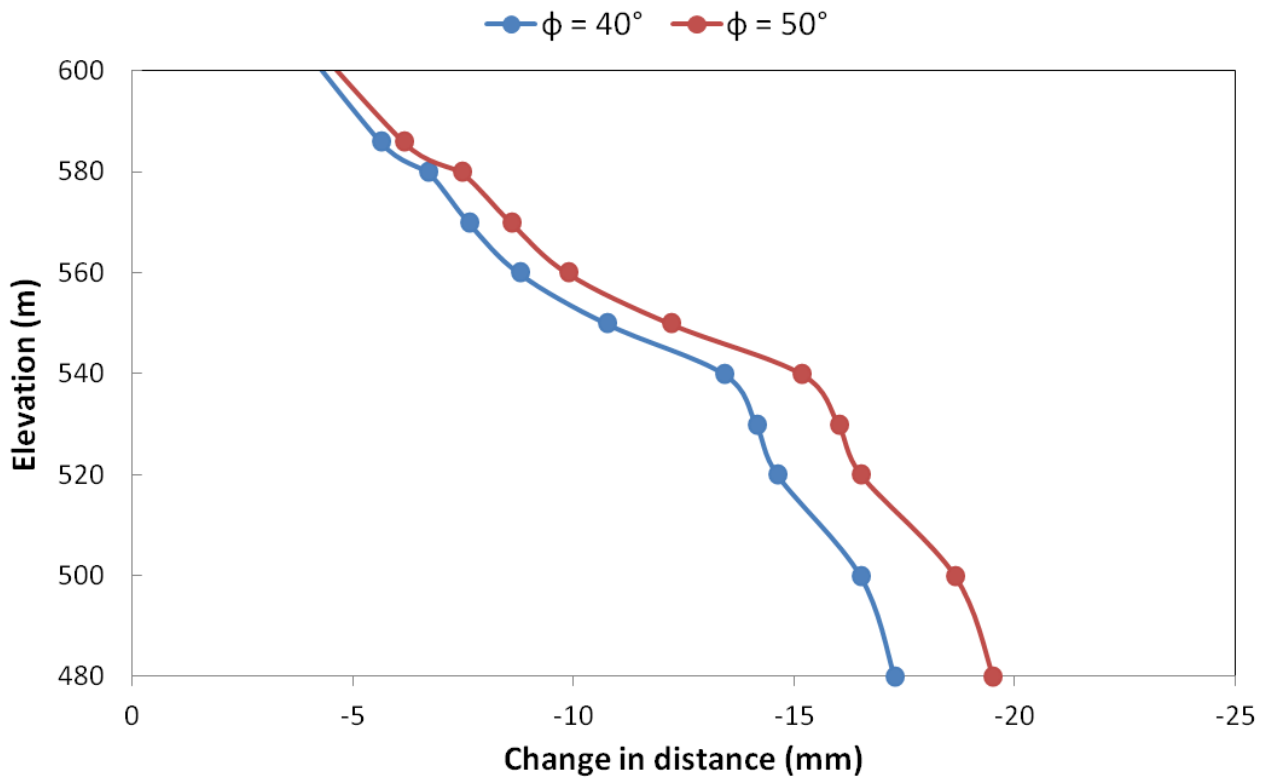

Fig.3.13: Change in distance calculated from SSR simulation results.

3.4.2 Analytical results and discussion

The surface displacement vector of the rock slope at ϕ = 40° is shown in Fig. 3.12 with the shear strain distribution. The change in distance calculated from the surface displacement vectors is plotted against the quarry elevation for comparison, as shown in Fig. 3.13. Fig. 3.12 shows that

the downslope movement of the rock mass occurred at the top of the rock slope. The slope clearly slid relatively downward from the top to the intense shear strain zone in the middle of the slope, resulting in massive forward displacement of the middle of the rock slope surface. The change in distance decreased as a result of the downslope movement along the slope and at the beam generator point. The maximum decreasing rate of the distance at the footwall of the rock slope for both friction angles were also observed. As the shear sliding progressed in the rock slope owing to reduced rock mass strength, the distance decreased with the greatest magnitude at the foot of the slope. Based on comparison of the measured result Fig.2.12c and Fig. 3.13, it can be seen that both results have a similar tendency but different magnitude of displacement. This suggests that the rock slope displacement at south- side occurred not mainly as a result of lowered shear strength of rock mass. Thus, it is expected that the rock slope has low risk of shear failure.

3.5 Concluding remarks

From the numerical simulations, the following characteristics of slope displacement were estimated:

i. The change in distance calculated from the distribution of the surface displacement vectors along the slope and beam generator point decrease due to deterioration of clay-bearing rock, and the maximum decrease are seen at the middle of the slope. The change in distance owing to excavation of the pit floor depends on the rock stress conditions. The distance increases under gravity force conditions and decreases under horizontal stress conditions and shear sliding of rock slope. The magnitude of the decrease in distance is observed to be greatest at the foot of the slope.

ii. According to the characteristics of the measured and calculated results, the rock slope displacement at the Higashi-shikagoe limestone quarry is conclude to be mainly caused by excavation at the floor wall if the horizontal stress is sufficiently large. However, consideration of plastic deformation due to excavation is also important in assessing stability of rock slope at the quarry.

4 Estimation of regional stress state and Young's modulus of ground by 3-D back analysis

4.1 Introduction

As discussed in chapter 3 that excavation at the floor wall of the quarry is the main cause of rock slope deformation observed at Higashi-shikagoe quarry if the horizontal stress is sufficiently large. It is well known that information on the stress field in rock mass around excavation is of fundamental importance for ensuring the stability of mining and civil engineering projects. In open-pit mines, changes in the stress state of rock mass arising from mining activities have been extensively investigated by some researchers (Kaiser et al., 1990; Kaneko et al., 1997; Obara et al., 2000; Nara et al., 2011; Kodama et al., 2013). In these studies, excavation-induced stress changes of homogeneous rock slope were estimated considering surface geometry and tectonic stress. However, Nakamura et al. (2003) presented measurement of rock slope deformation due to excavation in a pit-type limestone mine using multi-stage extensometers and proposed that elastic deformation of rock slope formed in the pit-type quarry can be affected by geological structure and/or mechanical properties of rock types. This suggests excavation-induced stress changes of heterogeneous rock slope are also essential. However, excavation-induced stress changes of heterogeneous rock slope encompassed by clay-bearing rock have not been clarified yet, although layer of clay-bearing rock is often observed at limestone quarries.

In this chapter, excavation-induced deformation of the rock slope intersected by layer by clay-bearing rock, 70-m- thick at the footwall of the rock slope was estimated by 3-D back analysis. At first, effect of model sizes on deformation of the rock slope was investigated to find a model with adequate size. In Finite element method, displacements on surrounding boundary of model are usually fixed. Therefore, model with extensive area is better because it has less affects of boundary conditions. However, numbers of node and elements increases with the model size. These causes increase in computation time and computer with large memory size is also required. Thus, it is important to simplify the model for adequate memory size and shorter computation time. Thereafter, a stress state of the quarry and the elastic moduli of a rock mass around mining area of Higashi-shikagoe limestone quarry were estimated by varying Poisson's ratio of the ground to ensure the long-term stability of the rock slope. This is because the behavior of relative displacement depends on the magnitude of Poisson's ratio (Kodama et al.,

2009). Furthermore, effect of the ratio of the existing layer of the clay-bearing rock on excavation-induced stress changes of rock slope was also investigated. Then, stability of the rock slope is assessed by comparing calculated results to measured results.

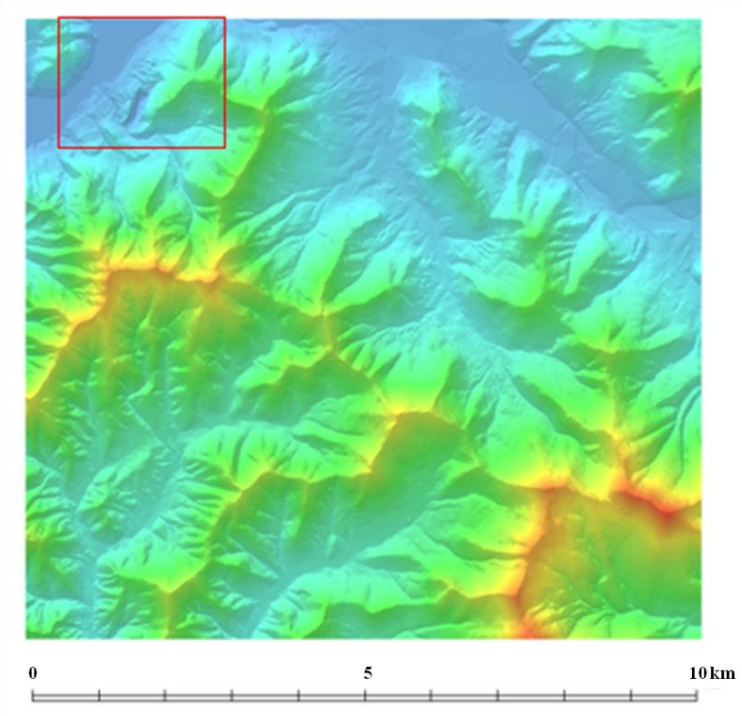

Fig. 4.1: Base map from the Geospatial Information Authority of Japan. The red frame indicates the studied area (the Higashi-shikagoe limestone quarry).

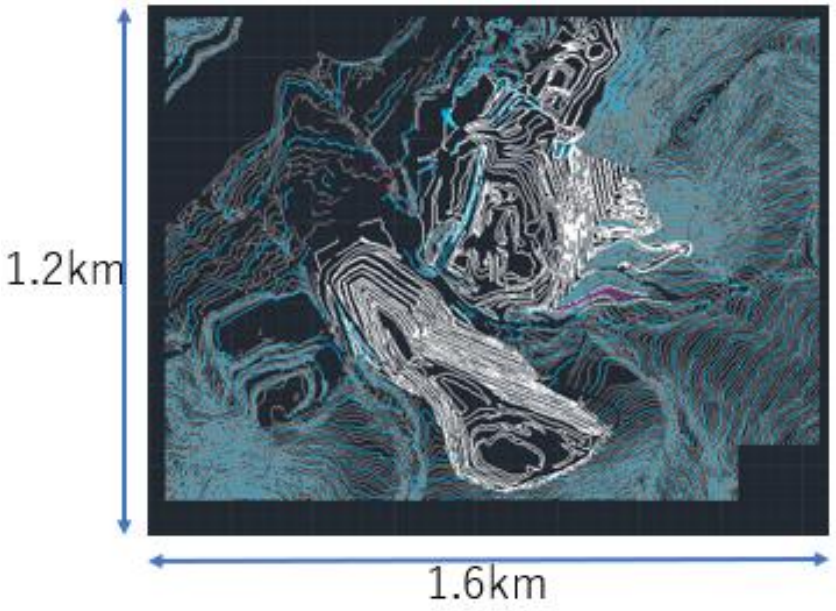

Fig.4.2: Elevations read from the regional contour map of the quarry.

4.2 Theoretical concept of back analysis

Back-analysis has become an integral part of the observational method commonly used in rock engineering. It has been applied to identify in-situ stress field (Kaiser, 1990), estimation of rock mass deformation modulus and strength parameters (Kodama et al., 2013), tunneling (Okuda et al., 1999; Sakurai et al., 2001), rock mass hydraulic properties (Cai et al., 2007), rock mass zoning, boundary conditions, loads acting on the tunnel linings, etc through numerical methods. In back analysis, a set of input parameters such as geological structure, mechanical parameters and in-situ stress that lead to outputs such as displacement and stress is determined by performing numerical simulation as model calibration using either least square or mathematical programming techniques of error minimization with observed data (Cai et al., 2007). Contrary to forward analysis, which has unique solution and determines the output such as displacement and stress from inputs such as geological structure, mechanical parameters and in-situ stress, back analysis cannot guarantee the uniqueness of the solution (Sakurai et al. 2003). Using back analysis, evaluation of several parameters, such as the mechanical parameters and the in-situ stress field, is achievable simultaneously. Thus, it is likely that back analysis would provide a more accurate estimation of displacement and rock stress in mining engineering (Kodama et al., 2013) on a large scale.

In open pit mine, the rock stress around the mine is often estimated by analyzing the mining-induced deformation arising from the stress state due to gravity and the given regional strains (Kodama et al., 2013). The mining-induced deformation occurs as a result of changes in the surface geometry arising from mining activity in an open pit mine. Thus, the effects of change in both the geometry and regional strain state by mining on the elastic deformation were investigated. The Young's modulus and regional strain of rock can be estimated based on Eq. (4.1) directly depend on varying Poisson's ratio. The relative displacements at position **x** induced by mining under a constant regional strain, **u** (**x**) is given by the following linear equation (Kodama et al., 2013):

$$\mathbf{u}(\mathbf{x}) = \mathbf{u}^0(\mathbf{x}, \rho g, E^G) + \mathbf{u}^X(\mathbf{x}, \varepsilon_{xx}{}^G) + \mathbf{u}^Y(\mathbf{x}, \varepsilon_{yy}{}^G) + \mathbf{u}^{XY}(\mathbf{x}, \gamma_{xy}{}^G) \quad (4.1)$$

Where $\mathbf{u}^0(\mathbf{x}, \rho g, E^G)$ is the displacement due to release of gravity by mining, ρg and E^G are the unit weight and Young's modulus of the ground, respectively. $\mathbf{u}^X(\mathbf{x}, \boldsymbol{\varepsilon}_{xx}{}^G)$, $\mathbf{u}^Y(\mathbf{x}, \boldsymbol{\varepsilon}_{yy}{}^G)$ and $\mathbf{u}^{XY}$

($\mathbf{x}$, $\boldsymbol{\gamma}_{xy}^{G}$) are the mining-induced displacement under the given normal strains ε_{xx}^{G}, ε_{yy}^{G} and shear strains γ_{xy}^{G}, respectively.

To estimate the Young's modulus and regional strain of ground by back analysis, the total displacement $\mathbf{u}(\mathbf{x})$ given by Eq. (4.1) using a unit Young's modulus, E^0 and unit regional strain (normal strain ε_{xx}^{0}, ε_{yy}^{0} and shear strain γ_{xy}^{0}) of the ground can be expressed by the following equation with the detail explained in Kodama et al., 2013:

$$\mathbf{u}(\mathbf{x}) = \boldsymbol{c}_E \mathbf{u}^0(\mathbf{x}, \rho g, E^0) + \boldsymbol{c}_X \mathbf{u}^X(\mathbf{x}, \varepsilon_{xx}^{0}) + \boldsymbol{c}_Y \mathbf{u}^Y(\mathbf{x}, \varepsilon_{yy}^{0}) + \boldsymbol{c}_{XY} \mathbf{u}^{XY}(\mathbf{x}, \gamma_{xy}^{0}) \quad (4.2)$$

where $c_E = E^0/E^G$, $\boldsymbol{c}_X = \varepsilon_{xx}^{G}/\varepsilon_{xx}^{0}$, $\boldsymbol{c}_Y = \varepsilon_{yy}^{G}/\varepsilon_{yy}^{0}$, $\boldsymbol{c}_{XY} = \gamma_{xy}^{G}/\gamma_{xy}^{0}$. The Eq. (4.2) is a linear equation with four unknown parameters $\boldsymbol{c}_E$, $\boldsymbol{c}_X$, $\boldsymbol{c}_Y$, $\boldsymbol{c}_{XY}$, which can be determined from displacement results in horizontal plane estimated by numerical analysis using the given values of Young's modulus E^0, normal strains ε_{xx}^{0}, ε_{yy}^{0} and shear strains γ_{xy}^{0}, respectively. Thereafter, the regional stress state can be calculated from the specified regional strain state using the following Hooke's law:

$$\begin{aligned} \boldsymbol{\sigma}_{xx}^{G} &= \boldsymbol{c}_1[(1-\nu)\,\boldsymbol{\varepsilon}_{xx}^{G} + \nu\boldsymbol{\varepsilon}_{yy}^{G}] \\ \boldsymbol{\sigma}_{yy}^{G} &= c_1[\nu\,\boldsymbol{\varepsilon}_{xx}^{G} + (1-\nu)\,\boldsymbol{\varepsilon}_{yy}^{G}] \\ \boldsymbol{\sigma}_{xy}^{G} &= c_2\boldsymbol{\gamma}_{xy}^{G} \end{aligned} \quad (4.3)$$

where $\boldsymbol{c}_1 = E^G/(1+\nu)(1-2\nu)$, $\boldsymbol{c}_2 = E^G/2(1+\nu)$, ν is the given Poisson's ratio.

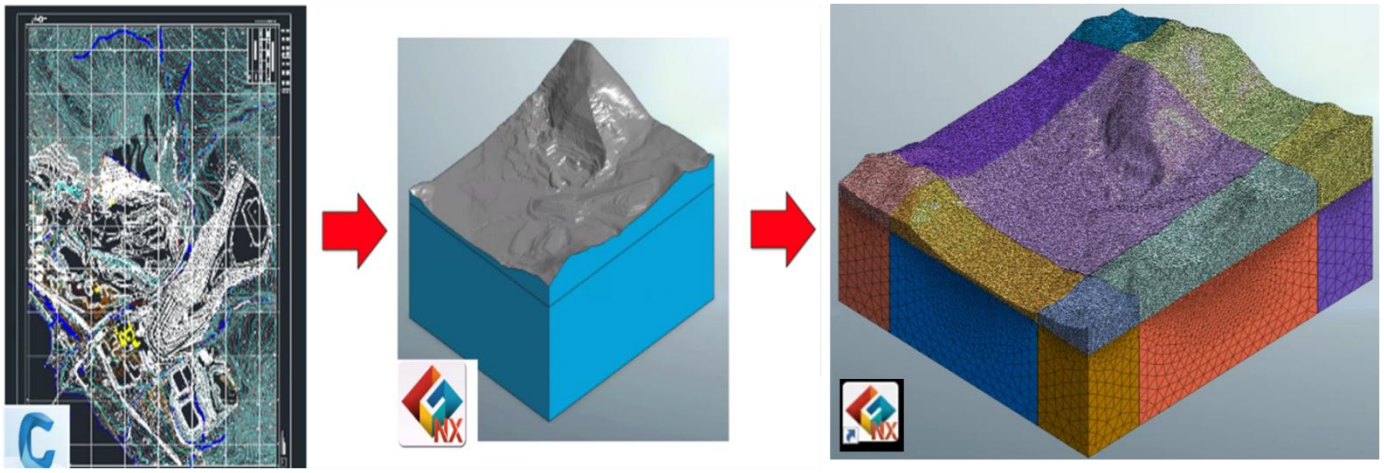

Fig.4.3: Procedures for creating 3D model.

4.3 Effects of model size and Poisson's ratio

In this section, effect of model size on elastic deformation of the rock slope induced by excavation is predicted. In FEM, large model including a vast surrounding area to excavation area is often more reliable as the effect of boundary conditions are significant smaller on the targeted area (Kodama et al., 2009). However, such large model required long computation time. A vast computer memory is also needed when the excavated area is extensive. Thus, it was necessary to simplify the model to bring it within the limits of the available memory size and shorter computation time. Thereafter, regional stresses and elastic modulus of the ground were estimated using the appropriate model size by back analysis based on varying Poisson's ratio of ground.

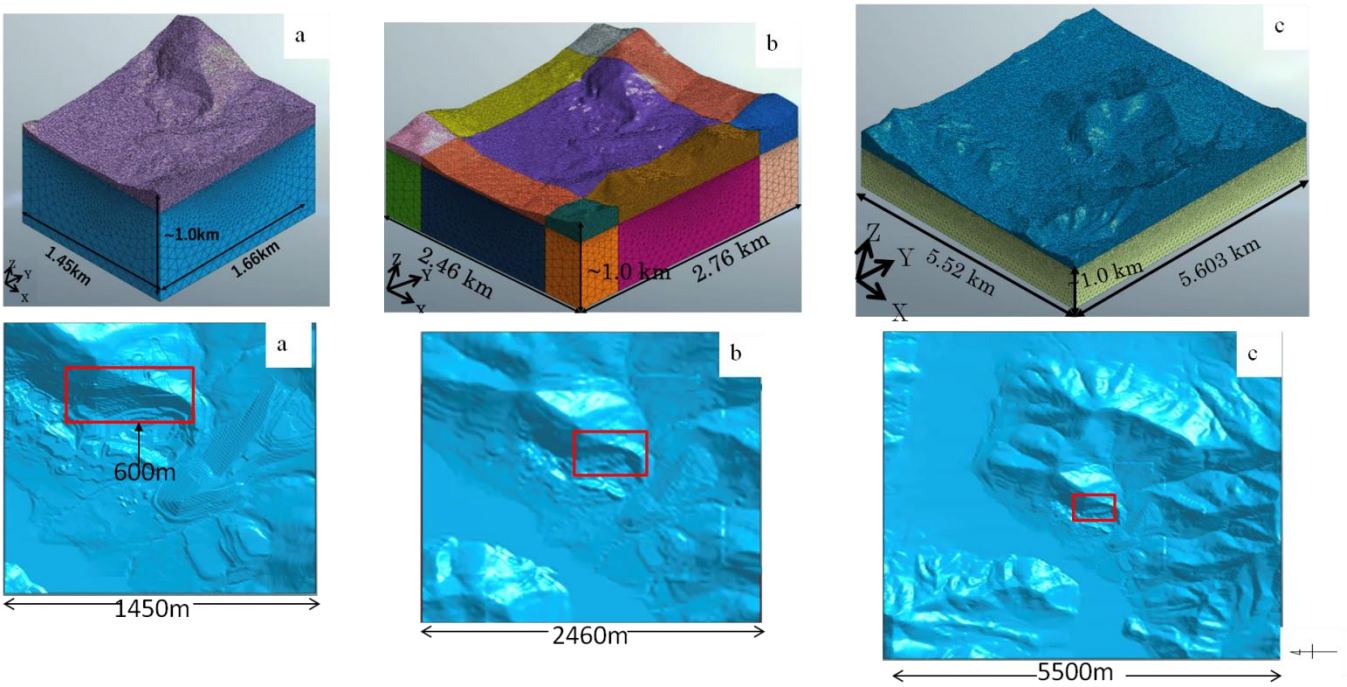

Fig. 4.4: The 3-D FEM model of the Higashi-shikagoe limestone quarry with different dimension designated as (a) small model, (b) medium model and (c) larger model. The red frame indicates the excavation area of 600m length.

4.3.1 Analytical method

Base map from the Geospatial Information Authority of Japan and mine elevation data measured from May 2014 to July 2021 were used as the elevation data to express the surface geometry of the analysis target area. As shown in Fig.4.1, the red frame indicates the area containing base map information of the Higashi-shikagoe quarry in the bird's-eye view of the

Geospatial Information Authority of Japan. Then, the quarry elevation data (Fig. 4.2) provided by the mining company were synthesized using commercial CAD software. Thereafter, 3D meshes of the quarry for the eight years from 2014 to 2021 were generated using commercial software, MIDAS GTS/NX 2014 (V2.1) as show in Fig.4.3.

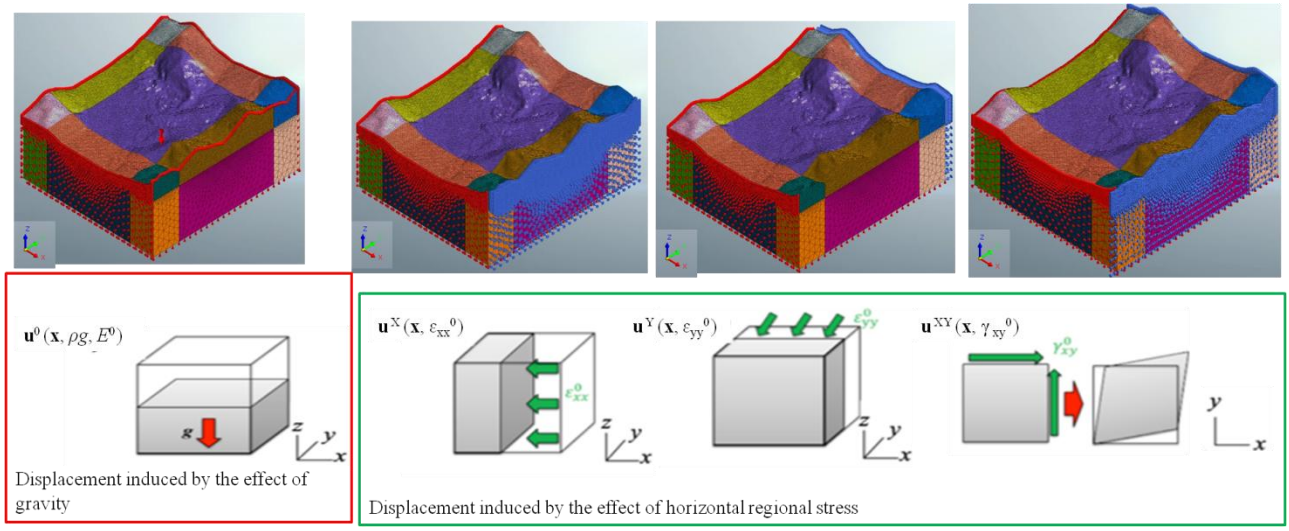

Fig.4.5: 3D-FEM model boundary condition used for mining-induced displacement analysis.

Fig.4.4 shows the entire 3-D models of 2014 used for the numerical simulation. Three models of different dimensions were built to understand effects of model sizes and boundary conditions. The dimensions of the model were approximately 1.45 km and 1.66 km, 2.46 km and 2.76 km, 5.52 km and 5.60 km in the x-, and y-directions with depth of about 1.0 km for small, medium and larger model, respectively. The mining area is approximately 0.6km length, which is 2.0, 4.0 and 9.0 times lesser than the length of small, medium and larger model, respectively as indicates in Fig. 4.4. To model the change in surface geometry by mining better, the mesh size within the mining areas was set to 10 m, which is equal to one bench height. The directions of the x- and y-axes of the model were aligned to due south and east of the quarry, respectively, and z-axis was parallel to the vertical direction. The total number of nodes and elements in the model for 2014 are presented in Table 4.1.

Table 4.1: Number of elements and nodes of model for 2014.

Mesh size	Dimension (km)	Node	Element
Small model	1.45 x 1.66	571, 290	1, 225, 820
Medium model	2.46 x 2.76	1, 242, 050	7, 085, 126
Larger model	5.52 x 5.60	871, 290	4, 855, 820

The ground of the model was assumed to be homogeneous, isotropic, and elastic. This implies that the mechanical behavior of the rock mass affected by change in surface geometry by mining and the geological structure was approximated by the behavior of an equivalent elastic body. As shown in Fig.4.5, the nodal displacement of each model was calculated independently by applying the gravitational force and each forced displacement corresponding to each regional strains. Based on Eq. (4.1), displacement induced by the effect of gravity, $\mathbf{u}^0(\mathbf{x}, \rho g, E^0)$ is evaluated by applying the unit weight of the ground while displacements on the side surfaces and the basal surface of the model are fixed to zero. Subsequently, displacement induced by the effect of horizontal regional stress, $\mathbf{u}^X(\mathbf{x}, \boldsymbol{\varepsilon}_{xx}^0)$, $\mathbf{u}^Y(\mathbf{x}, \boldsymbol{\varepsilon}_{yy}^0)$ and $\mathbf{u}^{XY}(\mathbf{x}, \boldsymbol{\gamma}_{xy}^0)$ are evaluated applying horizontal displacement of the side surfaces, which is equal to the given regional strains, ε_{xx}^0, ε_{yy}^0 and γ_{xy}^0. The nodal displacements on the basal surface and the side surface of X and Y-planes were fixed to zero. The mechanical properties presented in Table 4.2, as adopted from Obara et al (2000) are used. Thereafter, the relative displacements, $\mathbf{u}^0(\mathbf{X}, \rho g, E^0)$, $\mathbf{u}^X(\mathbf{X}, \varepsilon_{xx}^0)$, $\mathbf{u}^Y(\mathbf{X}, \varepsilon_{yy}^0)$ and $\mathbf{u}^{XY}(\mathbf{X}, \gamma_{xy}^0)$ at each elevation to beam generator point induced by mining were calculated.

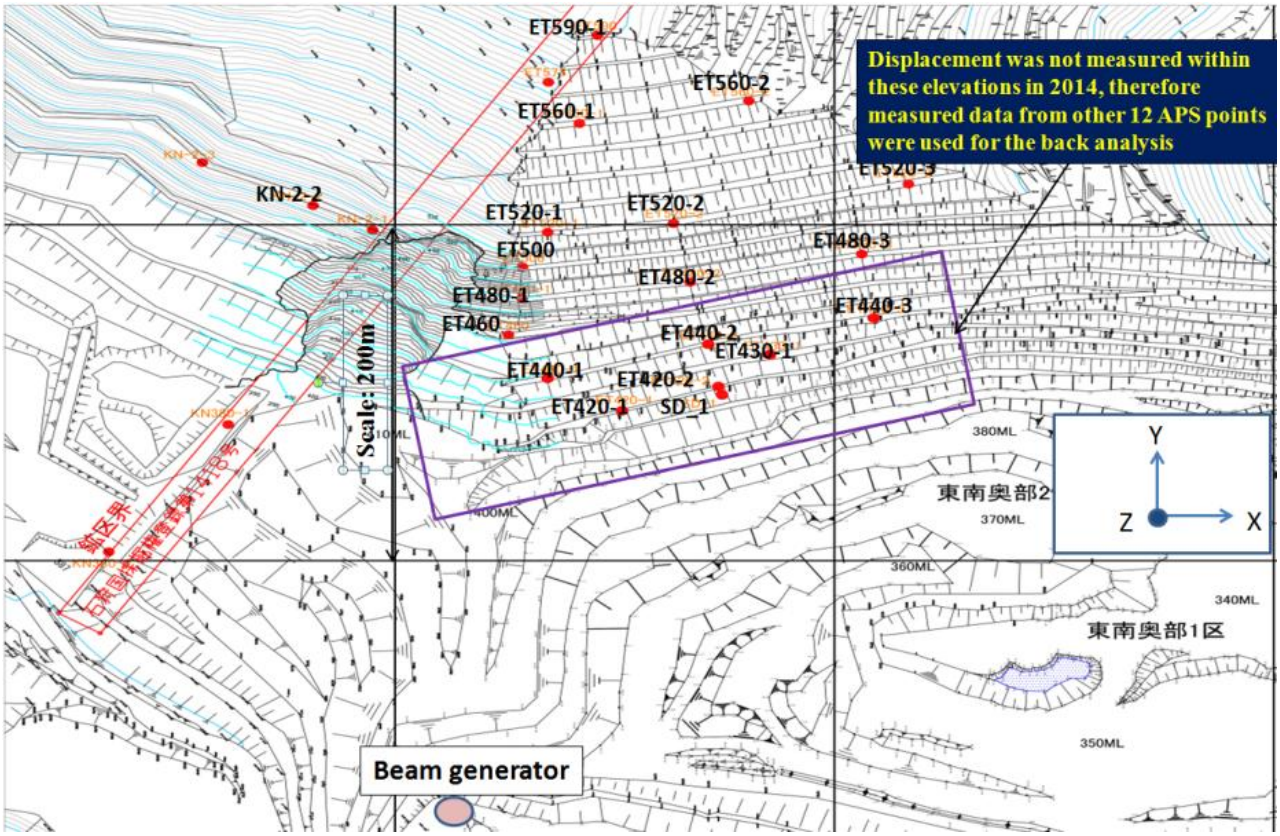

Fig.4.6: Layout of APS mirrors used for back analysis on mining area.

Table 4.2: Mechanical properties of the ground material.

Parameters	Ground
Unit weight, γ (kN/m^3) [a]	26.2
Poisson's ratio, v[b]	0.10, 0.20 and 0.30

[a]The Obara et al. (2000), [b]Assumed

Table 4.3: Unknown constant and regional stress values.

Mesh size	c_E	c_X	c_Y	c_{XY}	σ_{xx}	σ_{yy}	τ_{xy}
Small model	1.955	-0.018	1.930	0.380	-0.206	-2.013	-0.345
Medium model	0.219	0.431	2.122	-0.370	-0.682	-2.219	-0.336
Larger model	0.220	0.310	1.810	-0.670	-0.530	-1.890	-0.609

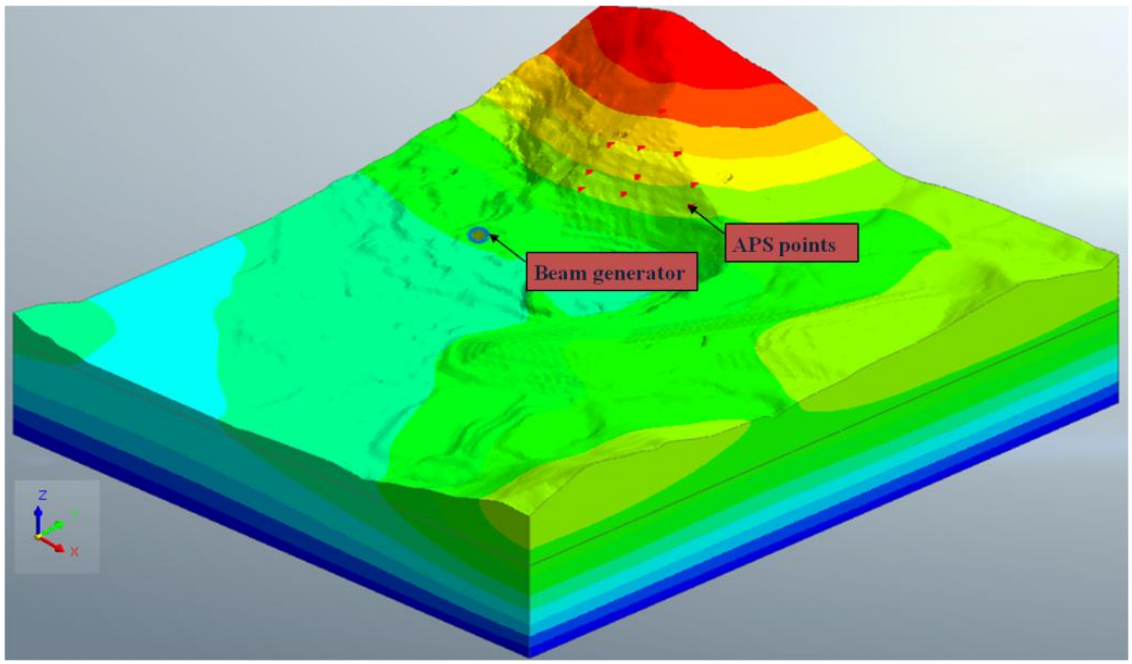

Fig. 4.7: Layout of APS mirrors used for back analysis on 3-D model. Relative displacement of each mirror point to beam generator point was calculated.

4.3.2 Analytical results and discussion

To account for deformation induced by mining, the relative displacements of both measured and calculated in the horizontal plane between each of the 12 APS mirrors (see Fig.4.6 and Fig. 4.7) on the slope surface at different elevations and beam generator point as described in section 2.3.2 were used for back analysis. The relative displacement between 2014 and 2017 of both

measured and calculated results were used to estimate the four unknown parameters: c_E, c_X, c_Y, c_{XY} of Eq. (4.2). The regional strain state and Young's modulus of rock were then estimated by back analysis using Eq. (4.2). The magnitude and direction of the principal regional stress states of the different models estimated by Eq. (4.3) are shown in Fig. 4.8. The estimated unknown parameters and values of regional stresses are presented in Table 4.3. It is noted that all models have similar compressive stress state. The magnitude of maximum principal stress is -2.10 MPa, -2.09 MPa and -2.12 MPa at the maximum principal direction of N11°E, N22°W and N21°W for the small, medium and larger model, respectively. The estimated Young's modulus of the ground for seven year is shown in Fig.4.9. The Young's modulus range of -0.8-0.5 GPa, 3.5-4.57 GPa, and 2.5-6.0 GPa are estimated under small, medium and larger model, respectively.

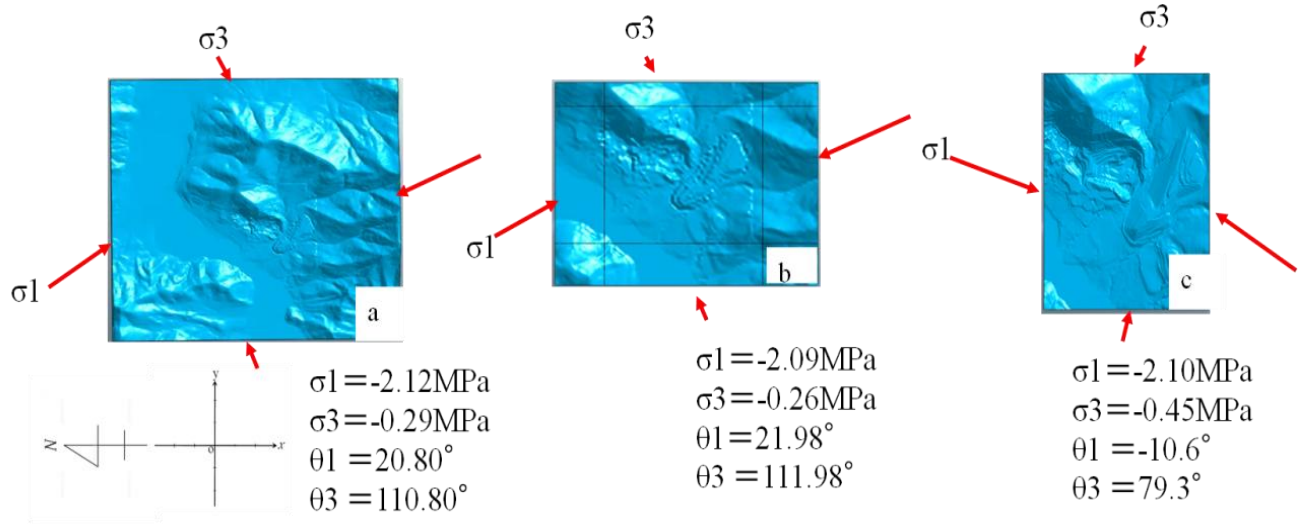

Fig. 4.8: The magnitude and the direction of the estimated principal regional stress. In Fig. 4.8, Rectangle in the figure depicts the model used. (a) Large model with a dimension of nine (9) times larger than that of the mining area, (b) medium model with a dimension of four (4) times larger than that of the mining area, and (c) small model with a dimension of two (2) times larger than that of the mining area.

For more clarification, the estimated unknown parameters (see Table 4.3) were used to calculated displacement in the horizontal plane. The calculated displacements were compared with the measured results as shown in Fig. 4.10. From Fig. 4.10, it can be seen that the measured results agreed with the calculated results with error of 15.56, 9.86, and 10.39 for small, medium and large model, respectively.

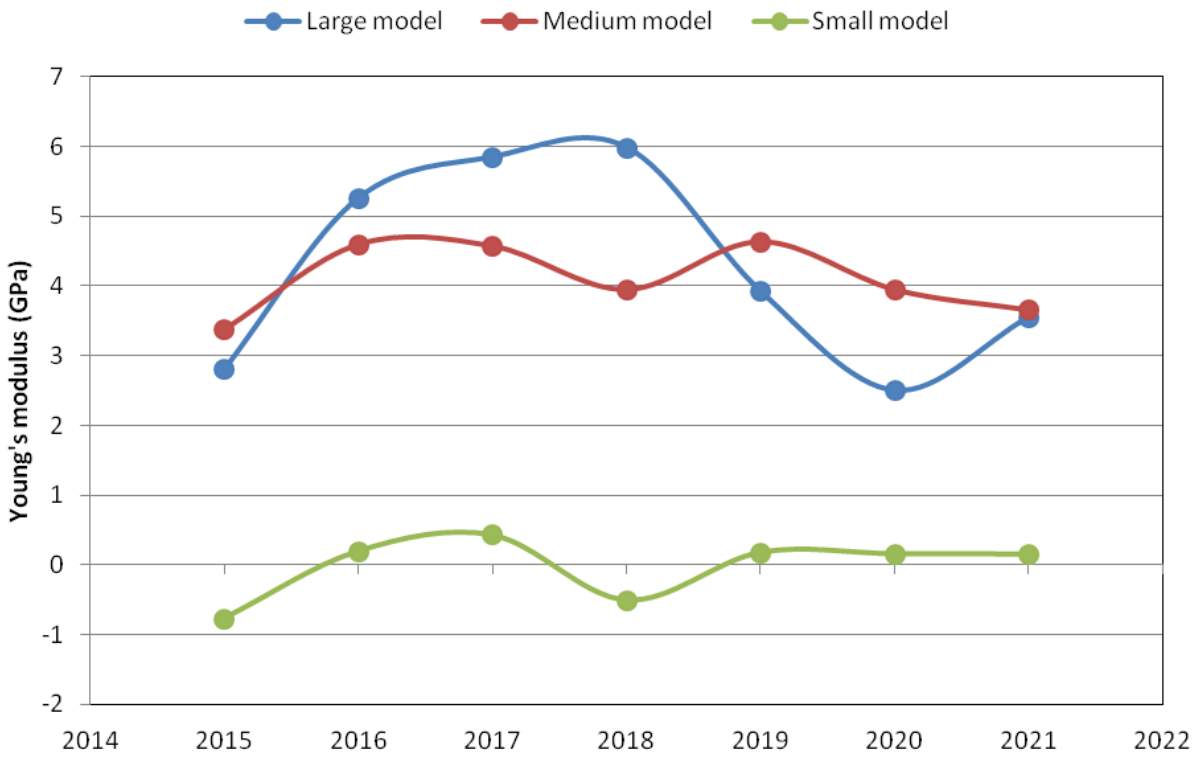

Fig.4.9: The estimated Young's modulus at Poisson's ratio, 0.2.

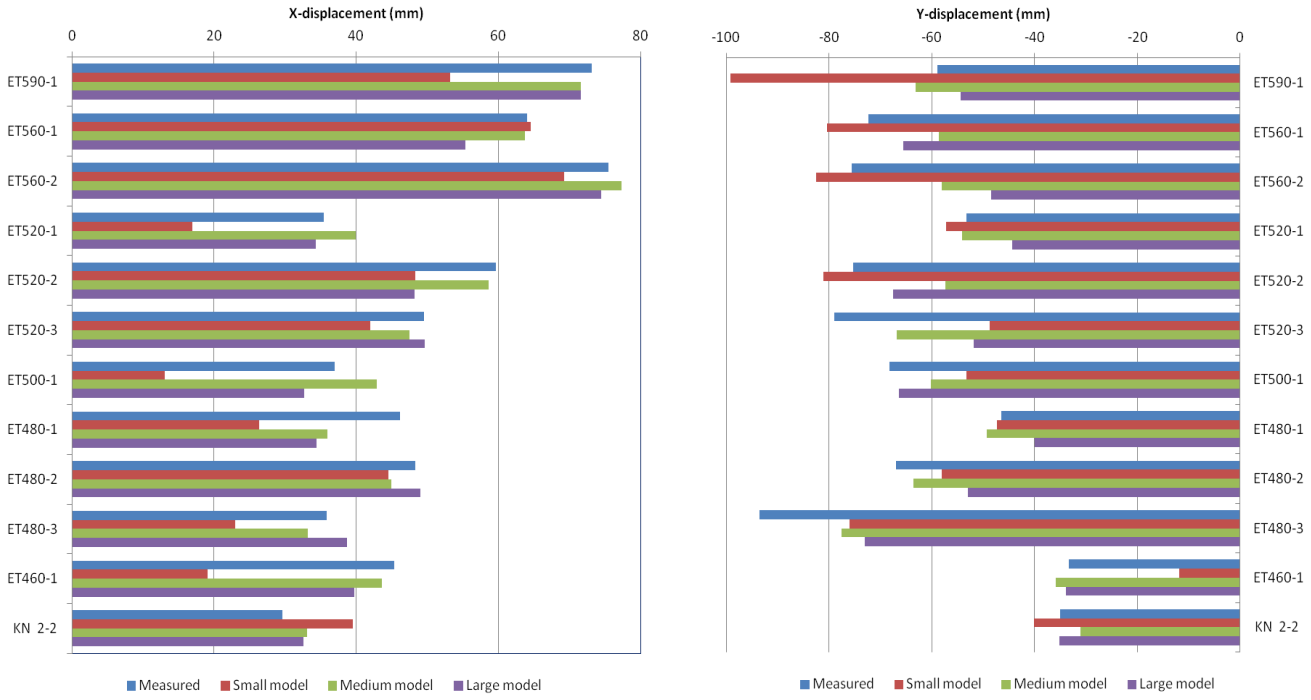

Fig. 4.10: The relationship between measured and calculated displacement of different models at Poisson's ratio, v=0.2.

It can also be observed that the calculated displacements with the small model deviated considerably from the measured displacement, mainly because effect of change in the surface geometry due to mining and boundary condition is larger on the small model. Conversely, the magnitudes of the calculated displacement with medium model are closer to that of large model. It also indicates that estimated error from the calculated displacement with medium model is almost equal to that from large model. Thus, it can be concluded that the medium model with a dimension of four times larger than that of the mining area is large enough for simulation. Not only that it has lesser effect of boundary condition, but also it may require lesser computation time and computer memory than the large model with extensive excavated area.

Subsequently, the medium model was used to identify an appropriate Poisson's ratio of the ground by varying the Poisson's ratio from 0.1 till 0.3 since all terms in Eq. (4.1) depends on Poisson's ratio. Fig. 4.11 shows estimated Young's modulus at different Poisson's ratio by back analysis. It can be noted that the Young's modulus increases in order of Poisson's ratio of 0.2, 0.1, and 0.3 with maximum value of approximately 4.7 GPa at Poisson's ratio, v = 0.2 in 2019.

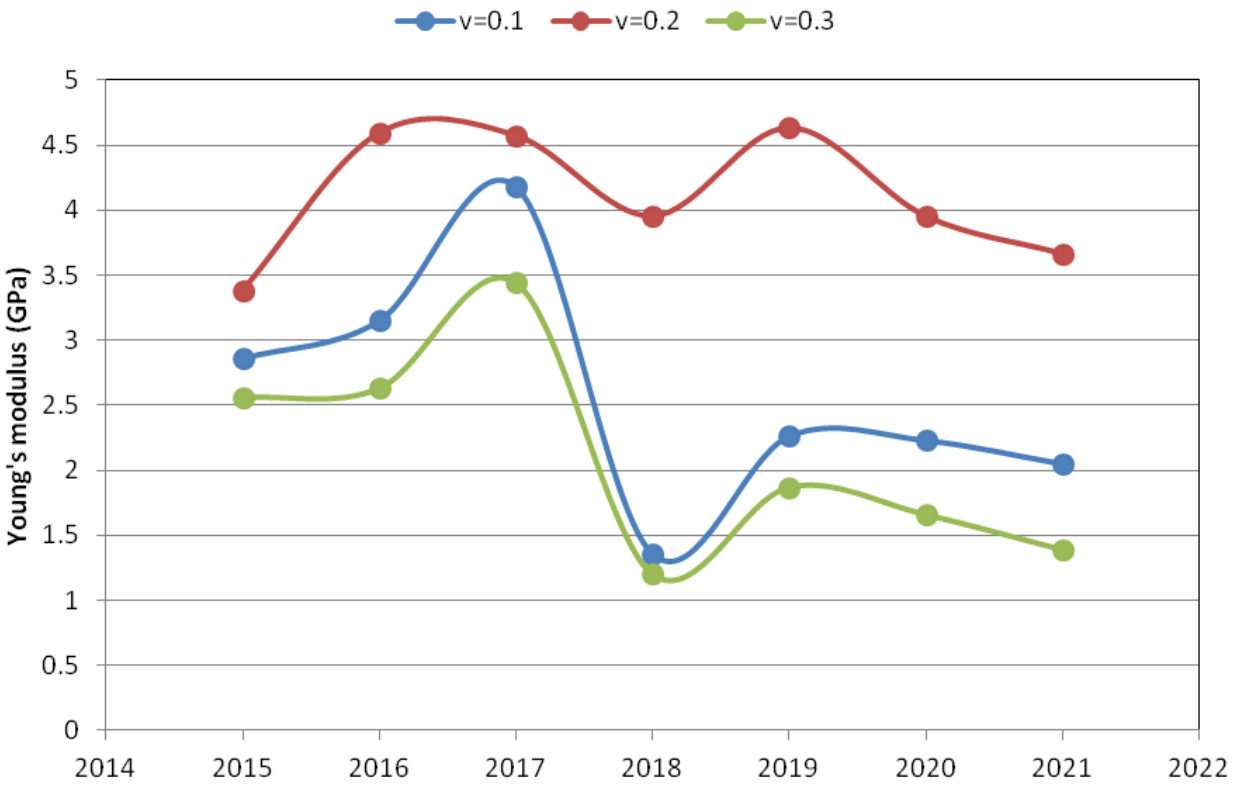

Fig.4.11: The estimated Young's modulus at different Poisson's ratio.

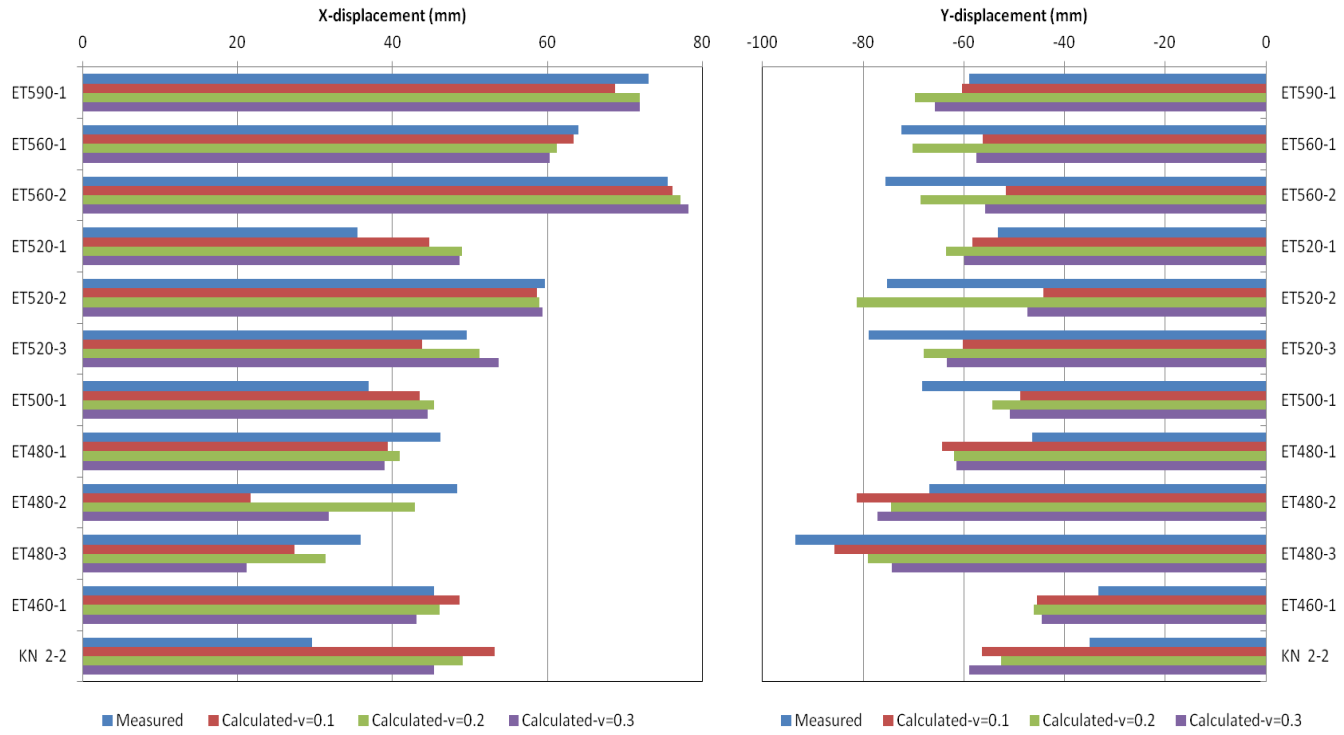

Fig. 4.12: The relationship between measured and calculated displacement with medium model at varying Poisson's ratio.

The estimated unknown parameters based on Eq. (4.2) were also used to calculated displacement in the horizontal plane with medium model at varying Poisson's ratio of 0.1, 0.2 and 0.3 as shown in Fig. 4.12. The result shows that the calculated displacement of all the Poisson's ratio have similar trend with the measured displacements. In addition, the estimated errors are of order: 14.90, 9.86 and 13.68 for Poisson's ratio of 0.1, 0.2, and 0.3, respectively. The estimated errors indicated that calculated displacement at Poisson's ratio of 0.2 is closest to the measured displacement. Then, the displacements vector at Poisson's ratio, v = 0.2 were compared with that of measured displacement as shown in Fig.4.13. As can be seen in Fig.4.13, the vector indicates that both the measured and calculated displacements trend forward toward the southern part of the quarry. It can be concluded that the values for Poisson's ratio of 0.2 and Young's modulus range of 3.5 -4.57 GPa estimated with medium model are reasonable. The estimated Young's modulus of rock mass by back analysis is close to that of Young's modulus by GSI of 4.01 GPa (see Table 2.2). The estimated Young's modulus also fall within the range of estimated Young's modulus of ground in Torigatayama limestone mine (Kodama et al., 2013).

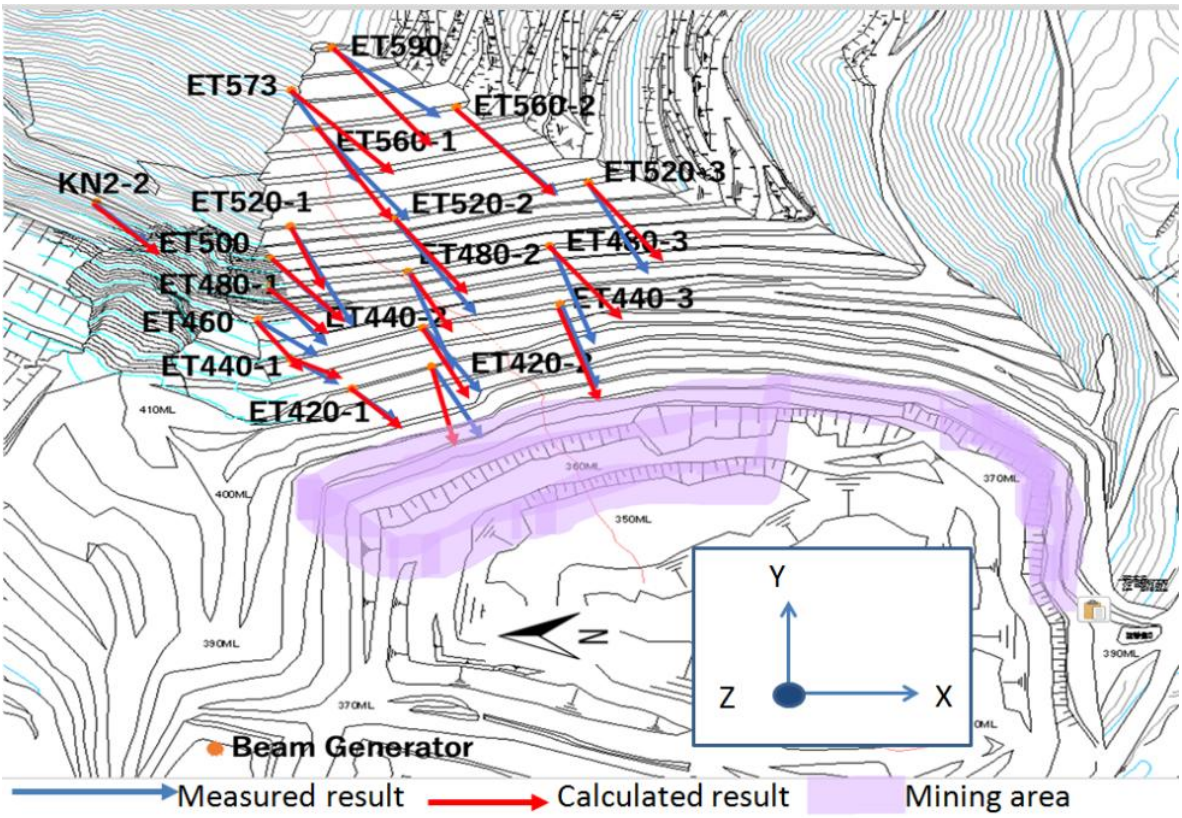

Fig.4.13: Displacement vector of the measured and calculated results in the horizontal plane.

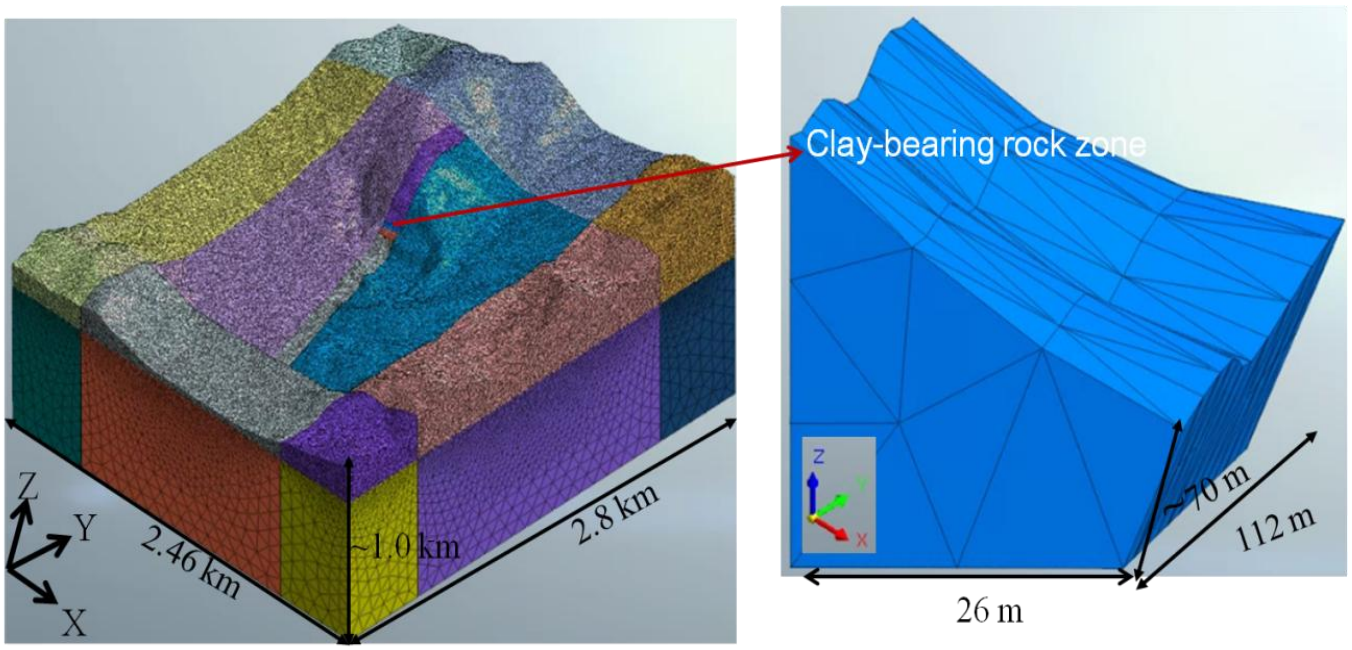

Fig.4.14: 3-D FEM model of the quarry including the clay-bearing rock zone.

4.4 Effects of clay-bearing rock zone on slope displacement

In this section, effect of the existing layer of clay-bearing rock on changes in regional stress due to excavation was investigated by 3-D back analysis. Afterward, stability of the rock slope is assessed by comparing calculated results to measured results. The relative displacements of both measured and calculated in the horizontal plane between each of the 12 APS mirrors on the slope surface at different elevations and beam generator point as described in section 2.3.2 were used for back analysis.

4.4.1 Analytical method

A 3D mesh of the quarry was generated using commercial software, MIDAS GTS/NX 2014 (V2.1) as described in section 4.2.1. The zone of clay-bearing rock, 110 m thick was inscribed in the medium model (Fig. 4.4b) at the elevation of 440-420 m. For simplicity, the shape of the inscribed clay-bearing rock was the same with that of cross-sectional line of V32 (see Fig. 2.7a). The entire 3-D FEM model is shown in Fig.4.14. The dimension of the entire model is the same as that of Fig.4.4b whereas the dimension of the inscribed clay-bearing rock zone is approximately 26 m, 112 m and 70 m in the x-, y- and z-directions. The total number of nodes and elements in the model for 2014 were 1,303,315 and 7,354,776, respectively. For better model of the change in surface geometry by mining, the mesh size within the mining areas was set to 10 m, which is equal to one bench height. The directions of the x- and y-axes of the model were aligned to due south and east of the quarry, respectively. The ground of the model was assumed to be isotropic and elastic. The boundary conditions are the same as shown in Fig.4.5 were used, the nodal displacement of each model was calculated independently by applying the gravitational force and each forced displacement corresponding to each regional strain.

As seen in Fig.4.14, the rock mass consists of two geological layers, it is therefore important to investigate the effects of changes in the surface geometry and the mechanical properties of the clay-bearing rock. The known parameters of the ground presented in Table 4.2, with the estimated Young's modulus of 4.01 GPa by GSI are used. The unknown parameters of clay-bearing rock, the unit weight, Poisson's ratio and elastic moduli were generated empirically by the ratio of known properties of rock mass presented in Table 4.2. The linear equations of the ratio of the mechanical properties of clay-bearing rock to that of rock mass were formulated as given in Eq. (4.4)-(4.6). The mechanical properties of clay-bearing rock are presented in Table

4.4. To estimate the parameters of the clay-bearing rock, it is necessary to conduct back analysis by changing mechanical properties of clay-bearing rock and then determine the parameters that can provides the minimum error in Eq. (4.2).

$$\text{Young's modulus, } E = 0.02\alpha + 4.0(1-\alpha) \quad (4.4)$$

$$\text{Poisson's ratio, } \nu = 0.2\alpha + 0.3(1-\alpha) \quad (4.5)$$

$$\text{Unit weight, } \gamma = 26.2\alpha + 18.0(1-\alpha) \quad (4.6)$$

where, α is the ratio of clay in the ground.

Table 4.4: Estimated parameters of weak rock by ratio to parameters of the ground material.

Young's modulus, E (GPa)	Clay ratio, α	Poisson's ratio, ν	Unit weight, γ (kN/m^3)
0.02	1.000	0.300	18.00
0.5	0.870	0.288	18.98
1.0	0.750	0.276	19.97
1.5	0.623	0.263	21.05
2.0	0.497	0.250	22.08
2.5	0.365	0.238	23.11
3.0	0.240	0.225	24.15
3.5	0.120	0.213	25.13
4.0	0.000	0.200	26.20

4.4.2 Analytical results and discussion

The regional strain state and Young's modulus of rock were then estimated by back analysis using Eq. (4.2). The relative displacement between 2014 and 2017 of both measured and calculated results were used to estimate the four unknown parameters: $\boldsymbol{c}_E$, $\boldsymbol{c}_X$, $\boldsymbol{c}_Y$, $\boldsymbol{c}_{XY}$ of Eq. (4.2). The estimated unknown parameters and values of regional stresses are presented in Table 4.5. The relationship between Young's modulus and magnitude and direction of the principal regional stress states estimated by Eq. (4.3) are shown in Fig. 4.15. It is observed that the estimated principal stresses show similar trends and stress state is almost uniaxial compression. This indicates that the magnitude and direction of the estimate regional stress is independent of Young's modulus of the existing layer of clay-bearing rock. The results as shown in Fig. 4.16 reveal the magnitude of maximum principal stress ranges from -2.10 to -2.62 MPa at principal

directions range of N16.9°W to N21.0°W. Fig. 4.17 shows the estimated errors, which indicates that Young's modulus of 20 MPa have a lesser errors of 12.6. Naga et al. (2009) reported the direction of stress measured at a point of about 50 km northwest of the Higash-shikagoe limestone quarry as N18°W. The direction of the measured stress was compared with that of the estimated principal stress as shown in Fig. 4.18. The result indicated that the direction, N21°W of the estimated maximum principal stress is close to that of measured stress, N18°W. Thus, the stress state in the quarry could also be influenced by regional stress due to tectonic activity.

Table 4.5: Unknown constant and regional stress values.

Young's modulus (GPa)	c_E	c_X	c_Y	c_{XY}	σ_{xx}	σ_{yy}	τ_{xy}
0.02	0.999	0.471	2.232	-0.766	-0.740	-2.340	-0.700
0.5	0.948	0.091	1.678	-0.500	-0.284	-1.726	-0.455
1.0	0.899	0.373	1.923	-0.501	-0.600	-2.009	-0.456
1.5	0.881	0.346	2.032	-0.614	-0.585	-2.118	-0.558
2.0	0.958	0.335	1.941	-0.483	-0.563	-2.023	-0.439
2.5	1.026	0.397	2.026	-0.487	-0.636	-2.117	-0.443
3.0	1.038	0.454	2.106	-0.494	-0.704	-2.205	-0.449
3.5	1.058	0.108	2.239	-0.732	-0.365	-2.302	-0.665
4.0	1.003	0.326	2.072	-0.511	-0.569	-2.156	-0.465

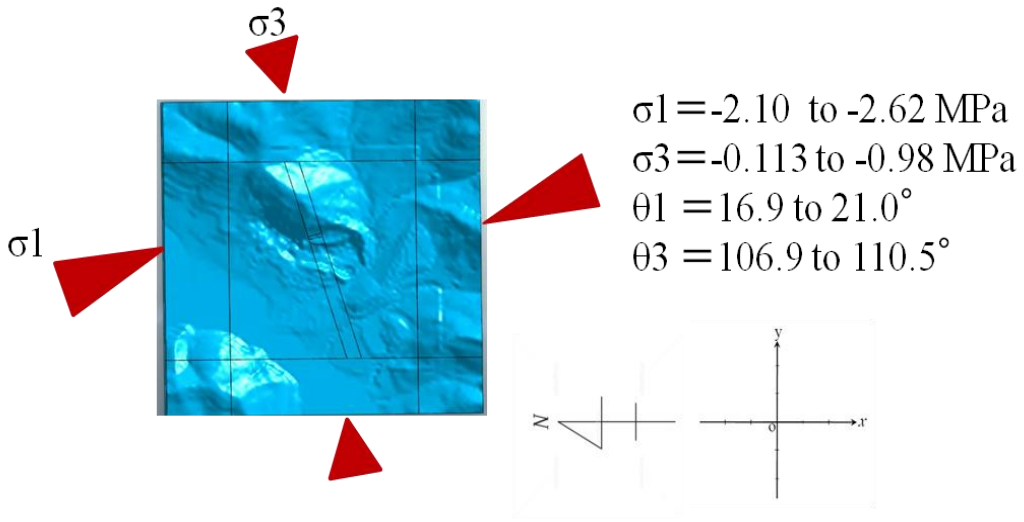

Fig.4.15: The magnitude and the direction of the estimated principal regional stress. The rectangle in the figure depicts the model used.

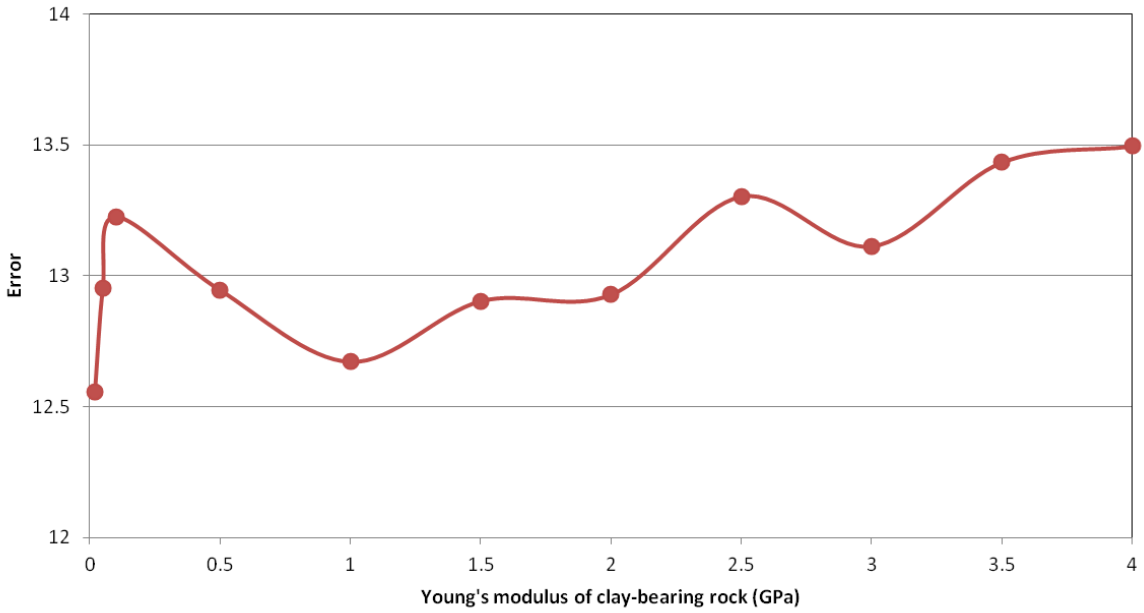

Fig.4.16: The estimated errors at different Young's modulus of clay-bearing rock.

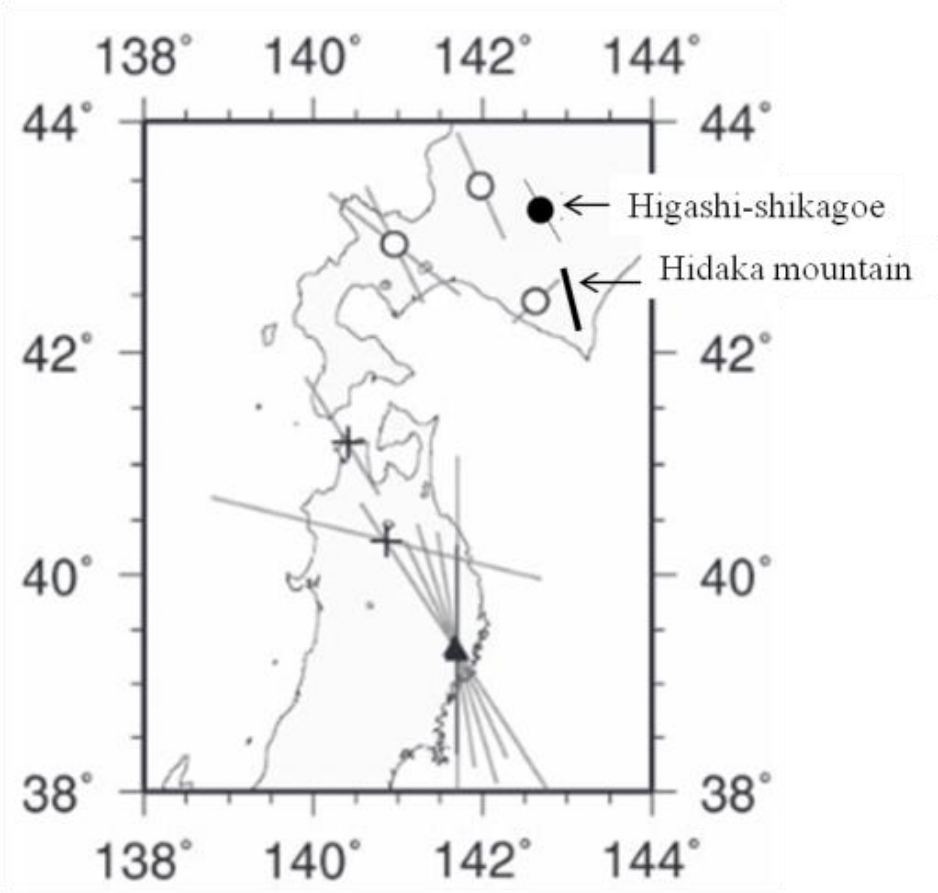

Fig.4.17: The estimated and measured regional stress as adopted from Naga et al., 2009.

4.5 Concluding remarks

Based on the characteristics of the calculated results, the findings of the 3-D back analyses are as follows:

i. The results of the medium model are almost equal to that of large model. Thus, model with a dimension of four times larger than that of the mining area is large enough.

ii. The estimated Young's modulus, 4.57 GPa of rock mass at Poisson's ratio of 0.2 by back analysis is close to that of Young's modulus, 4.01 GPa estimated by GSI.

iii. The magnitude and direction of regional stress is independent of Young's modulus of the existing layer of clay-bearing rock.

iv. The estimated stress state of the quarry is almost uniaxial compression. The maximum principal stress is estimated to be between -2.10 and -2.62 MPa.

v. The direction, N21°W of the estimated maximum principal stress is close to that of measured stress, N18°W. Thus, the stress state in the quarry could also be influenced by regional stress due to tectonic activity.

5 Estimation of mining-induced deformation by 3-D numerical analysis

5.1 Introduction

As found in chapter three that excavation at floor of the quarry is a dominant cause of the slope displacement observed at Higashi-shikagoe quarry if horizontal stress is sufficiently large. From chapter three, it was also revealed that plasticity of clay-bearing rock affects magnitude of the slope displacement due to excavation. These indicate that detail analysis of elasto-plastic behavior of the clay-bearing rock under regional stress is significantly important for estimation of long-term rock slope deformation. Previously, extensive studies have been done on deformation of homogenous rock slopes in pit-type mines by many researchers (Kaneko et al., 1996; Kaneko et al., 1997; Obara et al., 2000; Kodama et al., 2003; Kodama et al., 2009). In these studies, the elastic deformation of rock slope due to excavation has been cleared. However, the mining-induced plastic deformation of rock slope intersected by weak rock formation such as clay-bearing rock has not been investigated even though yielding of the clay bearing rock is likely affects the rock slope deformation. In this chapter, mining-induced deformation resulting from the plastic behavior of clay-bearing rock at the quarry was estimated by 3-D elasto-plastic analysis.

As described in chapter four, gravitational force and regional strains were applied to the model independently in order to estimate elastic deformation induced by excavation. In contrast, gravitational force and regional strains should be applied to the model simultaneously in order to estimate elasto-plastic deformation due to excavation. However, it is impossible to apply shear strain and normal strains simultaneously to the model as used in chapter four. To overcome this, a 3-D elasto-plastic analysis under regional stress by model rotating technique was proposed.

In this chapter, firstly, the validity of the proposed model rotating technique was verified to apply principal stress instead of the usual normal and shear strains. Then, causes of the rock slope deformation are considered by comparing calculated results from elastic and elasto-plastic analysis to measured results.

5.2 Analytical method

5.2.1 Validation of model rotating technique

To validate the new proposed rotation model, the surrounding of the mining area of the model shown in Fig.4.14 was rotated to 20° in anticlockwise direction. Fig.5.1 depicts the entire rotation model. The dimension of the entire model is the same as that of Fig.4.14. The mesh size within the mining areas was set to 10 m, which is equal to one bench height. The ground of the model was assumed to be isotropic and elastic. The parameter at Young's modulus of clay-bearing rock, 20 MPa as presented in Table 4.4 were used with Young's modulus, Unit weight and Poisson's ratio of ground as 4.01 GPa, 26.2 kN/m^3 and 0.2, respectively.

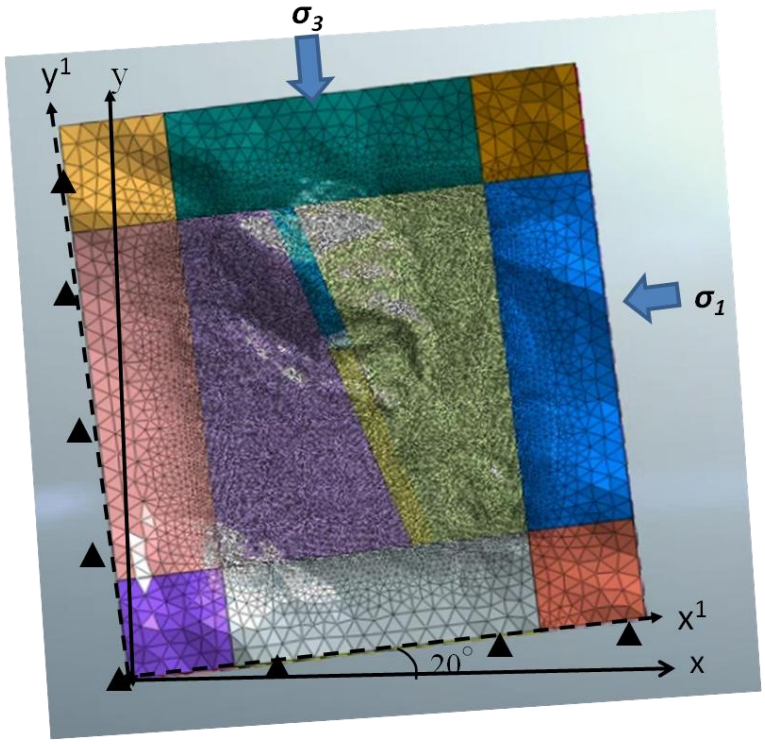

Fig.5.1: 3-D FEM rotation model of the quarry.

In this model, a 3-D elastic analysis was carried out under regional stress by the model rotating technique. The principal stresses at Young's modulus of clay-bearing rock, 20 MPa as presented in Table 5.1 estimated by back analysis based on Eq. (4.3) were applied on the model. Nodal displacement on the side surfaces (x- and y-directions) and the basal surface were fixed. Nodal displacement was calculated by simultaneously applying the gravitational force and principal stresses estimated by back analysis as shown in Fig. 5.1. To validate the model, nodal

displacement was also calculated independently by applying the gravitational force and each forced displacement corresponding to each regional strain using the estimated the four parameters: $\boldsymbol{c}_E$, $\boldsymbol{c}_X$, $\boldsymbol{c}_Y$, $\boldsymbol{c}_{XY}$ of Eq. (4.3) based on boundary conditions described in section 4.3.1 on the model shown in Fig. 4.14. $\boldsymbol{c}_E$, $\boldsymbol{c}_X$, $\boldsymbol{c}_Y$, $\boldsymbol{c}_{XY}$ at Young's modulus of clay-bearing rock, 20 MPa as presented in Table 4.5 were used.

To interpret deformation within the mining area, the relative displacements of 2014 to 2017 of both boundary conditions of rotation model (Fig.5.1) and model of Fig.4.14 in the horizontal plane were analyzed. The calculated displacements from the two models were designated as normal model and rotational model. Fig. 5.2 shows the calculated displacements. It can be seen in Fig. 5.2, the magnitude of calculated displacements in x- and y-direction are almost equal. This implies that the rotation model is reliable for the new proposed 3-D elasto-plastic analysis under regional stress by the model rotating technique.

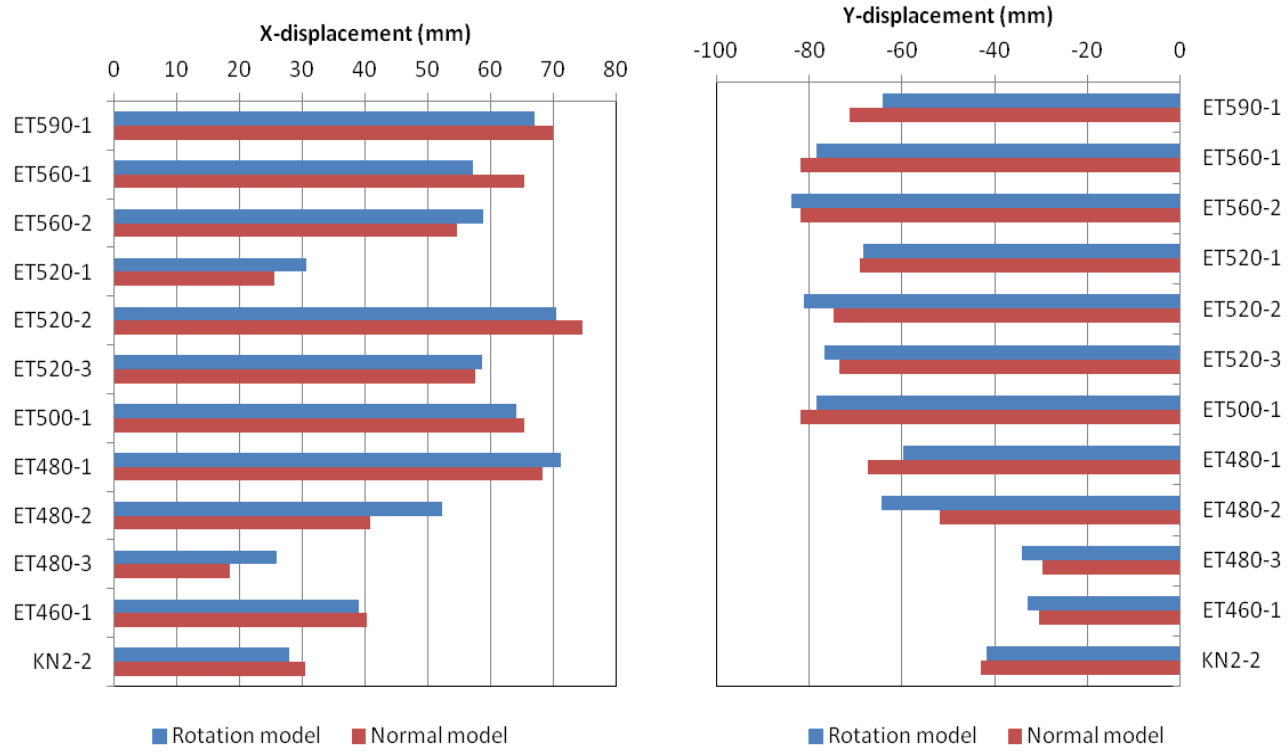

Fig. 5.2: Comparison of the calculated displacement from normal and rotation model.

5.2.2 Elasto-plastic analysis under regional stress

A 3-D elasto-plastic analysis was carried out under regional stress by the model rotating technique to apply regional stress to the model. Fig.5.3 shows the entire 3-D FEM model with

the dimension of the model shown in Fig.4.14. The limestone is assumed to be isotropic and elastic whereas the clay-bearing rock is assumed to behave as elasto-plastic material under Hoek-Brown criterion. In this model, the surrounding boundaries of the mining area were rotated to 20°, the direction of maximum principal stress estimated by back analysis. Nodal displacement on the side surfaces (x- and y-directions) and the basal surface were fixed. The maximum and minimum principal stress estimated by 3-D back analyses as presented in Table 5.1 were applied to side surface of the -y and -x plane, respectively. The nodal displacement of each model was calculated simultaneously by applying the gravitational force and the principal stress. Generalized Hoek-Brown criterion (Hoek and Brown, 1980) as shown in Eq. (5.1) was used as a failure criterion for elasto-plastic analysis on clay-bearing rock. Generalized Hoek-Brown parameters for clay-bearing rock are presented in Table 5.1. The parameters of the ground used are presented in Table 4.2, with the Young's modulus of 4.01 GPa and GSI of 45. The unit weight, Poisson's ratio and elastic moduli of clay-bearing rock were presented in Table 4.4.

$$\sigma_1 = \sigma_3 + \sigma_{ci}(m_b \frac{\sigma_3}{\sigma_{ci}} + s)^a \quad (5.1)$$

Where, σ_1 and σ_3 are the major and minor principal stresses, σ_{ci} is the uniaxial compressive strength of the intact rock, m_b, a and s are Hoek-Brown material constants, where s =1 for intact rock.

The GSI of clay-bearing rock was estimated from Young's modulus based on Equations given by Majdi et al., 2012.

$$Erm = 0.35 * exp^{0.06GSI} \quad (5.2)$$

Where *Erm* is Young's modulus of clay-bearing rock presented in Table 4.4, and GSI is the geological strength index

When the GSI value of clay-bearing rock is estimated, the following equations are used to determine the Hoek-Brown material constants, m_b, s and a:

$$m_b = m_i exp\left(\frac{GSI-100}{28}\right) \quad (5.3)$$

When,$GSI > 25$, the rock is considered as a good quality, then a=0.5 and s is estimated from the following equation as

$$s = exp\left(\frac{GSI-100}{9}\right) \quad (5.4)$$

When,$GSI < 25$, the rock is considered as poor quality, then s=0 and a is estimated from the following equation as

$$a = 0.65 - \frac{GSI}{200} \quad (5.5)$$

Table 5.1: Mechanical properties of clay-bearing rock for elasto-plastic analysis.

Young's modulus (GPa)	Principal stress (MP**a)**		GSI	Generalized Hoek-Brown parameter		
	σ_1	σ_3		m_b	s	a
0.02	-2.60	-0.23	0.225	0.268	$1.5x10^{-5}$	0.664
0.5	-2.10	-0.31	13.30	0.428	$6.5x10^{-5}$	0.568
1.0	-2.22	0.38	23.83	0.623	$2.1x10^{-4}$	0.534
1.5	-2.30	-0.40	29.99	0.776	$4.2x10^{-4}$	0.522
2.0	-2.21	-0.33	34.37	0.908	$6.8\ x10^{-4}$	0.517
2.5	-2.39	-0.43	37.76	1.025	$9.9x10^{-4}$	0.513
3.0	-2.49	-0.51	40.53	1.131	$1.4x10^{-3}$	0.511
3.5	-2.58	-0.18	42.87	1.229	$1.8x10^{-3}$	0.509
4.0	-2.46	-0.37	44.9	1.323	$2.2x10^{-3}$	0.508

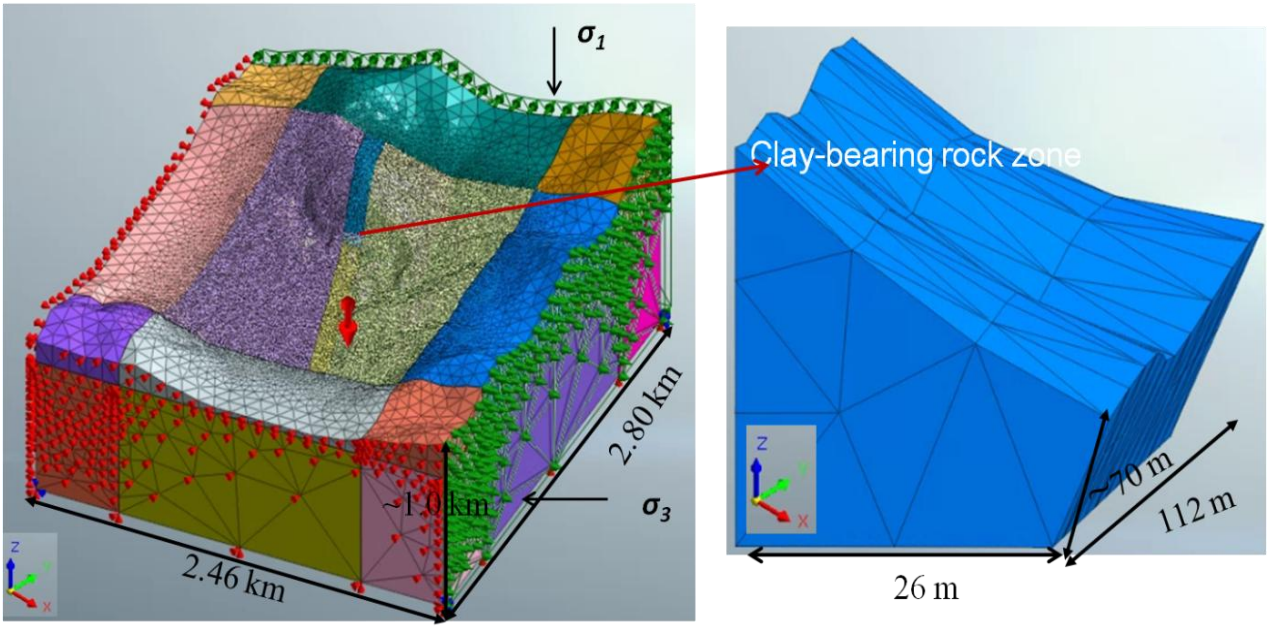

Fig.5.3: 3-D FEM model of the quarry used for elasto-plastic analysis.

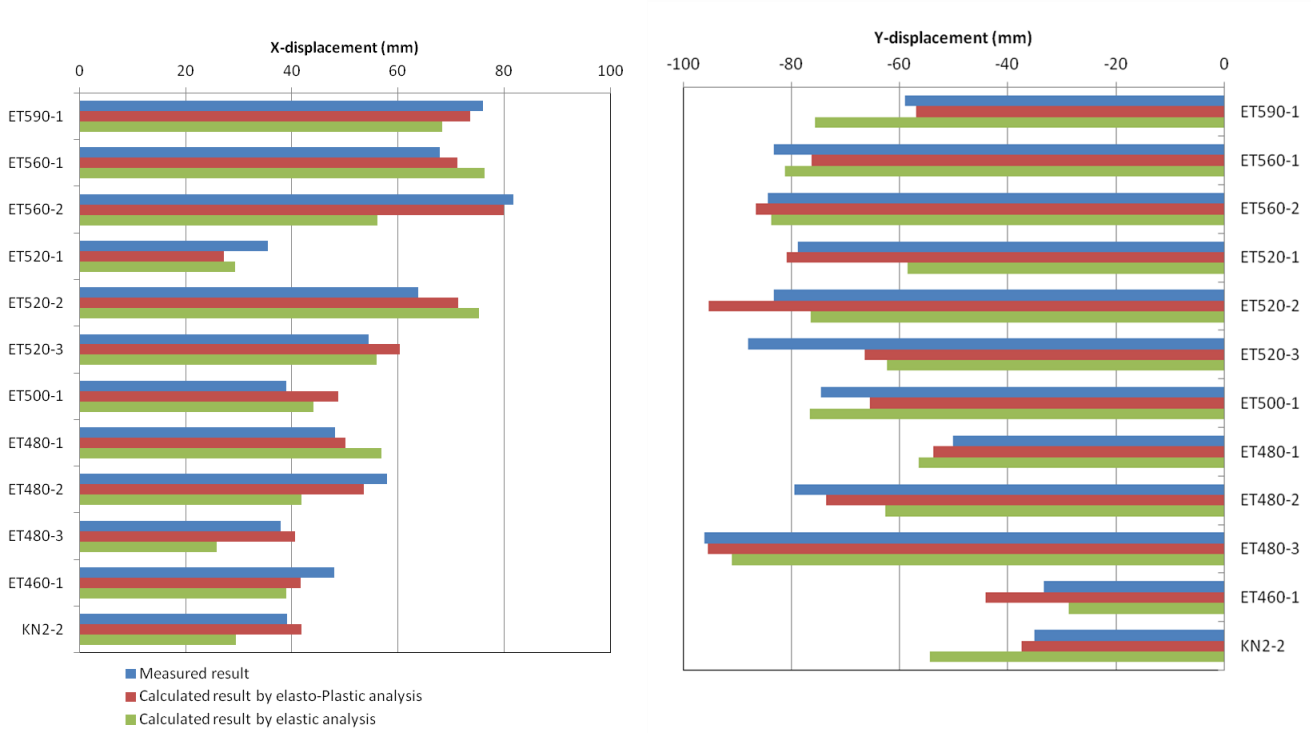

Fig. 5.4: Comparison of the measured and calculated results**.**

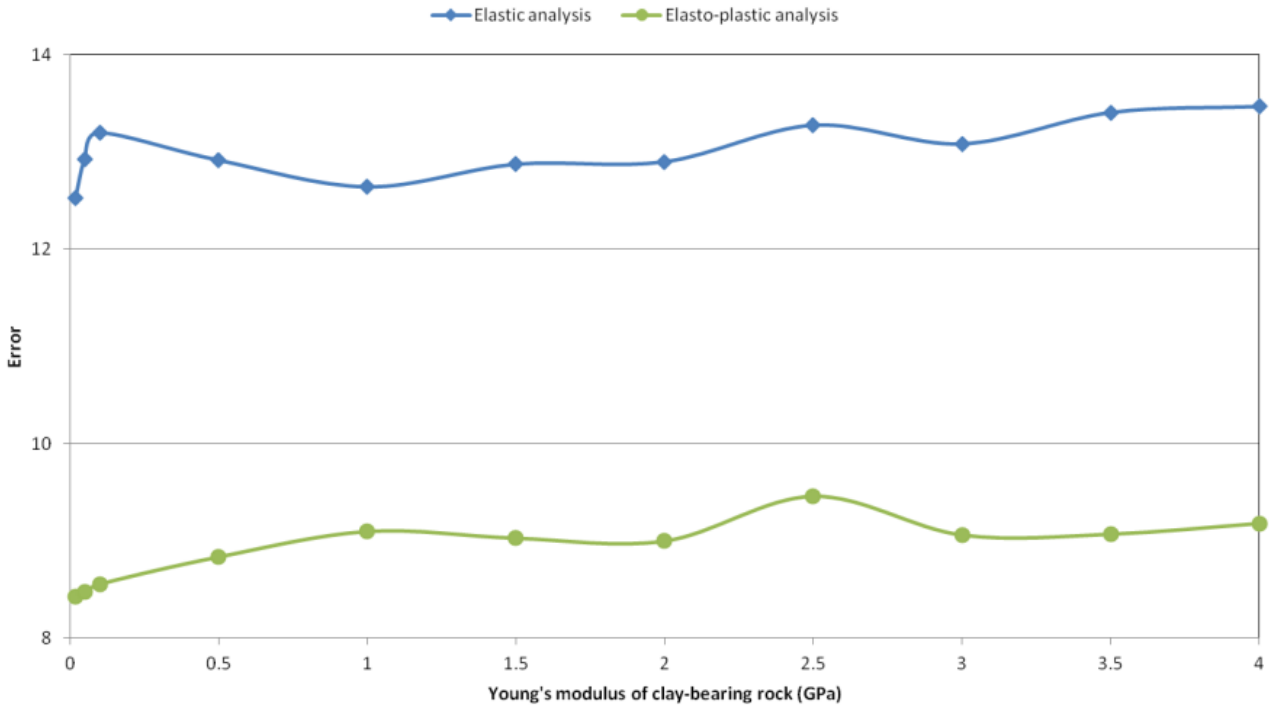

Fig. 5.5: Relationship between estimated errors and Young's modulus of clay-bearing rock.

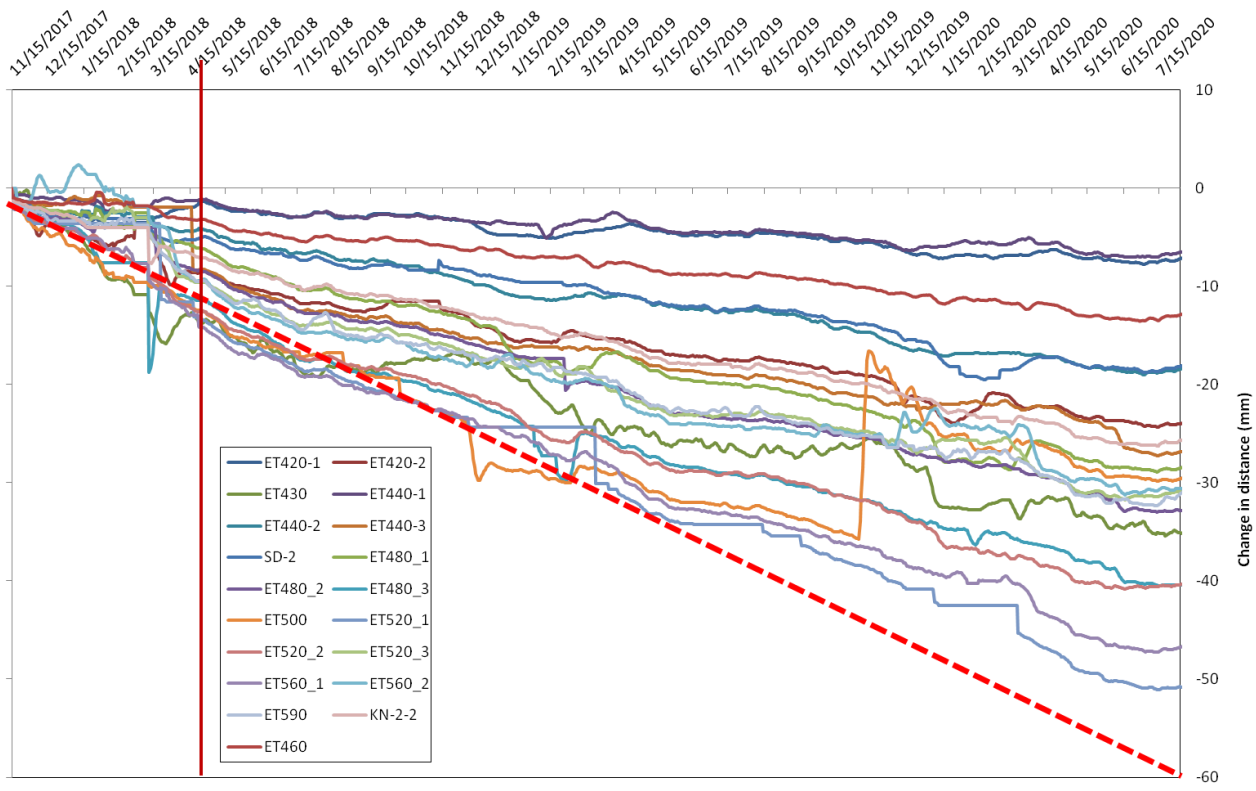

Fig. 5.6: Change in displacement rate after installation of shotcrete and rock bolting in April 2018.

5.3 Results of elastic and elasto-plastic analysis

To interpret deformation within the mining area, the relative displacements of 2014 to 2017 of both measured and calculated results in the horizontal plane were analyzed. The measured results from the 12 APS mirrors were compared with the calculated results by elasto-plastic and elastic analyses to identify the cause of the long-term deformation of the rock slope observed at the quarry. The calculated displacement by elastic analysis and elasto-plastic analysis are compared with the measured results as shown in Fig.5.4. The results show that the calculated displacements by the elasto-plastic analysis are closer to the measurement results than those of the elastic analysis. In addition, errors were estimated as shown in Fig. 5.5. As can be seen in Fig.5.5, the calculated results by the elasto-plastic analysis have lesser errors than that of elastic analysis. The estimated errors seem to be almost the same at all the Young's modulus of the clay-bearing rock, although a lesser error is estimated at the Young's modulus of 20 MPa. This means that the clay-bearing rock at the foot of the rock slope shown plastic behaviors between 2014 and 2017.

However, as seen in Fig.5.6, the deformation rate of the rock slope decreases constantly after April 2018. As mentioned in chapter two, countermeasure by rock bolts and shotcrete was installed from 2018. This indicates that the shotcrete and rock bolting at the periphery of the excavation surface of the existing layer of the clay-bearing rock is expected to have inhibited the plastic deformation of the rock slope because the decreasing rate in change in distance became smaller since 2018.

5.4 Concluding remarks

Based on the characteristics of the calculated results, the findings of the 3-D elasto-plastic analyses are as follows:

i. The proposed model rotating technique provides a useful basis for elasto-plastic analysis under regional stress.

ii. The calculated results of the elasto-plastic analysis are closer to the measurement results than those of the elastic analysis. Thus, it can be concluded that deformation of rock slope arising from excavation was predicted by considering plastic deformation of clay-bearing rock. Thus, clay-bearing rock shows plastic behaviors between 2014 and 2017.

iii. Countermeasure by rock bolts and shotcrete at excavation surface of the existing layer of the clay-bearing rock which commenced in 2018 is expected to have inhibit the plastic deformation of the rock slope because the decreasing rate of change in distance became smaller since 2018.

6 Conclusions and recommendations

6.1 Conclusions

In this research, the characteristics of the long-term rock slope deformation observed at the open-pit limestone quarry were investigated by field measurement and numerical analysis. At first, the change in distance between the beam generator and each of the 18 mirrors on the rock slope, and 3-D relative surface displacements arising from mining activities at the floor of the quarry for more than seven years were analyzed to clear deformation characteristics of the rock slope. The probable causes of the long-term continuous slope deformation were discussed based on the previous studies, deformation characteristics, geological conditions and mining progression. Afterward, the main cause of the long-term continuous slope deformation was investigated by 2-D elastic analysis. Excavation-induced deformation and effect of model sizes on the slope deformation were examined by 3-D back analysis. Based on regional principal stresses estimated by 3-D back analysis, mining-induced plastic deformation of the heterogeneous rock slope intersected by clay-bearing rock was also investigated. The contents and findings of this research are summarized as follows:

Chapter 1 reviewed the background, objectives of research, case study of deformation and failure of rock slopes similar to that of Higashi-shikagoe limestone quarry were described. Previous studies related to the estimation of regional stress by back analysis, causes and analysis of mining-induced deformation of rock slope were also reviewed.

Chapter 2 aimed at revealing the overall characteristics of the long-term slope displacement observed at the Higashi-shikagoe limestone quarry. In this chapter, the overview of the quarry and geologic conditions of the rock slope at the quarry were explained. The change in distance between the beam generator and each of the 18 mirrors on the rock slope for more than seven years was analyzed to clear deformation characteristics of the rock slope. The results revealed that the distance between the beam generator and each of the 18 mirrors decreases gradual at a continuous rate. It was also suggested that the decreasing rate differs between the center and north- and south-sides of the quarry. The analysis of 3-D relative surface displacements shows that continuous forward movement of the rock slope toward the southern side of the quarry is the dominant component of the displacement vectors. Finally, possible causes of slope deformation

were deduced based on the previous studies, geological conditions, deformation characteristics and mining progression of the quarry.

Chapter 3 aimed at identifying the main cause of the observed continuous deformation using two-dimensional (2-D) finite element method. Firstly, the effects of limestone excavation at the floor of the quarry, the deterioration of the 70-m-thick clay-bearing rock distributed at foot of the rock slope, and shear failure of the rock slope were investigated. From the results, it was observed that the change in distance decrease due to deterioration of clay-bearing rock, and the maximum decrease are seen at the middle of the rock slope. Also, it revealed that the change in distance induced by excavation at the pit floor depends on the rock stress conditions. The distance increases under gravity force conditions and decreases under horizontal stress conditions. The magnitude of the distance reduction under horizontal stress conditions is greatest at the foot of the slope. Based on the characteristics of the measured and calculated results, continuous excavation at floor of the quarry was deduced as the main cause of observed continuous slope deformation. It also revealed that displacement induced by excavation is quite significant if clay-bearing rock behaves as an elasto-plastic material.

Chapter 4 evaluated excavation-induced deformation of rock slope using 3-D back analysis. At first, effect of model sizes on deformation of the rock slope was investigated. Thereafter, regional stress state and the Young's modulus of a rock mass within the mining area of the quarry were estimated to ensure the long-term stability of the rock slope. Furthermore, effect of the clay-bearing rock on excavation-induced deformation of the rock slope was also investigated.

Reliable results can be obtained if entire model size is set at four times larger than that of the mining area. From the 3-D back analyses, it was found that the estimated Young's modulus, 4.57 GPa of rock mass at Poisson's ratio of 0.2 is close to that of Young's modulus, 4.01 GPa estimated by GSI. It was observed that the magnitude and direction of regional stress is independent of Young's modulus of the existing layer of clay-bearing rock. The estimated stress state of the quarry is almost uniaxial compression. The maximum principal stress is estimated to be between -2.10 and -2.62 MPa. Furthermore, the direction, N21°W of the estimated maximum principal stress was seen to be close to that of measured stress, N18°W.

Chapter 5 cleared the cause of the rock slope deformation using a newly proposed 3-D elasto-plastic analysis under regional stress by model rotating technique. First, validity of the new proposed model rotating technique for elasto-plastic analysis was verified. Then, mining-

induced deformation resulting from the plastic behavior of clay-bearing rock was estimated based on generalized Hoek-Brown criteria by applying the principal regional stresses estimated by 3-D back analysis to the rotation model. It was found that the calculated results of the elasto-plastic analysis are closer to the measurement results than those of the elastic analysis. This implies that the clay-bearing rock at the foot of the rock slope has shown plastic behaviors between 2014 and 2017. However, countermeasure by rock bolts and shotcrete at excavation surface of the existing layer of the clay-bearing rock which commenced in 2018 is expected to have inhibited the plastic deformation of the rock slope because the decreasing rate of change in distance became smaller since 2018.

6.2 Recommendations

Continuous deformation of rock slope is still observed at the quarry. Thus, considering the strong responses of the rock slope deformation to excavation, it is recommended that a detail investigation should be carried on countermeasures by rock bolts, shotcrete at the periphery of the excavation surface of the existing layer of the clay-bearing rock for ensuring long-term safety of the rock slope because yielding of the clay bearing rock will likely affects the rock slope deformation. Moreover, the countermeasure by shotcrete is likely to be effective in preventing rainfall inflow to rock slope. Thus, it is expected to effectively prevent further deterioration of the existing clay-bearing rock. Secondly, effect of changes in temperature and weather conditions should be investigated to further clarify the mechanisms of the continuous deformation. Thirdly, it is recommended that further studies should be undertaken on effects of blasting and discontinuity such as faults.

References

Amagu AC, Zhang C, Kodama J, Shioya K, Yamaguchi T, Sainoki A, Fukuda D, Fujii Y, Sharifzadeh M (2021a) Displacement Measurements and Numerical Analysis of Long-Term Rock Slope Deformation at Higashi-Shikagoe Limestone Quarry, Japan, Advances in Civil Engineering Vol. 2021, Article ID 1316402,15 pages.

Amagu AC, Zhang C, Kodama J, Iwasaki H, Ikegami S, Sainoki A, Fukuda D and Fujii Y (2021b) Numerical Analysis of Effects of Clay on a Cut Rock Slope Deformation at an Open-pit Limestone Mine, Japan, ISERME-S1-2, 10th December 2021, Colombo, Sri Lanka.

Ataei M, Bodaghabadi S (2008) Comprehensive analysis of slope stability and determination of stable slopes in the Chador-Malu iron ore mine using numerical and limit equilibrium methods, J China University Mining and Technology. 18:488-493

Ayalew L, Yamagishi H, Ugawa N (2004) Landslide susceptibility mapping using GIS-based weighted linear combination, the case in Tsugawa area of Agano River, Niigata Prefecture, Japan. Landslides 1:73-81.

Bandazi CN (2017) Measurement and analysis of rock slope displacement at Higashi Shikagoe limestone quarry, Japan; Master thesis, Hokkaido University.

Barla G (2016) Application of numerical methods in tunnelling and underground excavations: Recent trends. Rock Mechnics and Rock Engineering: from the past to the future-Ulusay et al. (Eds), Taylor and Francis Group, London, ISBN 978-1-138-03265-1.

Bell FG (200) Engineering properties of soils and rocks, 4th edn, Blackwell Scientific, Oxford.

Bian X, Hong ZS, Ding JW (2016) Evaluating the effect of soil structure on the ground response during shield tunneling in Shanghai soft clay, Tunn Undergr Sp Tech; 58:120-132.

Bishop AW (1955) The use of the slip circle in stability analysis of slopes, Geotechnique, 5(1):7-17.

Bommer JJ, Rodrı’guez CE (2002) Earthquake-induced landslides in Central America, Eng. Geol. 63:189-220.

Brown ET, Hoek E (1978) Trends in relationships between measured in-situ stresses and depth, Int J Rock Mech Min Sci; 15:211-215.

Brummer R, Li H, Moss A (2006) The transition from open pit to underground mining: An unusual slope failure mechanism at Palabora. In Proceedings of the International

Conference S44 Stability of Rock Slopes in Open Pit Mining and Civil Engineering, Cape Town, South Africa, 3–6 April 2006.

Bye AR, Bell FG (2001) Stability assessment and slope design at Sandsloot open pit, South Africa, Int J Rock Mech Min Sci., 38:449-466.

Cai F, Ugai K (2004) Numerical analysis of rainfall effects on slope stability, Int. J. Geomech. 4(2): 69-78

Cai M, Morioka H, Kaiser PK, Tasaka Y, Kurose H, Minami M, Maejima T (2007) Back-analysis of rock mass strength parameters using AE monitoring data, International Journal of Rock Mechanics & Mining Sciences 44, 538–549

Chai JC, Igaya Y, Hino T, Carter J (2013) Finite element simulation of an embankment on soft clay- Case study Computers and Geotechnics; 48:117-126.

Chai JC, Miura N (1999) Investigation on some factors affecting vertical drain behavior, J Geotech Geoenviron Eng, ASCE; 125 (3):216–26.

Corkum AG, Martin CD (2004) Analysis of a rock slide stabilized with a toe-berm: a case study in British Columbia, Canada, Int J Rock Mech Min Sci 41:1109-21.

Dahal RK, Hasegawa S, Masuda T, Yamanaka M (2006) Roadside Slope Failures in Nepal during Torrential Rainfall and their Mitigation, Disaster Mitigation of Debris Flows, Slope Failures and Landslides 503–514.

Dawson EM, Roth WH, Drescher A (1999) Slope stability analysis by strength reduction, Geotechnique, 49 (6):835-840.

Eberhardt E (2003) Rock Slope Stability Analysis—Utilization of Advanced Numerical Techniques; Earth and Ocean Sciences at UBC Report; University of British Columbia (UBC): Vancouver, BC, Canada, 2003.

Eberhardt E, Stead D, Coggan JS (2004) Numerical analysis of initiation and progressive failure in natural rock slopes-the 1991 Randa rockslide, Int J Rock Mech Min Sci 41: 69-87.

Erguler ZA, Shakoor A (2009) Quantification of fragment size distribution of clay bearing rocks after slake durability testing, Env Eng Geosci 15 (2): 81-89.

Erguler ZA, Ulusay R (2009) Water-induced variations in mechanical properties of clay-bearing rocks, Int J Rock Mech Min Sci 46: 355-370.

Farshidfar N, Nayeri A (2015) Slope Stability Analysis by Shear Strength Reduction Method, J Civil Eng Urban 5 (1): 35-37.

Fujiita H (1997) State of the art of the landslide control in Japan and the issues in the future, J Jpn Geotech Soc 45(6): 1-4 (in Japanese).

Gao W, Dai S, Xiao T, He T (2017) Failure process of rock slopes with cracks based on the fracture mechanics. Eng. Geol., 231, 190–199.

Gautama TP, Shakoor A (2013) Slaking behavior of clay-bearing rocks during a one-year exposure to natural climatic conditions, Eng Geo, 166:17-25.

Goodman RE (1989) Introduction to rock mechanics, 2nd edition, Wiley, New York Goodman RE, 1995, Block theory and its application, Geotechnique, vol.45 (3), pp.383–423.

Griffiths DV, Lane PA (1999) Slope stability analysis by finite elements, Geotechnique 49(3): 387-403.

GTS NX 2014 v2.1 MIDAS Information Technology Co., Ltd. http://www.midasGTSNX.com.

Hassan B, Hani M (2017) Application of rock mass classification systems to rock slope stability assessment: A case study, Int J Rock Mech Geotech Eng 9:993-1009.

He MC, Feng JL, Sun XM (2008) Stability evaluation and optimal excavated design of rock slope at Antaibao open pit coal mine, China, Int J Rock Mech Min Sci 45:289-302.

Hoek E, Bray JW (1981) Rock slope engineering, 3rd ed., Institute of Mining and Metallurgy, London.

Hoek E, Brown ET (1980) Empirical strength criterion for rock masses, J. Geotech. Eng. Div., ASCE, 106(GT9), 1013-1035.

Hoek E, Brown ET (1997) Practical estimates of rock mass strength, Int J Rock Mech Min Sci; 34(8):1165-86.

Hu Y, Ren F, Ding H, Fu Y, Tan B (2019) Study on the Process and Mechanism of Slope Failure Induced by Mining under Open Pit Slope: A Case Study from Yanqianshan Iron Mine, China. Adv. Civ. Eng. 2019, 1-27.

Hustrulid WA, McCarter MK, Van Zyl DJA (2000) Slope Stability in Surface Mining; Society for Mining, Metallurgy, and Exploration: Littleton, CO, USA, pp. 81-88.

Ishikawa T, Tokoro T, Seiichi M (2015) Geohazard at volcanic soil slope in cold regions and its influencing factors, Jpn Geotech Soc Spec 1:1-20.

Ivasuc T, Olinic E (2015) The effect of clay desensitization with granular materials on slope stability analysis, Agric Agric Sci Procedia 2015; 6:459-466.

Jessu KV, Kostecki TR, Spearing AJS, Zhang J (2017) Influence of varying bedding thickness of underclay on floor stability, Int. J Mining Sci Technol, 27(3), 517-523.

Jing L (2003) A review of techniques, advances and outstanding issues in numerical modeling for rock mechanics and rock engineering, International Journal of Rock Mechanics and Mining Sciences, 40:283-353.

Jing L, Hudson JA (2002) Numerical methods in rock mechanics, International Journal of Rock Mechanics and Mining Sciences, vol. 39, pp. 409–27.

Kaiser PK, Zou D, Lang PA (1990) Stress determination by back-analysis of excavation-induced stress changes—a case study, Rock Mech Rock Eng; 23(3):185–200.

Kaneko K, Kato M, Noguchi Y, Nakamura N (1997) Influence of initial stress on rock slope stability, Proceedings of the international symposium on rock stress, Balkema Roterdam 429-434.

Keefer DV (2000) Statistical analysis of an earthquake-induced landslide distribution-the 1989 Loma Prieta, California event, Eng. Geol 58:231-249.

Kodama J, Miyamoto T, Kawasaki S, Fujii Y, Kaneko K, Hagan P (2013) Estimation of regional stress state and Young's modulus by back analysis of mining-induced deformation, Int J Rock Mech Min Sci 63:1-11.

Kodama J, Nishiyama E, Kaneko K (2009) Measurement and interpretation of long-term deformation of a rock slope at the Ikura limestone quarry, Int J Rock Mech Min Sci 46:148-158.

Kolapo P, Oniyide GO, Said KO, Lawal AI, Onifade M, Munemo P (2022) An Overview of Slope Failure in Mining Operations. Mining, 2, 350–384.

Li G, Mizuta Y, Ishida T, Li H, Nakama S and Sato T (2009) Stress field determination from local measurements by numerical modeling, Int J Rock Mech Min Sci Geomech Abstr. 46,138–47.

Liu YC, Chen CS (2007) A new approach for application of rock mass classification on rock slope stability assessment, Eng. Geo. 89, 129-143.

Lu L, Wang ZJ, Huang XY, Zheng B, Arai K (2014) Dynamic and static combination analysis method of slope stability analysis during earthquake. Math Probl Eng 2014a; http://dx.doi.org/10.1155/2014/.573962.

Lu L, Wang ZJ, Song ML, Arai K (2015) Stability analysis of slopes with ground water during earthquakes, Eng Geol 193:288-296.

Majdi A, Bashari A, Beiki M (2012) Estimation of rock mass deformation modulus based on GSI system, Harmonising Rock Engineering and the Environment, pp. 2113-2117.

Marinos PV (2010) New Proposed GSI Classification Charts for weak or complex rock masses, Bulletin of the Geological Society of Greece, vol. 43, 1248-1258.

Matsu T, San K (1992) Finite element slope stability analysis by shear strength reduction technique, Soils and foundation 32(1): 59-70.

Matsuda H, Shimizu N, Yoshitomi I, Kawahata K, Chiba T, Tonsyo M (2003) Accuracy of displacement monitoring of Large slope by using GPS. MMIJ 119:389-395 (in Japanese).

Matsuda H, Shimizu N, Yoshitomi I, Kawahata K, Chiba T, Tonsyo M (2003) Accuracy of displacement monitoring of Large slope by using GPS. MMIJ 119:389-395 (in Japanese).

Matsuki K, Nakama S, Sato T (2009) Estimation of regional stress by FEM for a heterogeneous rock mass with a large fault, Int J Rock Mech Min Sci Geomech Abstr. 46, 31–50.

Matsuoka N (2008) Frost weathering and rockwall erosion in the southeastern Swiss Alps: long-term (1994–2006) observations. Geomorphol; 99:353-368.

Naga A, Kunimatsu S, Kanekawa T, Fujii M, Yokoyama Y, Ogawa K, Tanaka M (2009) Initial ground pressure conditions in underground rocks in Japan -Based on measured data by stress release method-. Geological Survey Research Report, 60 (7-8):413-47.

Najib, Fukuda D, Kodama J, Fujii Y (2015) The Deformation Modes of Rock Slopes due to Excavation in Mountain-Type Mines. MMIJ, Materials Transactions, 56 (8):1159-1168.

Nakamura N, Tsukayama Y, Hirata A, Kaneko K (2003) Displacement measurement of rock slope with cover rock and its interpretation. MMIJ 119: 547-552.

Nakai S, Sasaki Y, Kaibori M, Moriwaki T (2006) Rainfall index for warning and evacuation against sediment- related disaster: Reexamination of rainfall index Rf and proposal of R. Soils and Foundations, 46 (4), 465-475.

Nara Y, Kaneko K, (2006) Sub-critical crack growth in anisotropic rock, Int J Rock Mech Min Sci, 43, pp.437-453.

Nara Y, Koike K, Yoneda T, Kaneko K (2006) Relation between subcritical crack growth behavior and crack paths in granite, Int J Rock Mech Min Sci, 43, pp.1256-1261.

Nara Y, Cho SH, Yoshizaki T, Kaneko K, Sato T, Nakama S, Matsui H (2011) Estimation of three-dimensional stress distribution and elastic moduli in rock mass of the Tono area, Int J Japan Comm Rock Mech, 7(1), pp.1-9.

Nicholas DE, Sims DB (2000) Collecting and Using Geological Structure Data for Slope Design; Hustrulid, W.A., McCarter, M.K., Van Zyl, D.J.A., Eds.; Society for Mining, Metallurgy, and Exploration: Golden, CO, USA, 2000.

Nicholson DT, Hencher SR (1997) Assessing the potential for deterioration of engineered rock slopes, In: Marinos, P.G., Koukis, G.C., Tsiambaos, G.C., Stournaras, G.C. (Eds.). Eng Geol the Env. Balkema, Rotterdam, 911-917.

Nicholson DT, Nicholson FH (2000) Physical deterioration of sedimentary rocks subjected to experimental freeze–thaw weathering. Earth Surface Processes and Landforms 25:1295-1307.

Nilsen B (2011) Case of instability caused by weakness zones in Norwegian tunnels, Bulletin Engineering Geology and Environment, 70:7–13.

Nishiyama E, Miyamoto T, Kodama J, Kaneko K (2010) Estimation of regional stress state and Young's modulus by analyzing mining induced deformation. In: Proceedings of the ISRM regional symposium, 681-4.

Noguchi Y, Okada Y (1999) Monitoring of rock slopes in the Ikura limestone quarry Limestone. MMIJ 297:28-35 [in Japanese].

Obara Y, Nakamura N, Kang SS, Kaneko K (2000) Measurement of local stress and estimation of regional stress associated with stability assessment of an open-pit rock slope. Int J Rock Mech Min Sci 37:1211-1221.

Ohtsuka S, Matsuo M (1995) Rigid plastic dynamic deformation analysis of structures, Proceedings of 1st International Conference on Earthquake vol. 2. Geotechnical Engineering, Tokyo, Japan, 1147-1152.

Okata K, Sugiyama T, Muraishi H, Noguchi T, Samizo M (1994) Statistical risk estimating method for rainfall on surface collapse of a cut slope. Soils Found 34(93):49-58.

Okuda M, Abe T, Sakurai S, (1999) A non-linear back analysis procedure for shallow tunnels excavated in unconsolidated grounds. J. Geotech. Eng. JSCE 638(III-49), 383-388.

Orense RP (2012) Soil liquefaction and slope failures during the 2011 Tohoku, Japan Earthquake. 2012 NZSEE Annual Technical Conference and AGM, New Zealand, Paper ID 007: 1-8.

Pankow KL, Moore JR, Hale JM, Koper KD, Kubacki T, Whidden KM, McCarter MK (2014) Massive landslide at Utah copper mine generates wealth of geophysical data. Geol. Soc. Am., 24, 4-9.

Pantelidis L (2009) Rock stability assessment through rock mass classification systems, Int J Rock Mech Min Sci 46: 315-325.

Park DS, Kutter BL (2015) Static and seismic stability of sensitive clay slopes, Soil Dyn Earthq Eng 2015;79:118-129.

Read JR, Stacey PF (2009) Guidelines for Open Pit Slope Design, CSIRO Publishing, Collingwood, Australia.

Rose ND, Hungr O (2007) Forecasting potential rock slope failure in open pit mines using the inverse-velocity method. Int J Rock Mech Min Sci 44:308-20.

Sakurai S (1982) In-situ test of rock masses and interpretation of the results, J Soc Mat Sci Japan; 8:759-769. [in Japanese].

Sakurai S, Akutagawa S, Takeuchi K, Shinji M, Shimizu N (2001) Back analysis for observational methods in tunnelling engineering, Proceedings of the International Symposium on Modern Tunnelling Science and Technology, IS-Kyoto 2001, Oct. 30–Nov. 1. pp. 1165–1188.

Sakurai S, Akutagawa S, Takeuchi K, Shinji M, Shimizu N (2003) Back analysis for tunnel engineering as a modern observational method. Tunnel Underground Space Technol.; 18(2-3):185-96.

Sano O (2005) Measurement methods of Contemporary stress field and rock mechanics, J Geogr; 114:1003-21.

Serna, M, Williams D, Ruest M (2016) Analysis of Kennecott Utah copper's Bingham Canyon mine pit wall slides. In Proceedings of the Tailing and Mine Waste, Denver, CO, USA, 2–5 October 2016.

Sha L (2016) Analysis of slope instability factors and protection. Int. J. Multidiscip. Res. Dev., 3, 181–182.

Sharifzadeh M, Fahimifar A, Esaki T (2002) Classification and modelling of water effect on mechanical behaviour of intact rock and rock joint. In: Proceedings of the Fourth International Summer Symposium, Kyoto, Japan, pp 263-266.

Sharifzadeh M, Javadi M (2017) Groundwater and underground excavations: From theory to practice. In Rock Mechanics and Engineering: Analysis, Modeling and Design 3: 300-329.

Shen J, Priest SD, Karakus M (2012) Determinations of Mohr–Coulomb shear strength parameters from generalized Hoek–Brown criterion for slope stability analysis. Rock Mech and Rock Eng 45:123-129.

Shimizu N, Koyama S, Ono H, Miyashita K, Kondo H, Mizuta Y (1997) Field experiments and data processing for continuous measurement by GPS displacement monitoring system. MMIJ113: 549-54.

Shuin Y, Hotta N, Suzuki M, Ogawa K (2012) Estimating the effects of heavy rainfall conditions on shallow landslides using a distributed landslide conceptual model. Physics and Chemistry of the Earth, Parts A/B/C, 49, 44–51. doi:10.1016/j.pce.2011.06.002.

Stead D, Eberhardt E, Coggan JS (2006) Developments in the characterization of complex rock slope deformation and failure using numerical modeling techniques, Eng Geol 83: 217-235.

Study committee on slope stability and environmental preservation in Chichibu area (1996), Study of cooperative development and slope stability at Mt.Bukoh, 112: 665-669 (in Japanese).

Sugawara K (2000) Next-generation measuring technology for risk management of rock slopes in open-pit limestone quarries. MMIJ 307:43-62 [in Japanese].

Sugiyama T, Okata K, Muraishi H, Noguchi T, Samizo M (1995) Statistical rainfall risk estimating method for a deep collapse of a cut slope. Soils Found 35(4):37- 48.

Va´n Eeckhout EM (1976) The mechanisms of strength reduction due to moisture in coal mine shales, Int J Rock Mech Min Sci 13:61-7.

Vásárhelyi B, Ván P (2006) Influence of water content on the strength of rock. Eng Geol 84: 70-74.

Voight B, Kennedy BA (1979) Slope failure of 1967–1969, Chiquicamata Mine Chile. In Rockslides & Avalanches; Voight, B., Ed.; Developments in Geotechnical Engineering, 14b; Elsevier: Amsterdam, The Netherlands, 1979; pp. 595-632.

Willie DC, Mah CW (2004) Rock Slope Engineering, 4th edition, Spon Press, New York, pp. 320-327.

Yamaguchi U, Shimotani T (1986) A Case Study of Slope Failure in a Limestone Quarry. Int J Rock Mech Min Sci Geomech Abstracts 23: 95-104.

Yamamoto K, Yabe Y, Yamamoto H (1997) Relation of in-site stress field to seismic activity as inferred from the stresses measured on core samples, In:Proc. Int. Sym. on rock stress, Kumamoto,Japan,7–10 October, p.375–80.

Yeh HF, Wang JG, Shen KL, Lee CH (2015) Rainfall characteristics for anisotropic conductivity of unsaturated soil slopes, Environmental Earth Sciences, 73: 8669–8681. doi:10.1007/s12665-015-4032-4.

Zhang WQ, Sun Q, Zhang, Y (2018) Correlation analyses of effects of temperature on physical and mechanical properties of clay, Environmental Earth Sciences 77:614.

Zienkiewicz OC, Humpheson C, Lewis RW (1975) Associated and non-associated visco-plasticity and plasticity in soil mechanics. Geotechnique 25(4): 671-689.